# INVESTIGATION AND CHARACTERIZATION OF LVOF SPRAYED BIMODAL COMPOSITE COATINGS FOR BIOMEDICAL APPLICATIONS

Thesis Submitted for the Award of the Degree of

**DOCTOR OF PHILOSOPHY**

**in**

**Mechanical engineering**

**By**

**Gaurav Bafila**

**Registration Number: 42100207**

**Supervised By**

**Dr. Hitesh Vasudev (24804)**

**School of Mechanical Engineering**

**(Professor)**

**Lovely Professional University, Punjab**


**LOVELY PROFESSIONAL UNIVERSITY, PUNJAB**

**2025**

# DECLARATION

I, hereby declare that the presented work in the thesis entitled "INVESTIGATION AND CHARACTERIZATION OF LVOF SPRAYED BIMODAL COMPOSITE COATINGS FOR BIOMEDICAL APPLICATIONS" in fulfilment of the degree of Doctor of Philosophy (Ph. D.) is the outcome of research work carried out by me under the supervision Dr. Hitesh Vasudev, working as Professor, in the School of Mechanical Engineering of Lovely Professional University, Punjab, India. In keeping with the general practice of reporting scientific observations, due acknowledgments have been made whenever the work described here has been based on the findings of another investigator. This work has not been submitted in part or full to any other University or Institute for the award of any degree.

**(Signature of Scholar)**

Name of the scholar: GAURAV BAFILA

Registration No.: 42100207

Department/school: Mechanical Engineering

Lovely Professional University,

Punjab, India

# CERTIFICATE

This is to certify that the work reported in the Ph.D. thesis entitled "INVESTIGATION AND CHARACTERIZATION OF LVOF SPRAYED BIMODAL COMPOSITE COATINGS FOR BIOMEDICAL APPLICATIONS" submitted in fulfilment of the requirement for the reward of degree of **Doctor of Philosophy (Ph.D.)** in the School of Mechanical Engineering, is a research work carried out by Pardeep Singh, Registration No. 42100207 is bonafide record of his/her original work carried out under my supervision and that no part of thesis has been submitted for any other degree, diploma or equivalent course.

**Supervised By**

**Dr. Hitesh Vasudev (24804)**

**School of Mechanical Engineering**

**(Professor)**

**Lovely Professional University, Punjab**

# ABSTRACT

The metallic materials are widely employed as bio-implants in human body for mechanical features and reasonable biocompatibility. However, these materials suffer from corrosion, which is a serious problem. Research and development on metallic biomaterials have shown that surface coating/ modifications of metallic implants by using a suitable bioactive material is a widely accepted alternative to minimize the harmful effects of corrosion.

This study examines the surface modification of SS-31254 surgical steel using Hydroxyapatite (HA) and alumina ($Al_2O_3$)-based bioactive powders, implemented via the Low Velocity Oxy-Fuel (LVOF) method. The research used four distinct coatings: pure hydroxyapatite (HA), hydroxyapatite with 10wt% micron-sized aluminum oxide (HALC), hydroxyapatite with 10wt% nano-sized aluminum oxide (HALN), and a hybrid of hydroxyapatite with 5wt% micron-sized and 5wt% nano-sized aluminum oxide (HALB). The objective was to improve the mechanical, corrosion-resistant, and bioactive characteristics of the substrate, specifically for biomedical applications.

The coating technique established a robust mechanical link between the surface-modified layers and the SS-31254 substrate, with no notable flaws, such as interface cracking, observed. This underscores the efficacy of the LVOF approach in generating well-adhered coatings. Subsequent to deposition, all coatings were subjected to a thermal treatment at 700°C for a duration of two hours. The objective of this post-treatment was to enhance the mechanical properties of the coatings by converting the amorphous phases in the as-deposited coatings into crystalline phases.

X-ray diffraction (XRD) examination indicated that, after heat treatment, the crystalline phases of α-tricalcium phosphate (α-TCP), β-tricalcium phosphate (β-TCP), and octa-calcium phosphate (OCP) were generated in the changed surface layers. The intensity of the amorphous phases markedly diminished in the heat-treated samples. Furthermore, the pronounced sharpening and shifting of the XRD patterns in the heat-treated coatings indicated a decrease in residual stresses that were originally generated during the LVOF spraying procedure.

Porosity is a crucial factor influencing both mechanical and biological efficacy in coatings. The porosity investigation indicated that the as-sprayed HA coating exhibited the greatest porosity, quantified at 7.6%. The incorporation of $Al_2O_3$ markedly decreased porosity: HALC demonstrated a porosity of 6.8%, HALN 6.3%, and HALB attained the minimal porosity of 4.6%. Post-heat treatment, the porosity of all coatings decreased, with HA exhibiting 6.9%, HALC 5.8%, HALN

4.7%, and HALB demonstrating the lowest porosity at 4.1%. This illustrates that heat treatment, along with the incorporation of $Al_2O_3$, especially in the HALB coating, significantly enhances the densification of the coatings, reduces porosity, and strengthens their mechanical integrity.

The microhardness investigation demonstrated that the mechanical characteristics of the coated surfaces were improved by the incorporation of $Al_2O_3$ and subsequent heat treatment. The as-sprayed HA coating exhibited an average hardness of 290.2 HV, while the addition of micron-sized $Al_2O_3$ in the HALC coating elevated the hardness to 296.9 HV. The HALN coating, which contains nano-sized $Al_2O_3$, exhibited a marginally increased hardness of 298 HV. The HALB coating attained the maximum hardness, including both micron- and nano-sized $Al_2O_3$, achieving 332.9 HV in its as-sprayed state. Post heat treatment, the hardness of HALB rose to 353.3 HV, illustrating the efficacy of using $Al_2O_3$ with varying particle sizes to improve the mechanical characteristics of the coating.

The corrosion resistance investigation indicated that the uncoated SS-31254 had the greatest corrosion rate of 0.328 mm/year. The use of HA and $Al_2O_3$-based coatings markedly enhanced corrosion resistance. The corrosion rates for HALC, HALN, and HALB coatings were 0.031 mm/year, 0.032 mm/year, and 0.022 mm/year, respectively. The heat treatment significantly improved corrosion protection, resulting in the heat-treated HALB coating attaining the minimal corrosion rate of 0.005 mm/year.

The bioactivity investigation evaluated the development of a bone-like apatite layer on the coated surfaces after immersion in simulated bodily fluid (SBF). The uncoated SS-31254 exhibited no weight change, indicating an absence of bioactivity. The as-sprayed HA coating exhibited a weight increase of 0.20 g, indicating substantial apatite production. The HALN coating exhibited a weight increase of 0.22 g, while HALB had the greatest as-sprayed weight gain of 0.26 g. Post-heat treatment, the HALB coating had the highest weight increase of 0.28 g, indicating higher bioactivity and the possibility for improved bone integration in biomedical applications.

# ACKNOWLEDGEMENT

I would like to express my deepest gratitude to my dissertation supervisor, **Dr. Hitesh Vasudev,** Professor at the School of Mechanical Engineering, Lovely Professional University, for his invaluable guidance and unwavering support throughout this research work.

I am profoundly grateful to my parents for their blessings and for being the cornerstone of my inspiration. A special note of thanks goes to my father, **Advocate Ganga Singh Bafila**, and my mother, **Mrs. Ganga Bafila**, for their constant care, love, and advice. I would also like to extend heartfelt thanks to my spouse, **Mrs. Suchita Bafila**, for her unwavering encouragement and financial support in pursuing my higher studies. My deep appreciation also goes to my son, **Rundrash**, my daughter, **Kuhu**, and my sister and brother-in-law**, Mr. Mohit Lal Sah** and **Mrs. Pranjali Sah**, for their love and care.

I extend my heartfelt thanks to everyone who has supported me in completing this work successfully. I apologize for not being able to mention everyone individually. Above all, I offer my sincere gratitude to the Almighty for granting me the strength, courage, and patience to carry out this research.

**(GAURAV BAFILA)**

## TABLE OF CONTENTS

# TABLE OF FIGURES

# LIST OF TABLES

# ABBREVIATIONS

| | |
|---|---|
| APS | Atmospheric Plasma Spray |
| HA | Hydroxyapatite |
| HAP | Hydroxyapatite |
| Hap | Hydroxyapatite |
| HALC | Hydroxyapatite+10 wt.% $Al_2O_3$ (Micronmetric) |
| HALN | Hydroxyapatite+10 wt.% $Al_2O_3$ (Nanonmetric) |
| HALB | Hydroxyapatite+05 wt.% $Al_2O_3$ (Micronmetric)+5 wt.% $Al_2O_3$ (Nanonmetric) |
| LVOF | Low Velocity Oxy-fuel |
| BSE | Backscattered Electron |
| BSE | Back Scattered Electron |
| CNT | Carbon Nanotube |
| EDS | Energy-Dispersive X-ray Spectroscopy |
| FE-SEM | Field Emission Scanning Electron Microscope |
| PS | Plasma Spray |
| PS-PVD | Plasma Spray-Physical Vacuum Deposition |
| SLM | Standard litre per minute |
| SPPS | Solution Precursor Plasma Spray |
| SPS | Suspension Plasma Spray |
| SS | Stainless Steel |
| TBC | Thermal Barrier Coating |
| TBCs | Thermal Barrier Coatings |
| TSC | Thermally Sprayed Coatings |

# CHAPTER 1

# INTRODUCTION

## 1.1 DEMAND OF BIOMATERIALS

The use of bio-implant increases in daily life. Thus, research in this area is very important to reduce costs and improve properties. Until 1860, as illustrated in **Fig.1.1,** it was possible to successfully implant metallic devices such as bone pins made of iron, or gold in experimental trials. However, after the industry experienced extraordinary growth, the biomaterials are used in knee implants also. It has been reported that between 2005 and 2030, the anticipated growth in primary TNA operations in the United States is over 673%, whereas the estimated increase in primary THA procedures is approximately 174% . Factors such as the ageing of the baby boomer generation, the rising average human lifespan, and the epidemic of obesity all contribute to the increased stress that is being placed on our weight-bearing joints.

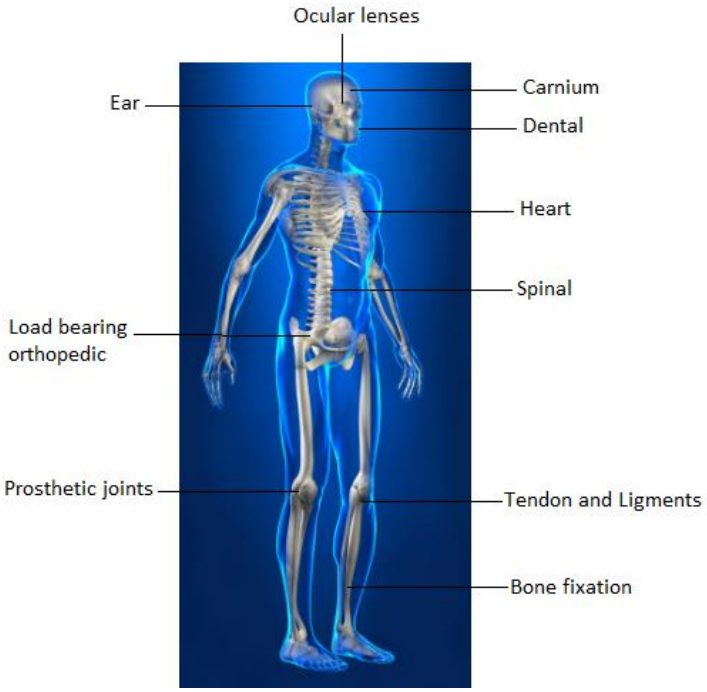


**Fig. 1.1** Biomaterials in human body parts.

The joint replacement was mainly done through metallic biometal (SS-316L, Ti-6Al-4V), because they possess adequate strength required to sustain loads in load bearing joints. **Table 1.1** illustrates the various metallic materials used as implant material in a number of applications.

**Table 1.1**
Biomaterials of metallic materials (Geetha et. Al, 2009)

| Class | Application | Use and approval |
|---|---|---|
| Stainless steels (Fe based biomaterials) | Replacement of the hip joint<br>Temporary implants | |
| Co-based materials | Joint replacement in surgery for use in dentistry | Applied routinely |
| Ti-based alloys | Mechanical devices and nails Hip replacement stem and cup | |
| Others | | |
| NiTi | Scleral stents Surgical anchors Wires used to guide catheters<br>Intracranial aneurysm clips | Approved by FDA |
| Mg | Biodegradable orthopedic implants | |
| Ta | To serve as a reference point in radiography<br>A plastic surgeon or neurosurgeon may utilise wire sutures. | |

## 1.2 BIOMATERIALS

The research is very important to reduce costs and improve properties of biomaterials. The joint replacement was mainly done through metallic biometal because they possess adequate strength required to sustain loads in load bearing joints (Balla et al., 2013; Balamurugan et al., 2002). In biomaterials, the metallic implants are used because they have adequate strength at reasonable cost. The austenitic stainless steels (ASS) are used as implant material for inner joint fixation orthopedic devices (Davis, J.R. ed., 2004). As compared to titanium alloys, the corrosion rate is low in stainless steel. Despite of this, at a very low cost, it has very good mechanical properties, used provisionally for inner parts like bone plates, screws and spine traction. Numerous kinds of stainless steel, including Rex-734, P-558, ASTM-F2581, and UNS.254, have been discovered by the authors for use in orthopaedics (Dehnavi et al., 2017; Tiwari and Mishra., 2021). In recent years, the use of UNS S31254 (254 SS), an austenitic stainless steel with maximal pitting corrosion resistance in chloride and phosphoric environments, outstanding

mechanical strength, and toughness, has risen in favour for use as implant material in the medical field.

## 1.3 IMPORTANT ASPECTS OF BIO-MATERIALS (METALLIC)

The biomaterials must have adequate biocompatibility. It also exhibits excellent corrosion resistant when interact with human body plasma. These materials must have adequate mechanical properties such as high wear resistant for load bearing applications. The implant upon implantation inside a human body must make a balance of all these properties. An implant should have the following features to serve for a longer time without failure in the human body. Furthermore, both scaffolding and scaffolds used in tissue engineering are constructed from metallic materials. This is the underlying cause of the problem (Bastan et al., 2018). Surface Coating Characteristics of Surgical Grade Stainless Steel Implants Coated with a Variety of Materials are as follows (Bodhak et al., 2011; Chai et al., 2021).

- Coverings made of stainless steel.
- Hardness that is superior and consistent.
- Exceptional longevity.
- Extremely effective defence against oxidation caused by wear and pressure.
- Strong resistance to corrosion as a result of the creation of a passive layer of $Cr_2O_3$ Excellent resistance to oxidation.
- Protection against chemical assault High bonding strength of the coating that is applied using thermal spraying.
- There is a thick covering with little porosity.

### 1.3.1. Mechanical Properties

The particular type of biomaterial needed for an application is determined by its mechanical properties. Biomaterials should have adequate strength and longer fatigue life for their excellent performance in the human body. An implant material must exhibit Young's modulus similar to that of the human bone depending on its biomedical applications. Ti6Al4V has modulus matches with that of the human bone whereas 316L stainless steel exhibit an exceedingly higher elastic modulus. Bone resorption at the implant/bone contact can occur if the implant material has a different modulus than the host tissue (M. Wang., 2003). The method employed to create a particular implant also has an impact on its mechanical qualities. **Table 1.2**

compares the properties of human bone to those of widely used implant materials Kamachimudali et al., 2003).

**Table 1.2** Important aspects related to implant material and bone (Kamachimudali et al., 2003).

| **Material** | **Strength (Tensile) ($MN/m^2$)** | **Strength (Yield)($MN/m^2$)** | **Hardness value (Vickers) (HV** | **Modulus (E) ($MN/m^2$)** | **Endurance limit ($MN/m^2$)** |
|---|---|---|---|---|---|
| **316L SS** | 649 | 279 | 490 | 209 | 0.27 |
| **Alloy Co-Cr** | 1540 | 1050 | 450 | 539 | 0.47 |
| **Cast Co-Cr alloy** | 689 | 489 | 300 | 239 | 0.30 |
| **Titanium** | 709 | 469 | - | 119 | 0.29 |
| **Ti6Al4V** | 999 | 969 | - | 119 | - |
| **Human Bone** | 140.3 | - | 26.3 | 30 | - |

### 1.3.2 BIOCOMPATIBILITY

The main prerequisite for any biomaterial is biocompatibility, which is a substance's ability to perform when used in the human body plasma. The biocompatibility is an essential primary requirement of any biomaterial (D.F. Williams., 2003). Biocompatibility of implant devices influenced by a number of parameters as depicted in **Fig. 1.2.**

These factors ultimately affect the performance of implant material and can lead to its failure (Manivasagam et al., 2010). Biocompatible materials, after their implantation in the human body must not release toxic substances, which may induce many complications such as allergies, choronic inflammation and unusual tissue formation (P. Itiravivong., 2001).

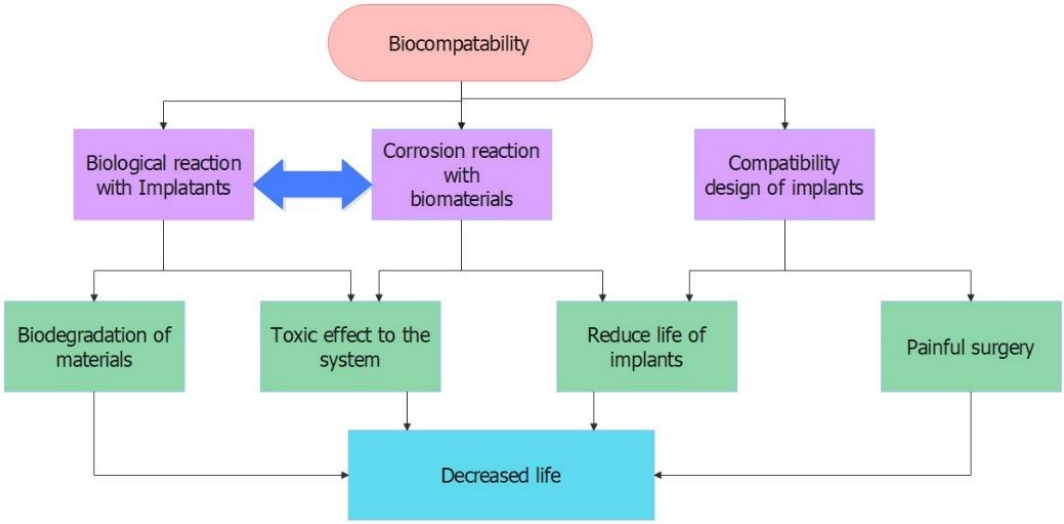


**Fig. 1.2** Various factors influencing the biocompatibility of biomaterial (Singh and Dahotre., 2007).

### 1.3.3 CORROSION RESISTANCE

Plasma-sprayed hydroxyapatite (HA) coatings are widely used in biomedical applications, especially for metallic implants, due to their excellent biocompatibility and bioactivity. However, pure HA coatings often exhibit poor corrosion resistance when exposed to physiological environments, primarily due to their porosity and tendency to dissolve under acidic conditions (Wang et al., 2009). To overcome this limitation, researchers have explored the incorporation of alumina ($Al_2O_3$), a chemically stable and corrosion-resistant ceramic, into HA coatings. The addition of $Al_2O_3$ significantly enhances the corrosion resistance of the composite coatings by refining the microstructure and reducing porosity, thereby limiting electrolyte penetration (Ramesh et al., 2007).

HA+$Al_2O_3$ composite coatings exhibit improved electrochemical stability in simulated body fluids (SBF), as evidenced by higher open circuit potentials and lower corrosion current densities compared to pure HA coatings (Han et al., 2012). The presence of alumina particles in the HA matrix acts as a physical barrier, impeding the diffusion of corrosive ions and improving coating integrity over time. Moreover, alumina contributes to better mechanical interlocking and adherence to metallic substrates, thereby reducing the risk of delamination and subsequent corrosion (Heimann et al., 2016).

Studies have also indicated that the phase stability of HA is retained better in the presence of alumina during plasma spraying, which further enhances the durability of the coating under physiological conditions (Gowthaman et al., 2014). The HA+$Al_2O_3$ coatings not only maintain the biological advantages of hydroxyapatite but also provide superior corrosion resistance, making them more suitable for long-term implant applications (Jastrzębska et al., 2018).

### 1.3.4 WEAR

In the case of knee and hip joint prostheses, wear is the leading cause of implant failure (Roychowdhury et al., 2004). Low wear resistance resulted in the wear debris to build up and cause a variety of tissue reactions. According to Niinomi (2008), these reactions have the potential to result in the premature failure of implants. A primary area of emphasis within orthopaedic research involves the enhancement of fixation and wear properties pertaining to whole joint components (Geetha et al., 2009). Hence, it is imperative to develop materials that possess elevated levels of hardness and corrosion resistance in order to enhance the longevity of implants within the human body (Eliaz et al., 2002).

Biomedical implants provide substantial benefits to patients requiring joint replacement, cardiovascular support, and other medical procedures, greatly improving their quality of life. However, the durability of these implants is a crucial factor that directly affects their efficacy and longevity.

The wear performance of biomedical implants is greatly affected by essential factors including surface polish, hardness, toughness, and corrosion resistance.

## 1.4 METAL IMPLANT MATERIALS WITH MODIFIED SURFACES

Further, HA having chemical formula $Ca(PO_4)_6(OH)_2$ is the frequently used material in the dentistry and prosthesis area of applications due to its excellent biocompatibility and tissue regeneration property (Tiwari and Mishra., 2021). Thus, the biocompatibility of metallic implant surface can be improved with pure biometal such as HA or its composite material. The main function of HA implant coatings is its participation in human tissues on the implant surface (Bergant and Grum., 2009; Bergant et al., 2014).

The coating of HA on the metal substrates are introduced on the surfaces by using various well established surface modifications techniques like sol-gel, biomimetry, chemical vapour deposition, sputtering, dip coating, immersion coatings, ion bean assisted deposition, plasma sintering, electrophoretic deposition, electro hydrodynamic spraying, pulsed laser deposition based surface modification of metallic implant with reinforced HA material, thermal spray methods, and flame spray etc. (Bergmann and Vicenzi., 2011; Birks et al., 2006; Bolelli et al., 2008a; Bolelli et al. 2008b; Boulos et al., 2021; Calvarin et al., 2000; Campo et al., 2009; Chatha et al., 2013; Chatha et al., 2016; Chatterjee et al., 2001; Ctibor et al., 2006; Daram and Banjongprasert., 2020.) Each of these coatings have significant advantages and limitations with respect to a particular fields/ application. For example, the plasma spraying is a complex process for performing HA based coating son the metallic implant because a lot of factors were involved in its coatings. The laser assisted surface modifications is a costly process on the other hand.

**1.5 MOTIVATION**

There is a huge demand for biomaterials in future. The metallic biomaterial is commonly used for the fabrication of implant because they exhibit better mechanical properties at reasonable cost. However, the metallic implant lacks in providing the required biocompatibility when they are come in contact with human body plasma. Therefore, a suitable coating has been done on this implant material. The metallic biomaterials can be effectively shielded against various sorts of degradations like corrosion and wear by applying a biocompatible coating. There are number of coatings methods were available as discussed above. However, there are limitations associated with these processes such as high-temperature associated with plasma spray, decomposition of HA and formation of unwanted phases, responsible for reduced crystallinity of the coating. To overcome the limitations of the existing compositions and coating techniques, a new process LVOF has selected in the present work due to its lower temperature and high-velocity as compared to plasma spraying on stainless SS-31254. The addition of ceramic ($Al_2O_3$) with features such as inertness, phase stability and high density has been selected in this research work. Further, the different scales (micron, nano and bi-modal) of $Al_2O_3$ were expected to achieve multiple set of properties.

## 1.6 CHAPTER WISE DETAILS

### Chapter 1: Introduction

This chapter outlines the growing demand for biomaterials in biomedical applications, emphasizing the need for surface modification of metallic implants to improve biocompatibility and corrosion resistance. It discusses the shortcomings of metallic implants such as corrosion and lack of bioactivity, prompting the use of bioactive coatings. Hydroxyapatite (HA) is highlighted as a preferred coating material due to its similarity to bone mineral. The chapter introduces the low-velocity oxy-fuel (LVOF) spraying technique as a promising method to deposit bioactive coatings at relatively lower temperatures compared to plasma spraying. The addition of alumina in micro, nano, and bimodal forms is proposed to enhance mechanical and biological performance.

### Chapter 2: Literature Review

This chapter surveys existing research on biomaterials, focusing on corrosion issues and surface engineering techniques for implants. It reviews various coating technologies, including plasma and microwave-assisted spraying, noting their limitations in achieving optimal phase composition and adhesion. Special emphasis is placed on the limited use of LVOF spraying in biomedical fields, marking a key research gap. It also introduces the potential of hybrid reinforcement (micro- and nano-$Al_2O_3$) in HA coatings for improved properties. The chapter concludes by identifying the need for further research on structure-property relationships and advanced composite coatings.

### Chapter 3: Experimental Equipments and Methodology

The methodology details the preparation of SS-31254 stainless steel substrates and the development of HA-based coatings using the LVOF technique. The process includes mixing HA with micro, nano, and hybrid alumina powders followed by spraying and subsequent heat treatment at 700°C. Characterization methods include SEM, EDS, XRD, microhardness, porosity, and corrosion testing using electrochemical techniques. In-vitro bioactivity is studied using immersion in simulated body fluid (SBF). This chapter establishes the foundation for evaluating the mechanical, structural, and functional performance of the coated specimens.

### Chapter 4: Characterization of Powders and Coatings

This chapter presents the morphological and phase characterization of HA and $Al_2O_3$ powders using SEM, EDS, and XRD. It confirms the purity and morphology of the powders used in

coating. The coatings displayed a mix of molten and partially molten particles, with improved microstructural uniformity observed in nano- and bimodal alumina composites. Cross-sectional SEM analysis indicated better adhesion and reduced porosity in HALB (hybrid alumina) coatings. Microhardness and porosity results showed enhancements in mechanical properties with alumina additions, especially in heat-treated samples.

**Chapter 5: In-vitro Biocompatibility Study and Corrosion Behaviour**

This chapter evaluates the corrosion resistance and bioactivity of as-sprayed and heat-treated coatings using electrochemical testing and SBF immersion. HALB coatings showed the lowest corrosion rate (0.005 mm/year) and highest weight gain (0.28 g), indicating superior bioactivity and protection. SEM images revealed a dense and uniform apatite layer in HALB after annealing, validating its enhanced surface reactivity. The EDS confirmed the presence of Ca and P in all coatings, supporting effective HA deposition. The combination of nano and micron-sized alumina and heat treatment significantly improved both corrosion resistance and biological performance.

**Chapter 6: Conclusions and Future Scope**

The final chapter summarizes that surface modification using HA and alumina composites via LVOF is effective in enhancing the surface characteristics of SS-31254. HALB coatings provided optimal results in terms of microhardness, corrosion resistance, and bioactivity. Heat treatment played a crucial role in reducing porosity and transforming the amorphous phase into crystalline forms, thereby improving coating integrity. The study recommends further exploration of alternative bioceramic reinforcements and optimization of LVOF process parameters. It concludes that the developed coatings are promising for long-term biomedical implant applications.

# CHAPTER 2

# LITERATURE REVIEW

This encompasses studies on implant corrosion and various surface modification techniques used for biomedical implants. The more emphasis is given on application of microwave energy for processing of various engineering materials.

## 2.1 BIOCOMPATIBLE METALLIC ALLOYS

As a direct consequence of this, a new era in the manufacturing of metals began with the first developments of medical implants that make use of metals that are biocompatible. A significant contributor to the increase in the number of applications for metal implants was the demand for treatments that attempted to heal bone, most frequently by performing internal fixation of long bone fractures. Implants made of metal had durability and corrosion issues in their early stages of development (Velu et al, 2019). Metal implant technology and its clinical uses have come a long way. Metal implants saw a rise in demand as the number of patients requiring internal treatment of lengthy bone fractures rose. Metals created from biologically acceptable materials have been employed in orthopaedic devices. In addition to more permanent devices like pins and screws, bone plates, and total joint replacements, they serve many different orthopaedic functions. When a broken bone has healed and cemented together, the metallic implant, such as a screw, is normally removed (Dehghanghadikolaei et al, 2019).

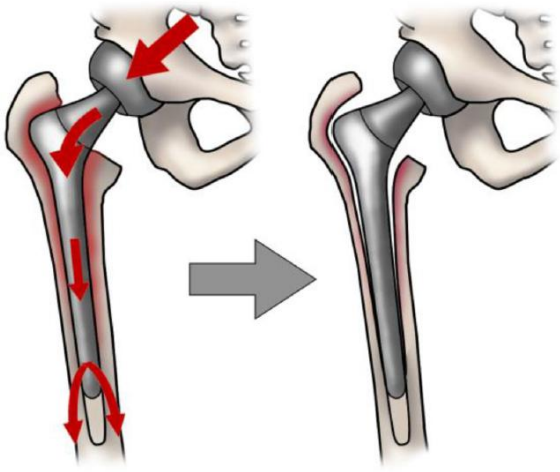

**Fig. 2.1.** Innovative loading conditions in stable surgical implants are depicted schematically (Degaard et al, 2020).

Nonmagnetic, high-density metals are preferred for implants. Figure 2.1 depicts a schematic representation of novel loading conditions that can be used on stable surgical implants. Before implants can be seen, imaging techniques like magnetic resonance imaging (MRI) and X-ray imaging need to be compatible with them. Because artificial implants are typically subjected to static or repetitive stresses, it is imperative that they possess both exceptional tensile and flexural strength. Metals have an advantage over ceramics and polymers when viewed from this perspective. The specific requirements for metals are decided by the function that the implant is supposed to serve. In order to open blood vessels that have become stenotic, stents and stent-grafts may be implanted (Priyadarshini et al, 2020). For dilatation to be supported, expansion plasticity and stiffness are both necessary characteristics. Metals must possess exceptional toughness, elasticity, stiffness, strength, and fracture resistance in order to be used in orthopaedic implants. It is essential for thorough joint replacement that metals have a high resistance to wear because this will prevent debris from accumulating as a result of friction. Dental reHALBilitation necessitates the utilisation of sturdy metals, including shaped memory alloys, in order to achieve optimal results. Wear stress is caused by the relative movement of an implant material and another material, such as bone, that exhibits a different stiffness behaviour under cyclic stress. This movement causes the implant material to rub against the bone. The issue of stress shielding is one that frequently arises in the context of biomaterials. Bone resorption is brought on by a disparity between the Young's Modulus of bone and the material that makes up the implant. Most metal-based biomaterials have Young's moduli that are much higher than those of cortical and trabecular bones. Manufacturing and material selection processes should be carried out to address the problem (Kamrani et al., 2019). Titanium alloys offer an alternative to other implant materials because their Young's Modulus is more comparable to bone than those of other implant materials. One more method for controlling bone's Young's modulus is by modifying the porosity of the bone. Therefore, solid metallic implants experience significant issues with bone loss in the vicinity of the implantation site when they are used in load-bearing applications (LBAs). Despite the potential for successful osseointegration after installation of the prosthesis, aseptic loosening continues to be the leading cause of all revisions for total hip replacements. Stress shielding, in which the neighbouring bone is protected from stress induced by new loading circumstances after implantation, is a common cause of the mechanism of failure. The remodeling process of bones begins when they are subjected to mechanical loading.

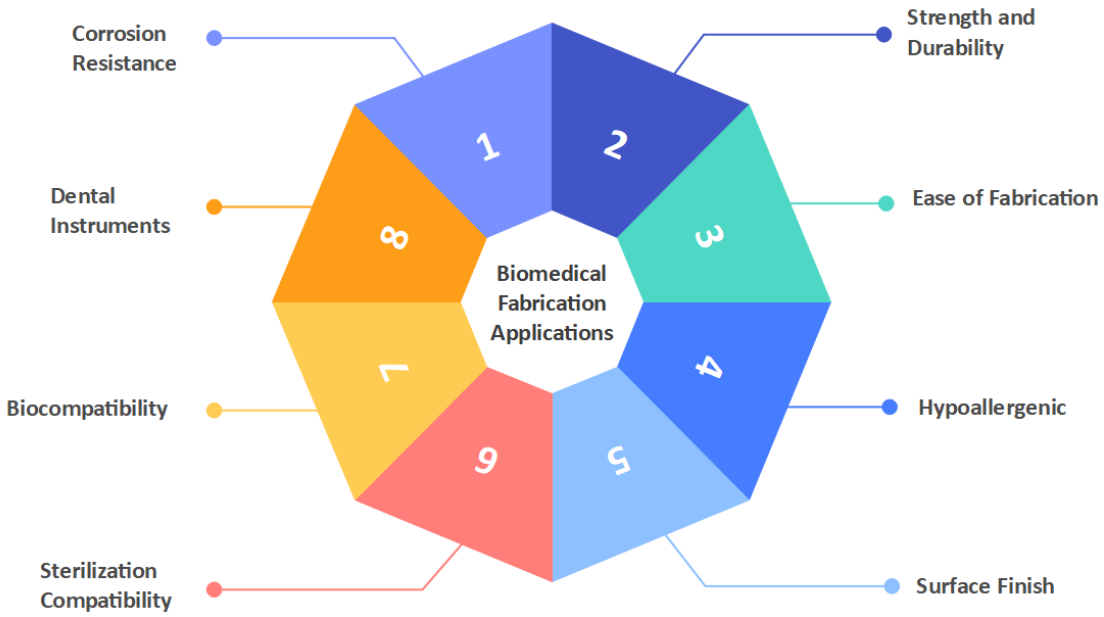


**Fig. 2.2.** Stainless steel (SS) is a common metal used in biomedical fabrication applications.

The Stainless steel (SS) is a metal that is widely used in the fabrication of applications related to biomedicine, as demonstrated in Fig.2.2. It has been used for several purposes, including the fabrication of durable prosthetic joints and transient implantation. Enhancements in the biocompatibility and durability of stainless steel remain under investigation, attributed to the challenges in addressing the material's issues (Resnik et al., 2020). The utilization of stainless steel in several contexts, including coatings, surface modifications, laser surface treatment, and grain refinement, was utilized to address these issues. Conversely, magnesium (Mg) is a biodegradable material that may serve as an alternative for bone. It has a comparatively low Young's modulus and exhibits biocompatibility (Rehman et al, 2020). Consequently, the bone tissue fails to fully repair prior to the compromising of the bone's mechanical integrity. Although a slower rate of magnesium biodegradability leads to a slower release rate, this also provides the body with more time to recover from the effects of the byproducts produced during the process of magnesium biodegradability. The rate at which magnesium degrades in biological systems can be controlled through the processes of alloying. MMCs, on the other hand, are helpful for selecting the appropriate reinforcements and modifying the properties of the material. In addition, it is of the utmost importance to discover methods by which the aggregation of particles, which occurred as a result of the use of traditional casting techniques, can be reduced. As a consequence of this, a number of researchers came to the conclusion that friction stir

processing, also known as FSP, is an efficient method for producing magnesium matrix composites. Magnesium as a biomedical material, in contrast to other medical metals currently in use, such as titanium and its alloy, alleviates patients' pain and eliminates the need for a second surgery once the wounds have healed. Magnesium also prevents the need for a second surgery. It has already been established that magnesium has biological effects during degradation, including promoting angiogenesis, bone growth, and wound healing. Other biological effects of magnesium include magnesium's role in promoting bone growth. Techniques known as severe plastic deformation (SPD) have become increasingly popular in recent years due to the obvious impact they have on grain refinement (Morsiya et al , 2022) [23]. By rotating the shoulder and pin tools, friction stir processing (FSP), which is one of these techniques, is primarily utilised to lessen the grain size of metal sheets or plates, which is the primary goal of the process. It is essential to keep in mind that the incorporation of $ZrO_2$ particles has the potential to boost the mechanical and biocompatibility features of the magnesium matrix. Researchers have found that FSP may support the microstructure and grain refinement of the composite, which relates to these findings.

## 2.2 USE OF BIOMEDICAL IMPLANTS PRESENTS SIGNIFICANT CHALLENGES

The use of biomedical implants, including but not limited to artificial joints, dental implants, pacemakers, and stents, poses numerous noteworthy obstacles, primarily centered on guaranteeing the safety, functionality, and sustained efficacy of these devices.

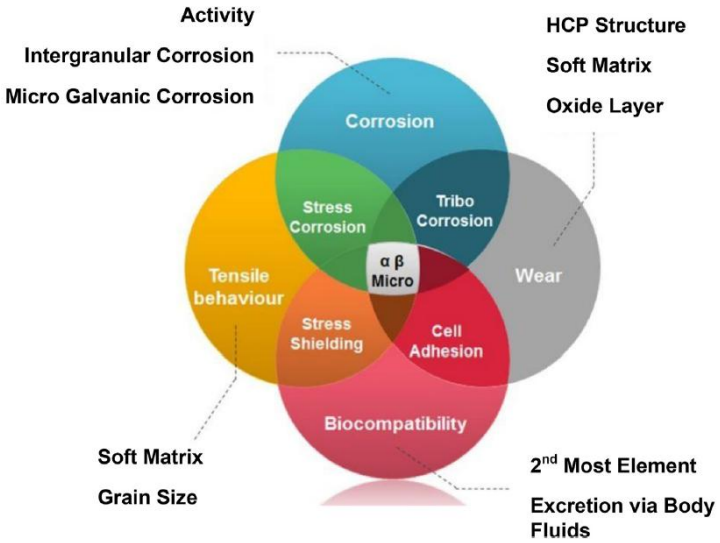


**Fig. 2.3** Concerns regarding the use of certain materials in biomedical implants (Nugyen et al, 2020).

To effectively tackle these difficulties, it is imperative to foster collaboration among diverse teams comprising engineers, materials scientists, doctors, and regulatory specialists. Ongoing research and development endeavours persistently aim to enhance the safety and performance of implant technology. When used in load-bearing applications, solid metallic implants run into major bone loss problems close to the implantation site. Aseptic loosening remains to be the primary failure, despite the prospect of good osseointegration following insertion of the prosthesis (Nugyen et al, 2020). The difficulties associated with employing alloys as a material for bioimplants are outlined in Fig. 2.3. The requirement to increase corrosion resistance and strength of technology, like changing the microstructure of an alloy using FSP, is advantageous because there is no addition of new phase materials to the alloy matrix. This was discovered after it was found that there was no addition of new phase materials to the alloy matrix.

## 2.3 DETERIORATION OF THE IMPLANT AS WELL AS CORROSION

The deterioration and corrosion of the implant is important factors to make while developing a reliable biomaterial. The degrading procedure that occurs within the biological environment might, depending on the applications, either be good or undesirable. The idea of "desired deterioration," which applies to biodegradable implants, states that these devices are only supposed to serve their intended purposes momentarily while promoting the healing of injured tissues, and then they are supposed to gradually break down after this period of time has passed. This concept applies to biodegradable implants (Munir et al, 2020). On the flip side, implant material is prone to undesirable degradation, which might manifest as surface corrosion, oxidation, or wear and tear over time. Unwanted degradation may result in the loss of the implant's structural integrity, the release of metal ions, and the production of wear debris, all of which may have a detrimental effect on the surrounding tissues on a biological level. The idea behind biodegradable implants is to break down the metal components in a biological environment so that they can be eliminated from the body through physiological channels without crossing a harmful threshold during the corrosion process. This is the fundamental idea behind biodegradable implants (Munir et al, 2020) . When it comes to biodegradable implants, one of the primary concerns that must be addressed is the fact that these implants must demonstrate an appropriate rate of deterioration while simultaneously ensuring that all damaged tissues will fully regenerate before they are completely broken down in vivo. Biodegradable

magnesium alloys usually demonstrate a high rate of deterioration, particularly in the early phases of implantation. This change in pH can have an effect on the rate at which tissues grow. To halt the quick deterioration taking place. In addition to slowing degradation, these particles promoted the growth of a biomineralized coating on the surface of the material.

The internal environment of a human being is chemically and physically different from the external environment. To give just one example, a metal that performs admirably in everyday conditions may be severely corroded in the biochemically active environment of the human body. Distinct differences in pH and oxygen levels can be found between different parts of the body. Even if an implant is functioning normally in one area of the body, it may develop corrosion in another area at unacceptable levels due to oxidation and acidic erosion.

**Table 2.1** displays the corrosive effects that a variety of biomaterials have on the host body. These effects are caused by corrosion. This study examines the impact of corrosion within the human body, resulting from the interaction of diverse metallic elements found in different biomaterials.

**Table. 2.1** The effects of corrosion in the human body, brought on by the presence of several metallic elements in various biomaterials. The presence of diverse biomaterials brings about this corrosion (Manivasagam et al, 2010).

| Different components in biomaterials | Effects on the body of a human |
|---|---|
| Ni | skin conditions such as dermatitis |
| Co | Preventing Fe from being absorbed into the bloodstream due to anemia B. |
| Cr | Causes ulcers and central nervous system abnormalities. |
| Al | Has an influence on the symptoms of epilepsy as well as Alzheimer's illness. |
| Va | Poisonous in its most fundamental form. |

The occurrence of various biomaterials contributes to the phenomenon of corrosion. This corrosion can lead to the release of toxic and carcinogenic substances, which can cause a variety of health problems. It is therefore important to understand the mechanisms and effects of corrosion to better control and manage its effects.

The implications for human health are serious, and further research is needed to better understand the potential risks of corrosion. It is important to develop strategies to prevent and mitigate the effects of corrosion, and to ensure that biomaterials used in medical devices are safe and biocompatible. Applicartions of bio-medical implants are shown in **Fig.2.4.**

Most stents are made of stainless steel, and depending on the circumstance, may be used with or without a coating. However, it was found that the element Ni released by the SS implant triggered allergic reactions when implanted into a human body. The implant itself brought on these reactions. In order to guarantee that a material will work correctly in its intended uses, it is necessary to test the material's resistance to corrosion in all possible adverse conditions (Jia et al, 2020).


**Fig 2.4.** Different materials used in the various bio-medical implants in corroiosn applications .

Corrosion is a critical factor contributing to the deterioration of biomedical implants, which can lead to significant clinical complications. The primary corrosion mechanisms include galvanic corrosion, pitting corrosion, and stress corrosion cracking. Galvanic corrosion occurs when dissimilar metals are in contact within a biological environment, leading to accelerated degradation of the less noble metal as presented in **Fig. 2.5.** Pitting corrosion, characterized by localized attack, can create small pits on the implant surface, compromising its structural integrity. Stress corrosion cracking arises from the combined effects of tensile stress and a corrosive environment, leading to the formation of cracks that can propagate over time. These corrosion processes are influenced by factors such as the implant material, the surrounding

biological fluids, and the physiological conditions of the body, ultimately affecting the longevity and performance of the implants. Understanding these mechanisms is essential for developing more durable materials and improving the design of biomedical implants to enhance their biocompatibility and resistance to corrosion.

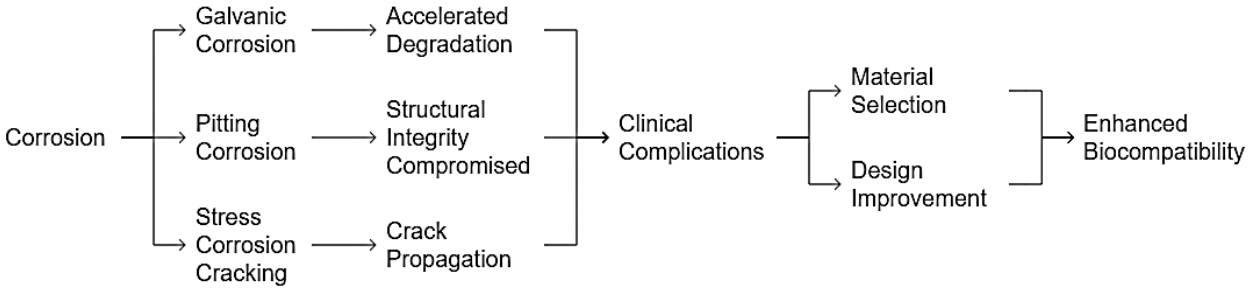


**Fig.2.5.** The corrosion mechanisms in bio-medical Implants (Revathi et al, 2017).

## 2.4 WEAR OF IMPLANTS

The consideration of wear resistance holds significant importance in the design of joint replacements within the human body, specifically for load-bearing joints such as the hip and knee. The durability and efficacy of these implants are directly influenced by their capacity to withstand wear and mitigate friction over an extended period. Joint replacement surgery is a surgical intervention that involves the substitution of a damaged or diseased joint with an artificial prosthesis. As depicted in **(Fig. 2.6),** many forms of joint replacement surgeries are conducted within the human body, contingent upon the specific joint that is afflicted (Kopava et al, 2019) . It is imperative to acknowledge that the attainment of wear resistance is merely one facet in the process of constructing efficacious joint replacements. The long-term effectiveness of joint replacements is contingent upon several crucial criteria, namely biocompatibility, implant fixation, and the mitigation of infection risk. Orthopaedic surgeons and biomedical engineers collaborate closely in the selection of materials and designs that best suit the individual requirements of each patient.

The contact between two hard, incongruent surfaces, heterogeneous strains developed in incongruent kinds like the knee and ankle joints shown in (**Fig.2.7**). In this scenario, metals and rigid polymeric materials are chosen over fragile ceramic materials because they are better able to withstand the stresses involved. The strains generated in the contact area are proportional to the applied force, with the higher force resulting in greater strain. The strain developed in the contact area is also dependent on the type of material used in the joint. The strain generated in

the contact area can also have an effect on the adhesive properties of the joint. If the strain is too high, the adhesive properties of the joint can be compromised. Therefore, it is important to select a material with an appropriate strain limit for the intended purpose.

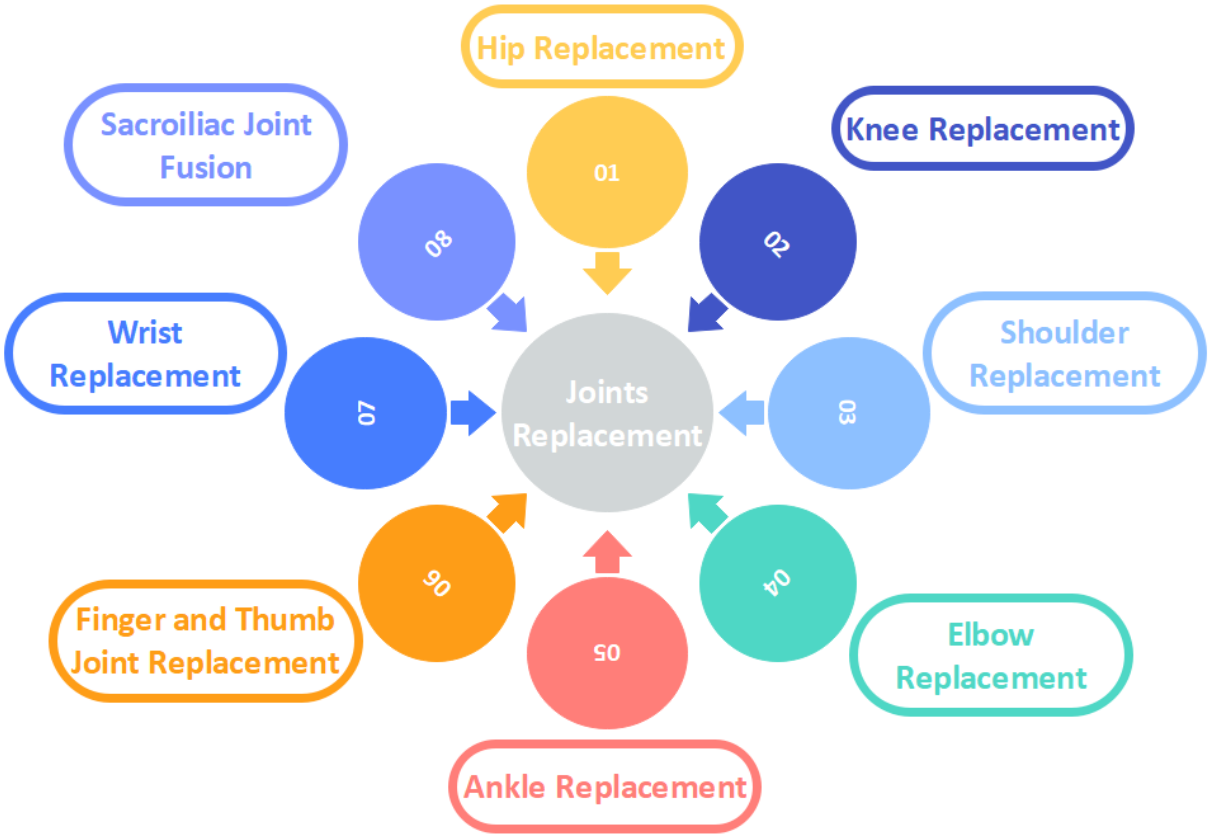


**Fig.2.6.** Types of joints replacement in the human body.


**Fig. 2.7.** (a) Knee and (b) ankle replacements are examples of artificial joints that do not align properly in the human body (Chen et al, 2015).

Concern has also been raised regarding the biological consequences as well as the long-term effects that the wear debris may have. It has been determined that wear is the primary factor responsible for osteolysis in THA. Submicron particles can reach the effective joint area and cause bone loss, which can result in a reaction known as a foreign body reaction (Hintermann et al, 2020). A significant number of people report diminished joint function as a consequence of the bone that surrounds the implant being thinner as a consequence of wear debris-driven osteolysis. The typical metal-on-polymer bearing setup causes wear debris whenever the acetabular cup rubs against the femoral head. This debris has the potential to cause severe damage to the living tissues that are in the area. In a nutshell, wear debris results in significant adverse reactions that call for revision surgery to be performed. Patients, physicians, and healthcare systems are all put under a significant amount of financial and logistical burden by revision operations. On the other hand, waste metals produced during use have the capacity to ionise and disperse themselves throughout the body (Mondal et al, 2020). People who have metal-on-metal implants have been found to have higher levels of metal in their blood and organs, which raises questions about the possibility of adverse effects on the body as a whole. This holds true despite the fact that a causal relationship between metal ions and health issues has not been verified. The discovery of new the improvement of wear resistance in materials or currently used materials for artificial joints has received heightened attention to reduce the frequency and severity of costly revision procedures caused by wear debris (Barg et al, 2011). This is done in order to avoid the complications that can arise from these procedures. High resistance to both wear and corrosion are consequently crucial qualities that determine how long joint implants will endure.

Biomedical implants are subject to various wear mechanisms **(Fig.2.8)** that can significantly impact their longevity and functionality. One of the primary wear mechanisms is abrasive wear, which occurs when hard particles or surfaces come into contact with the implant, leading to material loss. This is particularly prevalent in joint replacements, where the movement between surfaces can generate wear debris that contributes to inflammation and osteolysis. Another critical mechanism is adhesive wear, which happens when two surfaces slide against each other, causing material transfer and surface degradation. Fatigue wear is also a concern, especially in load-bearing implants, where cyclic stresses can lead to crack initiation and propagation over time. Additionally, corrosion wear can occur in the presence of bodily fluids,

leading to the breakdown of the implant material and the release of toxic ions. Understanding these wear mechanisms is essential for improving the design and material selection of biomedical implants to enhance their performance and lifespan.

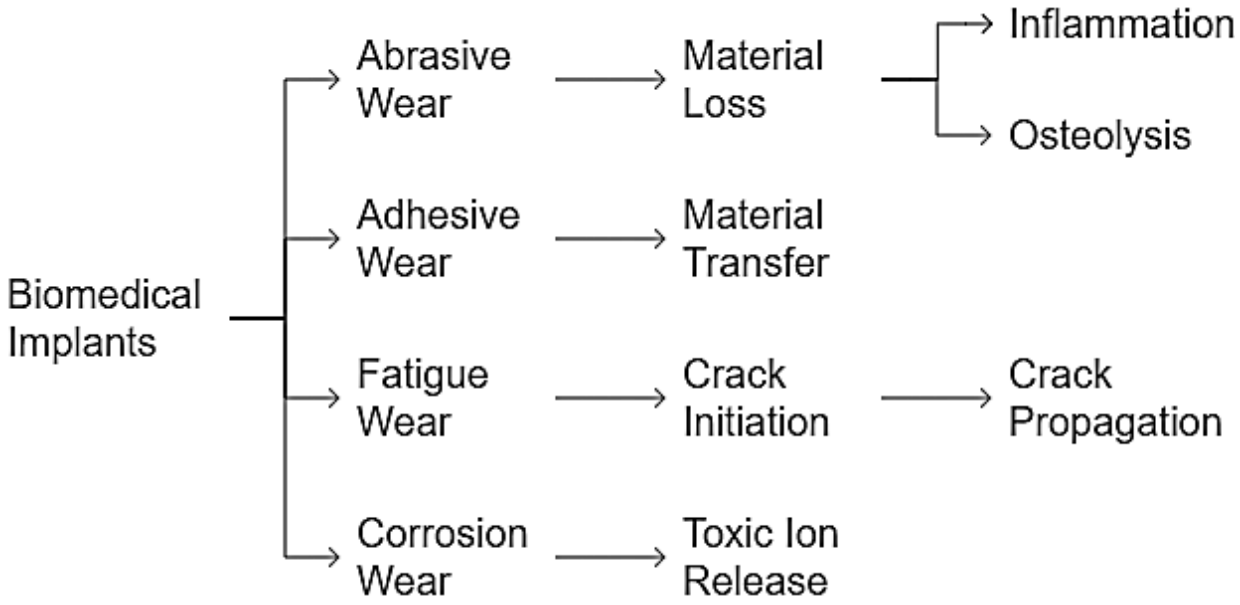


**Fig. 2.8.** Wear Mechanisms Responsible for the Deterioration of Biomedical Implants (Parcharoen et al, 2022).

**2.5 PREVENTION STRATEGIES TO REDUCE POSTOPERATIVE COMPLICATIONS**

All sorts of implants raise serious concerns when it comes to interactions with host tissue, which are normally evaluated. Therefore, modifying the surface of the prosthesis presents an opportunity to improve patient outcomes (Kumar et al, 2020). Prosthetics Surface modification implants is represented in **Fig.2.9.** On the other hand, it provides an information about the numerous materials that can be used in different conditions.). The thickness of the coating is the most important consideration, as it plays a role in the distribution of stresses at the interface between the coating and the implant and is therefore important for biomechanical analysis. Because of their superior mechanical strength, biocompatibility, and corrosion resistance, metallic biomaterials are typically used extensively for implants all over the world (Gibbs et al, 2020). Some of them, such as titanium, stainless steel 316L, and titanium alloys, are recommended for use in applications relating to orthopedics and biomedicine. In order for the medical device to function more effectively inside the body over a longer period of time, it must be non-toxic, even when it is in contact with living tissues (Quinn et al, 2020). Only then, it is able to maintain the position inside the body. In addition, there shouldn't be any cytotoxicity,

mutagenesis, or carcinogenesis associated with extended periods of time spent with medical equipment inside the body of a patient. However, metals and metal alloys cannot be transplanted directly into the human body because of corrosion. As a result, they are unfit for this purpose.

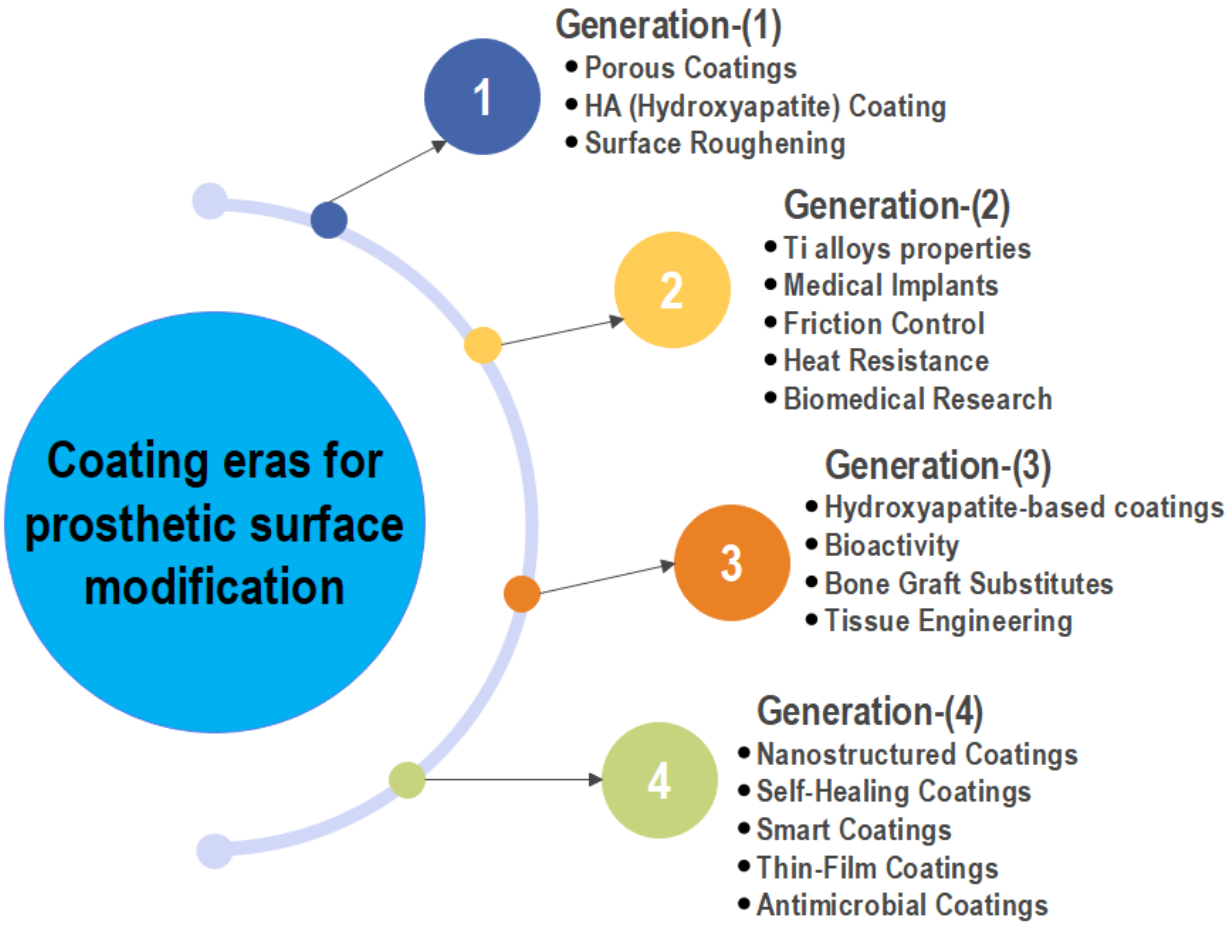


**Fig. 2.9.** Prosthetics Surface modification implants (Kumar et al, 2020).

These metals or alloys need to be covered in biocompatible materials and have a composition similar to bones for bone formation and development to proceed normally. By coating the metal implant with a bioactive and bioresorbable substance, it is possible to achieve these results. HAp is widely used as a covering material due to its excellent bioactivity, bioresorbility, biocompatibility, and osteoinducing qualities (Zafar et al, 2020).

In **(Fig.2.10),** we can see the crystal structure often linked to HAp. The fact that the Ca, $PO_4$, and OH ions in an appetite unit cell are so near to one other suggests that the mineral is crystalline.

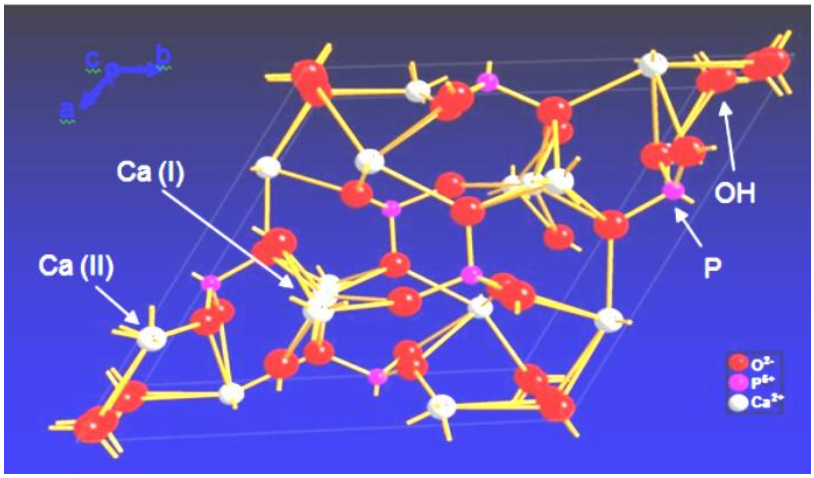


**Fig. 2.10.** Crystal structure of hydroxyapatite fluorapatite (Rivera et al, 2011).

Metallic implants can now have corrosion-resistant coatings, most commonly coatings based on HAp, deposited on them using any one of a number of different methods. This is made possible by the vast selection of coating materials. Things like the type of substrate and the applications of the coated material can have an effect on the technique that is ultimately selected. A wide variety of coating technologies exist, each with its own set of advantages; nevertheless, only a select handful are trustworthy enough for use in biomedical settings. By using these methods, the biocompatibility of the substrate as well as its ability to resist corrosion are both increased simultaneously. In biomedical applications, the TS coating technique is the one that is used the most frequently among the various coating methods that are available (Arcos et al, 2020). The fundamental concept that underpins this method, as well as several distinct applications of it, will be broken down in the sections that follow.

## 2.6 THERMAL SPRAY COATING TECHNIQUES

When biomedical implants like replacement joints are manufactured using thermal spray (TS). In this regard, high-performance TS coatings have been subjected to a significant amount of comparison research in recent years, alongside alternative manufacturing procedures (Beig et al, 2020) . For example, the TS process is absolutely necessary in order to manufacture high-quality prosthesis for medical implants. In order to make these implants suitable for human use, a TS method and extensive HAp spray-based coatings were applied to their surfaces. HAp-based coatings are selected because of their ability to generate a firm implant-bone interfacial

connection and because of their near resemblance to the main phase of the bone. This allows for enhanced prosthesis adhesion (Cheng et al, 2005).

In thermal spraying, a form of atomized spraying, powder, wire, or rod spray material is delivered into the heat source. It is possible for the feeding mechanism of the spraying pistol to be located either inside or outside. Because of the high temperature, the feedstock material will either be completely melted or short heated in order to become pliable (Awasthi et all, 2022). After this, the molten feedstock particles are accelerated or driven towards the surface of the substrate by a jet of gas. As a result of the interaction with the surface, the particles deform plastically into splats, which ultimately results in the formation of a coating. **Fig.2.11** provides a visual representation of the primary concept underlying thermal spraying.

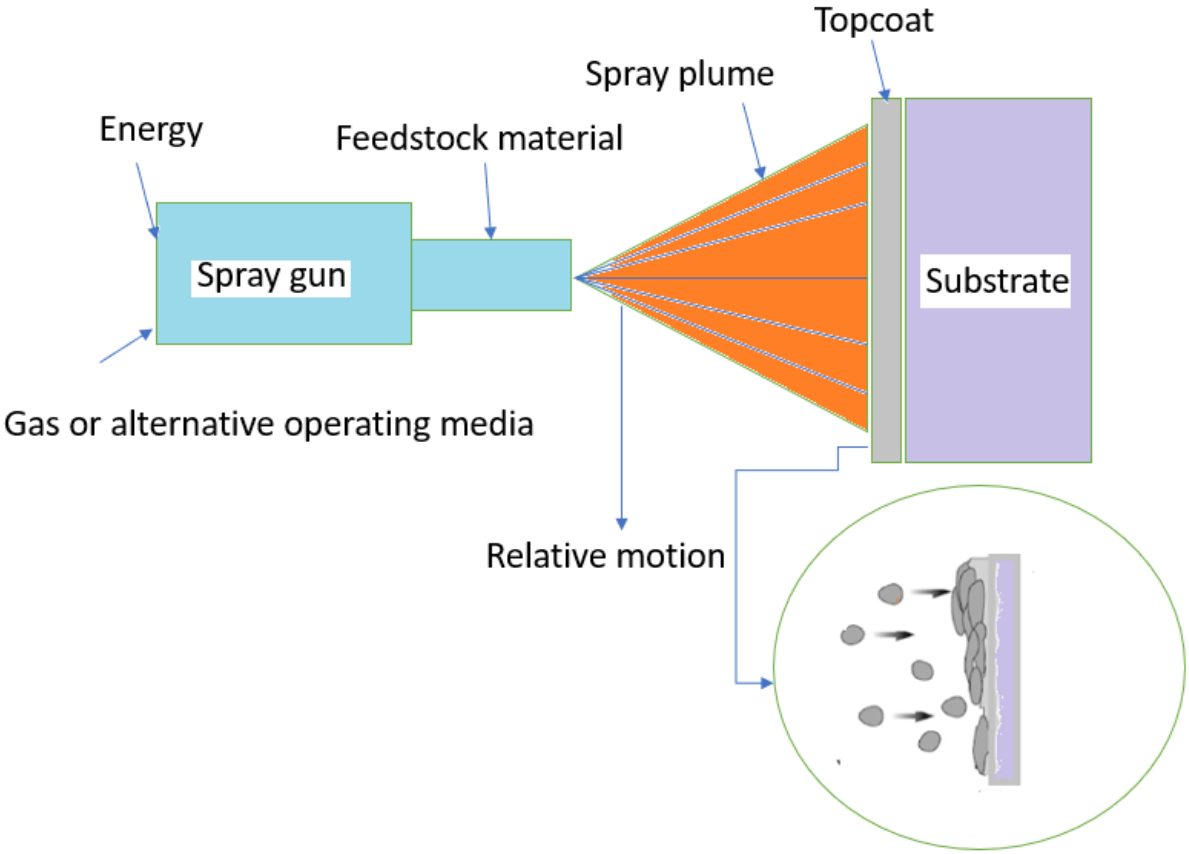


**Fig. 2.11.** Diagrammatic representation of the TS coating procedure

During the coating process, the surface of the substrate is not heated. The mobility of fluid and heat are two factors that determine the final shape of the splat that is produced when molten particles come into contact with a solid substrate. In the event of a hit, a splat may either fragment into smaller pieces or remain intact and crystallize into disc. TS technologies are applicable in a variety of different biomedical applications because of their inherent flexibility

and adaptability. These methods encompass the full range of applications, from maintenance to fixes to overhauls, and they vary according on the methodology that is utilised as well as the materials that are used for the coating and the substrate (Liu et al, 2020). The TS methods and coating materials for metallic implants that avoid corrosion and wear were the key focuses of this review's investigation. In TS, precursors are applied to the surface of the substrate in the form of a solution or a suspension in order to coat the substrate with the desired properties. The numerous varieties of thermal spray include flame, and plasma arc sprays. Coatings can be applied on biomedical implants utilising a wide number of methods, including as VPS, APS, Suspension PS, HVOF, and HVSFS (Maximov et al, 2021). The subsequent sections offer a description of the many TS coating modifications that are utilised in the deposition of coatings on biomedical implants.

## 2.7 HVSFS COATING TECHNIQUES

The HVSFS technology may produce coatings thick while maintaining their thinness. The HVOF coating technique has been expanded to create the HVSFS coating technique, It deposits a coating layer on surfaces using suspensions to achieve the desired composition (Maximov et al, 2021). This approach is also known as the "suspension coating technique." The following diagram is a schematic representation of the HVSFS, which highlights its core concept: **(Fig.2.12).**

## 2.8 PLASMA SPRAYING (PS) COATING TECHNIQUE

A powdered feedstock material for coating is mostly provided by the plasma jet in a radial direction, as seen in **Fig. 2.13.** The plasma jet then advances towards the substrate to apply the coating. The thickness of the coating is regulated by the velocity of the plasma jet and the concentration of the feeding material. The plasma jet may also be used to apply coatings on many substrates, including metals and ceramics.

In addition, the settings in which the (PS) approaches are utilized can be categorized in a variety of ways.

### *Atmospheric plasma spraying coating techniques*

The (APS) applications commonly make use of sintered ceramic feedstock powders with particle sizes ranging from 10 to 100 microns for the purpose of functioning as deposition particles. It is

necessary to make use of the processing methods that are most suited to the feedstock in order to have a prosperous coating production operation (Singh et al, 2020) .

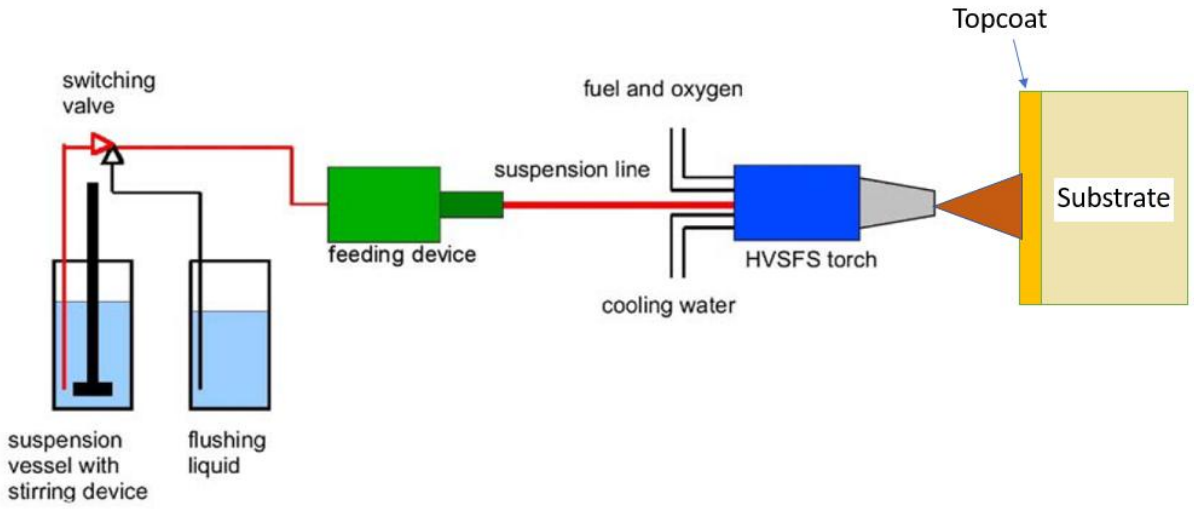


**Fig. 2.12.** A diagrammatic representation of the fundamental idea behind the HVSFS spraying technique.

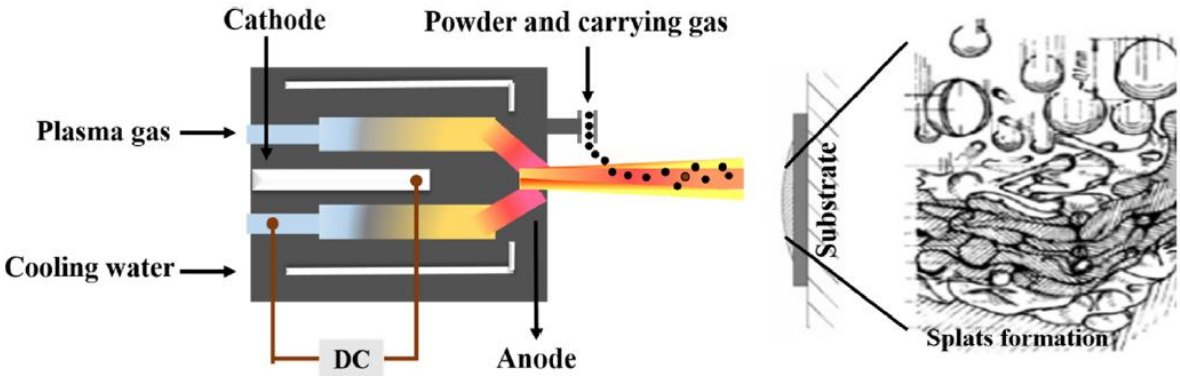


**Fig. 2.13.** Diagrammatic representation of the PS process (Rainer et al, 2010).

To accommodate a wide range of spraying requirements, there is a selection of spray gun configurations available, as well as a selection of power outputs for commonly used PS guns. APS coatings, on the other hand, have a high resistance to wear caused by sliding, adhesive, and abrasive forces (Hiemann et al, 2021).

With FDA clearance in hand, the APS method has emerged as the standard for manufacturing (HAp)-based coatings for metallic implants.

In contrast to the inert (VPS/LPPS) process, this method is carried out in an environment that is under strict control, but at a pressure that is slightly lower than that of the surrounding

atmosphere. The equipment necessary for this process is more expensive than the gear needed for spraying inert atmospheric agents.

The oxide layer on the substrate's surface must be removed via transferred arc etching before the coating can be deposited. To ensure appropriate completion of the coating process, the polarity is reversed (Kravanja et al, 2022). At high temperatures, the component and the coating material form a strong diffusion connection during the deposition process.

To achieve this, the coating substance and the component are heated to the same temperature (Yadav et al, 2020). This procedure is typically used to provide a coating to the turbine blades. The benefits of this method include, but are not limited to, improved bonding, elevated coating densities, improved of coating thickness still when applied to surfaces with irregular shapes, and exceptional deposition efficiency.

The tungsten electrode-equipped F4-VB spray gun was employed. The nozzle's outlet has a conical diverging portion. It is set up inside a vacuum chamber that has a pumping system that enables operation at pressures as low as 1 mbar, positioned on a fixed platform with a vertical translation axis unit. **Fig. 2.14** presents a schematic illustration of the configuration.

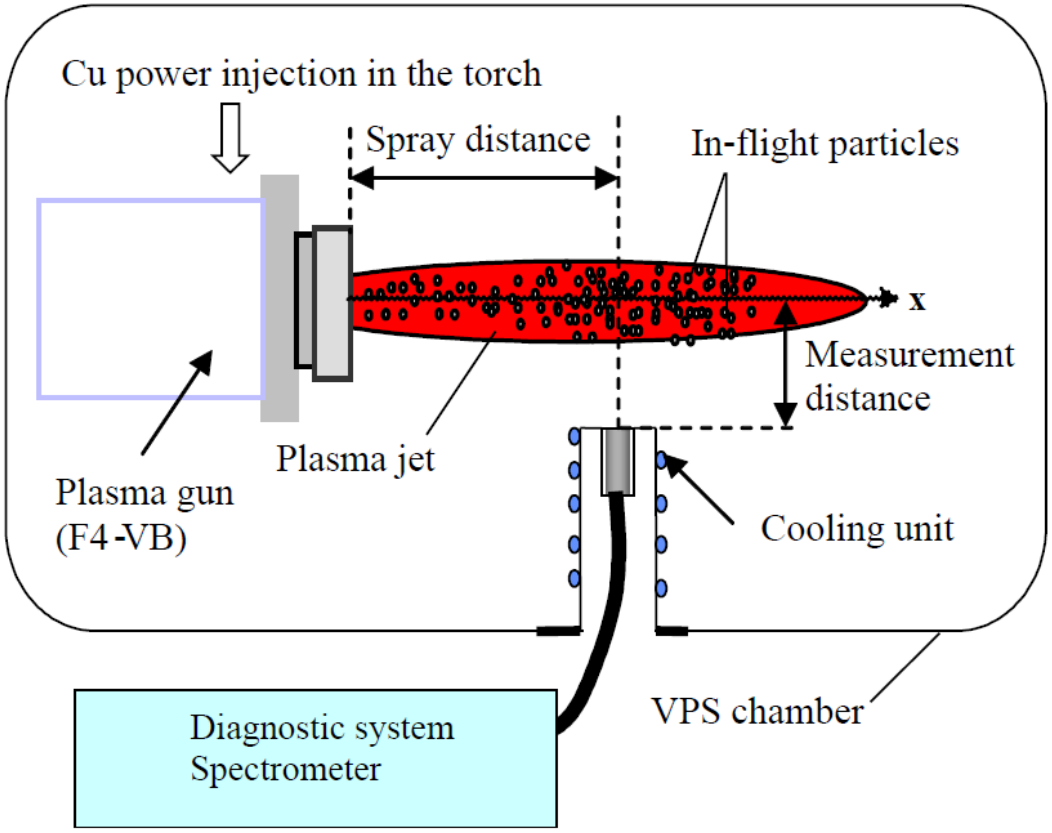


**Fig. 2.14.** The Configuration for (VPS or LPPS) process (Salhi et al, 2005).

In addition, when the pressure is low, the plasma's width and length become significant, and a high-velocity plasma jet can be created by employing convergent/divergent nozzles to direct the flow of the plasma.

The lack of oxygen and the capability to function under high temperatures allow for the production of coatings that have a low oxide content, are dense, and are sticky.

## 2.9 FLAME SPRAYING COATING TECHNIQUE

The flame spray method of coating deposition produces superior layer by employing a source of heat to combine the raw elements into a liquid state, which are commonly accessible in the forms of powder, wire, and rod. It is powered by a heat source that is produced as a result of a chemical interaction between the gases. It's a current of hot gas consisting of combustion by products is released at a high rate of speed from the spray torch, and this gas stream is the source of the heat. Compressed air is used to inject the spray material into the hot flame, where it melts before being propelled toward the surface of the substrate (Ratha et al, 2021). There are multiple thermal spray (TS) techniques that can be employed for the purpose of applying Hydroxyapatite (HAp) coatings onto metallic implants. Each of these techniques possesses distinct advantages and disadvantages. Upon completion of this phase, the spray substance is finalized. **Table 2.2** delineates the various thermal spray procedures available for the application of hydroxyapatite coatings on metallic implants.

**Table. 2.2**

The various thermal spray techniques used for applying hydroxyapatite coatings on metallic implants include distinct advantages and disadvantages.

| Technique | Layer thickness (t) | Benefits | Drawbacks | Reference |
|---|---|---|---|---|
| Plasma Spraying (PS) | <20µm | • Cost-effective as per economic point of view<br>• Smoother | • Poor adhesion between the HAp film and the metal surface.<br>• The density of the hydroxyapatite layer | (Grafts et al, 2004) |

| | | | | |
|---|---|---|---|---|
| | | surface<br>• anti-corrosive coating layer | may not be uniform. | |
| High-velocity suspension flame spraying | <50µm | • There is no requirement for any post treatment.<br>• Layer of coating that is inexpensive and consistent. | • A greater temperature is required. | ( Hameed et al, 2019) |
| Flame Spray (FS) | <250 µm | • The most cost-effective TS technique.<br>• Coating that is easily adjustable and porous. | • Post-treatment requirements.<br>• At lower temperatures, cracks may form. | (Rauch et al, 2009) |

## 2.10 TS-DEPOSITED HAP COATINGS OF VARYING PURITY AND REINFORCEMENT, AND THEIR RESPECTIVE PERFORMANCES

The phosphatic molecule known as HAp is quite widespread and occurs naturally all around the world. The chemical composition of HAp is extremely close to that of normal human bone, which is astonishing. On the other hand, there are concerns with the weak mechanical characteristics of HAp coatings, which restricts their clinical utility in orthopaedic applications.

These applications include knee replacements and hip replacements (Thompson et al, 2015). Extra brittleness, wear, and a lack of fracture toughness are all instances of such issues.

Table 2.3 illustrates how the addition of a variety of hard particles to HAp coatings affected the microhardness and tribological properties of the coatings in a variety of ways. In addition, it has been demonstrated in the research that the HAp's features can be improved by the incorporation of hard particles.

**Table. 2.3**

Evaluation of the performance of coatings reinforced with HAp.

| Method | Implanted metal | Feedstock material | Findings | Reference |
|---|---|---|---|---|
| • Flame Spray (FS) | Mild steel | HAp/polymer composite coating | • A greater young modulus, improved adhesion strength, acceptable dissolving behavior, and good fracture toughness are all properties of composite coating. | (Sun et al, 2002) |
| • Plasma Spraying (PS) | Ti6Al4V | HAp<br><br>HAp+CNT | • When compared to pure HAp coating, the wear resistance of HAp coating that has been supplemented by CNT is significantly higher.<br>• The use of CNT reinforcement increases both the biocompatibility | (Balani et al, 2007) |

| | | | | |
|---|---|---|---|---|
| | | | and the fracture toughness of the material.<br>• As a result of the CNT stretching and bridging, the reinforced covering experiences reduced loss in weight and volume, which contributes to the prevention of wear debris pinning. | |
| • Plasma Spraying | SUS 304SS | HAp<br><br>HAp+SiO2 | • Hard and dense coatings.<br>• The coating that is enhanced with SiO2 at a percentage of 30 percent by weight has the highest abrasion wear resistance.<br>• The inclusion of $SiO_2$ makes the adhesive more robust because it results in an increase in the coating bonding | (Morks et al, 2005) |

| | | | | |
|---|---|---|---|---|
| | | | strength at the interface. | |
| • Plasma Spraying | Ti6Al4V | Hap<br><br>HAp+10 wt% (80 Al2O3& 20 TiO2) | • The reinforcement causes the coating to become firm and devoid of cracks.<br>• The tensile strength of a structure sees an increase as a direct effect of reinforcement.<br>• When compared to pure HAp coating, the corrosion resistance offered by reinforced coatings is significantly higher. | (Singh et al, 2011) |
| • Plasma Spraying | SS 316L | HAp<br><br>HAp+YSZ (10, 20& 30 wt%) | • Hard and dense coatings.<br>• In addition, YSZ reinforcement promotes more cell adhesion and attachment during the process of cell growth tests.<br>• In terms of their ability to resist corrosion, | ( Yugeshwarab et al, 2012) |

| | | | | |
|---|---|---|---|---|
| | | | reinforced coatings perform better than pure HAp coatings in SBF. | |
| • High-velocity suspension flame spraying | Ti | HAp | • The stability of coatings made of water suspension is inferior than that of coatings made of di-ethylene glycol when placed in SBF solution.<br>• Diethylene Coatings made from glycol are more durable and crystallin than other types of coatings. | (Rath et al, 2012) |
| • Flame Spray | Ti | Zn-doped HAp coating | • The antibacterial and biocompatible properties of Zn-doped HAp coating have been significantly enhanced. | ( Yang et al, 2017) |
| • High-velocity suspension flame | SS 316L | HAp | • The reinforced coating possesses higher tensile | (Yao et al, 2018) |

| | | | | |
|---|---|---|---|---|
| spraying | | HAp+TiO2 | strength and wear resistance in contrast to a single layer of pure HAp coating. This is due to the coating's increased thickness. | |
| • Vacuum Plasma Spraying | SS 316L& Ti6Al4V | HAp<br>HAp+10 wt%Al2O3<br>HAp+10 wt%ZrO2 | • In terms of wear performance, as-sprayed coatings perform significantly better than heat-treated surfaces.<br>• The application of heat treatment, diffusion helps to reduce the number of pores and microcracks. | (Singh et al, 2018) |

## 2.11 REINFORCING HAP COATINGS WITH ZIRCONIA/YSZ

YSZ's high tensile strength makes this advancement possible. HAp coating mechanical, thermal and chemical properties were found to be enhanced by each of the four unique YSZ reinforcement compositions. This was shown in **(Fig. 2.15).**

In the research that was done, it was found that coatings reinforced with YSZ had improved mechanical properties. These findings were similar to what was found in the literature. to observe a rise in the bond strength between the second combination and the YSZ-reinforced coating as compared to the HAp coating by itself. The amount by which the bond strength

increased when YSZ reinforcement was included in pure HAp powder was comparable to or even greater. The use of YSZ as a reinforcing agent in pure HAp has a beneficial effect on the composite coating's mechanical properties (Safavi et al, 2021). They compared a pure HAp coating with a PS HAp/Ti6Al4V composite coating and a HAp/Ti6Al4V/YSZ composite coating. According to reports on PS YSZ reinforced HAp coatings, the incorporation of the second phase particle into composite coatings resulted in an improvement in the mechanical properties of the coatings when compared to bulk HAp alone.

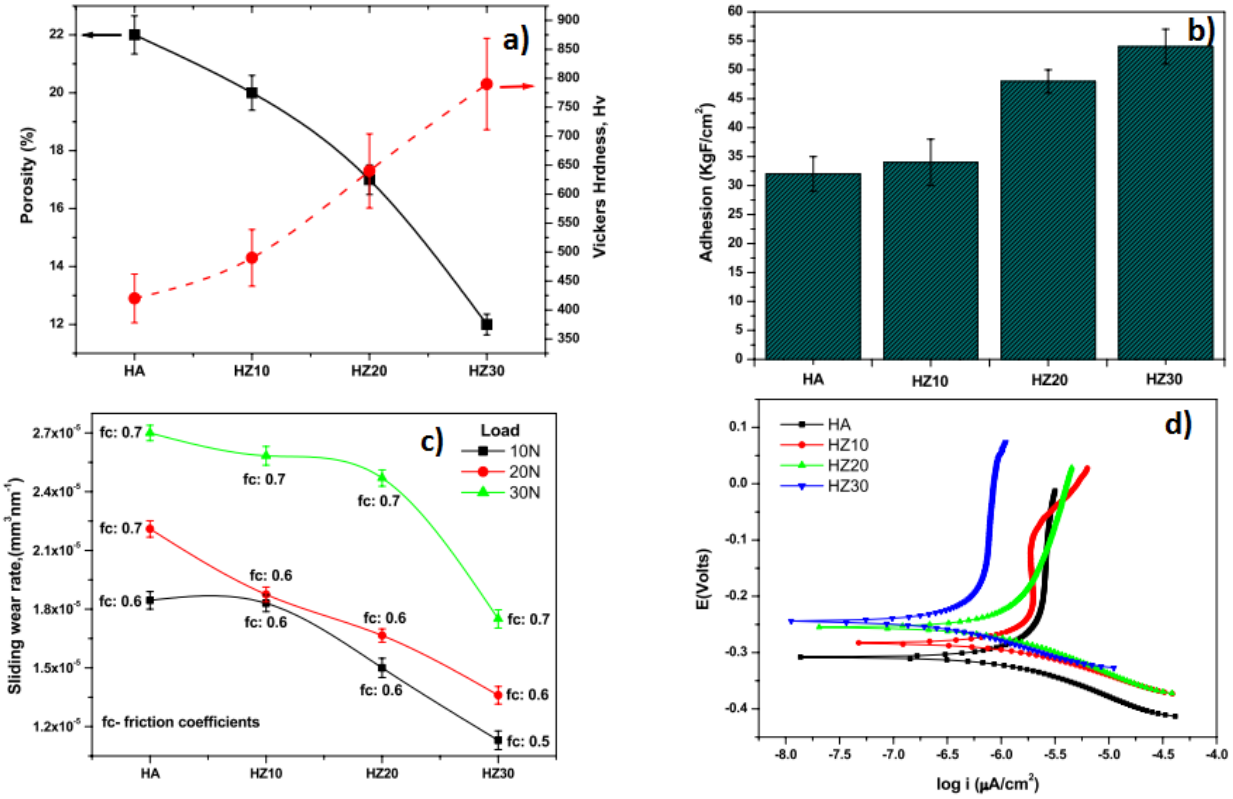


**Fig. 2.15.** The effect of adding four different compositions of YSZ on a) Coating properties can include microhardness and porosity, b) its ability of coatings to adhere to surfaces, c) the coefficients of wear and friction, and d) YSZ reinforced and pure HAp coatings' potentiodynamic polarisation curves were studied (Yugeshvaran et al, 2019).

## 2.12 THE REINFORCEMENT OFFERED BY CNTS IN HAP COATINGS

As seen in **(Figs. 2.16 and 2.17)**, the stretching and bridging of carbon nanotubes assist pin down wear debris, which results in a reduction in the weight and volume loss of the reinforced coating.

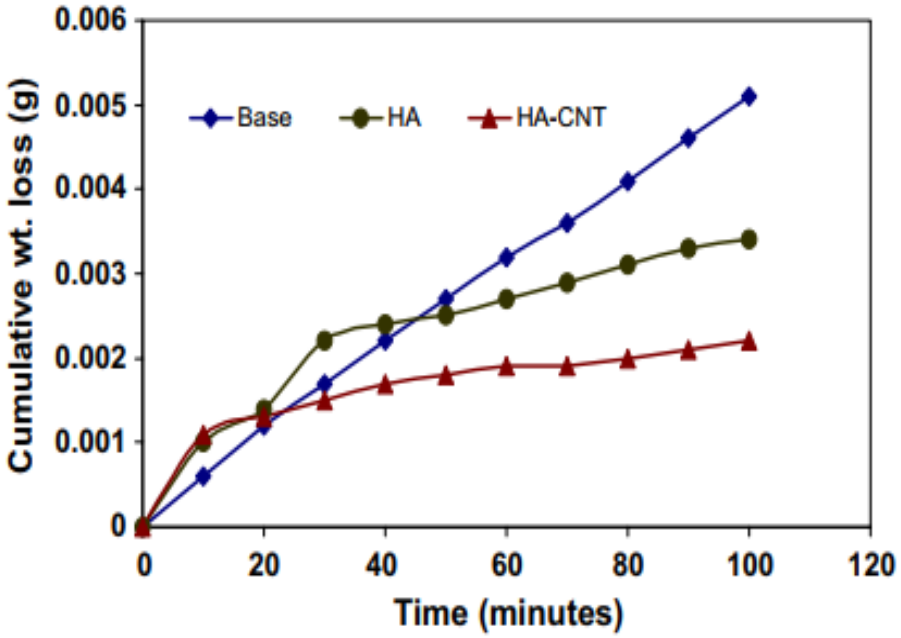


**Fig. 2.16.** The wear rates of the base metal, the HA-CNT composite coating, and the HA-P coated metal are all compared (Balani et al, 2007).

. This improvement in mechanical properties also leads to a better performance of the coating in terms of durability and corrosion resistance. Furthermore, the composite coating was found to be more stable compared to coatings without carbon nanotubes. The alumina-reinforced coatings increased fracture toughness by 158%, while CNTs with alumina increased it by 300%. Cell growth was examined across three coatings in SBF conditions. After one day in water, the cell growth rate of pure HAp was higher than that of $Al_2O_3$-CNTs enhanced hap coating ($23.75cm^2$/cell).

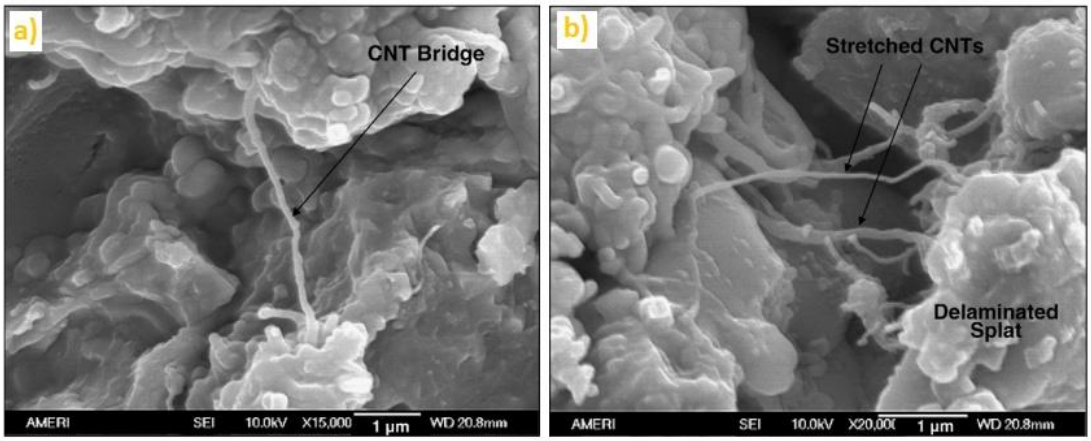


**Fig. 2.17.** SEM photos with high magnification displaying: a) Splats are bridged by CNTs, and b) Put on some stretched CNTs in order to secure the debris (Balani et al, 2007) .

The cell growth rate of $Al_2O_3$-CNTs enhanced hap coating increased to 34.25$cm^2$/cell after 2 days in SBF. The growth rate of the alumina-reinforced coatings increased even more to 54.25$cm^2$/cell. The CNTs with alumina coating showed the highest cell growth rate, reaching 70.00$cm^2$/cell after 3 days.

## 2.13 EFFECT OF SILICA REINFORCEMENT ON HAP COATINGS

In addition to this, it plays a part in the chemical process since the amount of silica present in bio-glasses, which is what determines their solubility in living organisms, is related to the bonding behaviour of these glasses to bone. Third, silica particles increase the HAp coating's tensile strength by a process called bonding mediated by particles, which either stops or deflects cracks (Sarifianjazi et al, 2020).. Both the micro-hardness and wear resistance of the improved coating with a weight percentage (Farhadian et al, 2020).

## 2.14 TITANIA'S FUNCTION IN HAP COATINGS AS A REINFORCING MATERIAL

The following picture illustrates how the incorporation of TiO2 reinforcement may alter coating qualities, including tensile strength and corrosion resistance **(Fig. 2.18).** The reinforcement further aids in minimizing fractures and porosity, hence enhancing mechanical qualities.

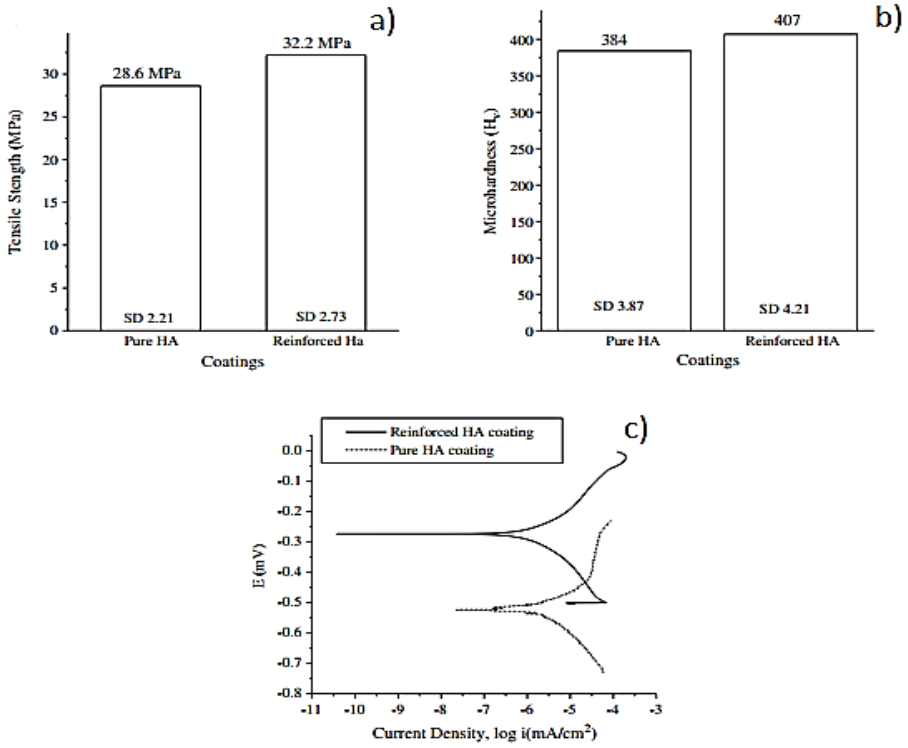


**Fig. 2.18.** Mechanical properties of pure and reinforced HAp coatings (Singh et al, 2011).

The enhancement of the mechanical characteristics of HAp by the incorporation of CS led to the formation of the HAp-CS composite material. In a distinct line of inquiry, several weight-to-composition ratios of the HAp-CS composite were established. The research authors discovered that increasing the concentration of CS in HAp resulted in an enhanced rate of mesenchymal stem cell proliferation in the bone marrow (Dulski et al, 2021). It has been reported that the HAp reinforced CS (10 & 20 wt%) coatings that were applied to Ti alloy by the PS method have increased in their ability to resist corrosion. In order to evaluate the resistance of the PS coated samples to corrosion, electrochemical tests were carried out in an SBF solution. **(Fig. 2.19)** depicts the potentiodynamic polarisation curves of pure HAp PS coatings as well as HAp-CS composite coatings in their respective graphical forms. The CS coating on HAp is clearly superior exhibits a high level of corrosion resistance.

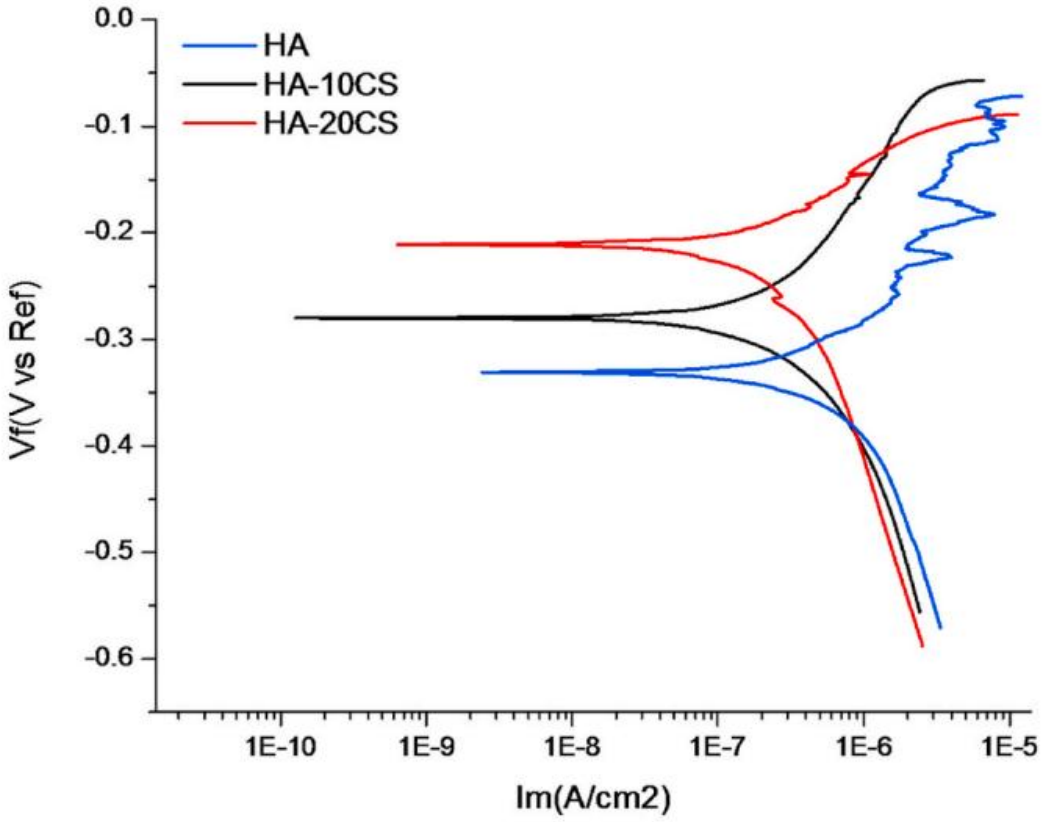


**Fig. 2.19.** Curves of potentiodynamic polarization.

The reinforcement level is higher, and it continues to develop as the weight percent of reinforcement in CS in HAp increases. It is possible that the substantial fraction of crystalline HAp phase that is present in those coatings is responsible for the improved corrosion resistance

of the HAp-CS coatings that was demonstrated in **(Fig. 2.20).** The pure HAp coating, the HAp-10 CS coating, and the HAp-20 CS PS coating each have a crystallinity that is 76.77%, 77.36%, and 79.82%, respectively.

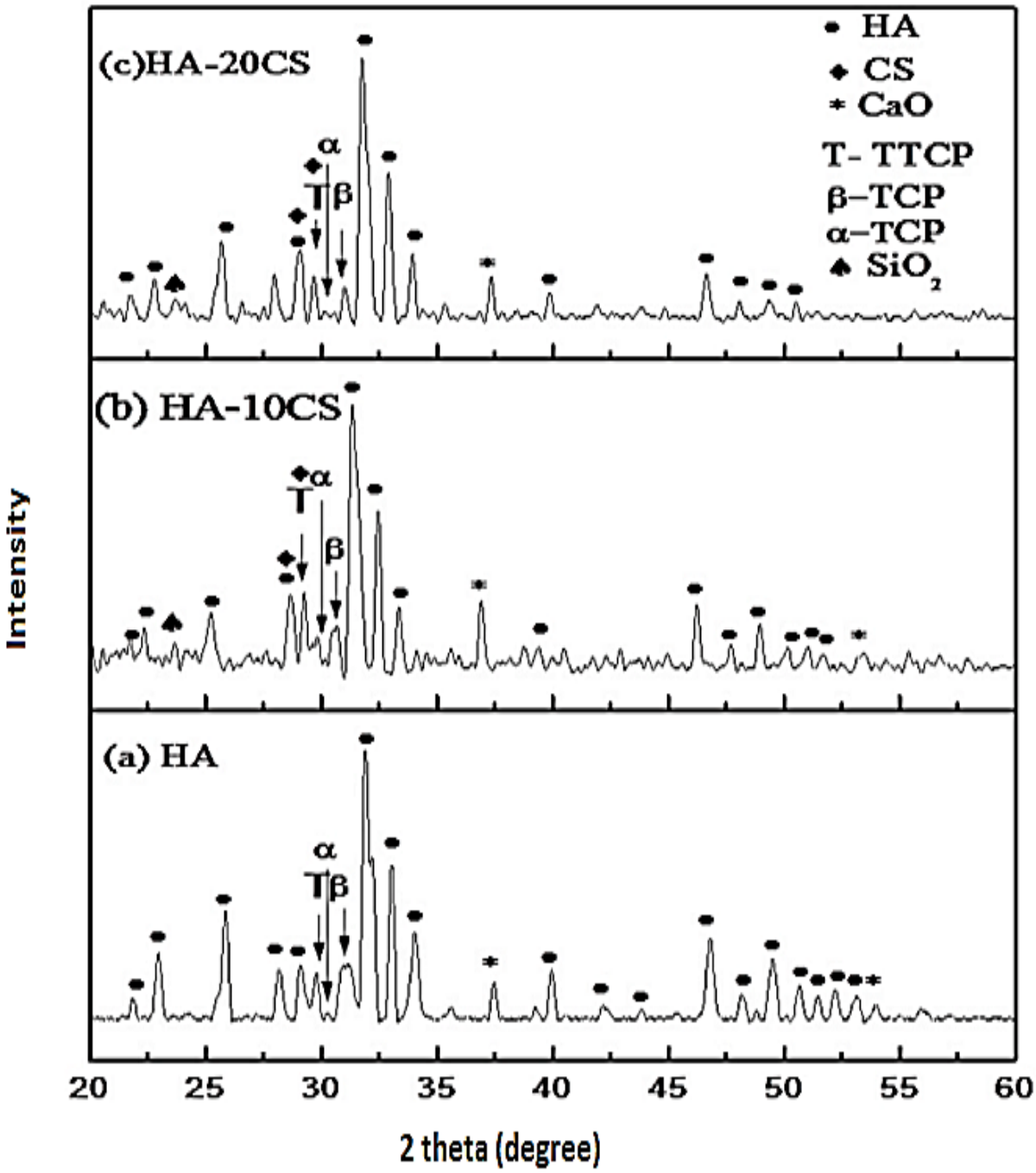


**Fig. 2.20.** Coatings' deposited XRD patterns (Singh et al, 2021).

## 2.15 MAGNESIUM (Mg) REINFORCEMENT IN THE HAP COATINGS

Double layer coatings of HAp and HAp-Mg produce potentiodynamic polarisation curves **(Fig. 2.21).** Because of the intermediate dense HAp layer, the (HAp-10wt.%Mg) has the best corrosion resistance.

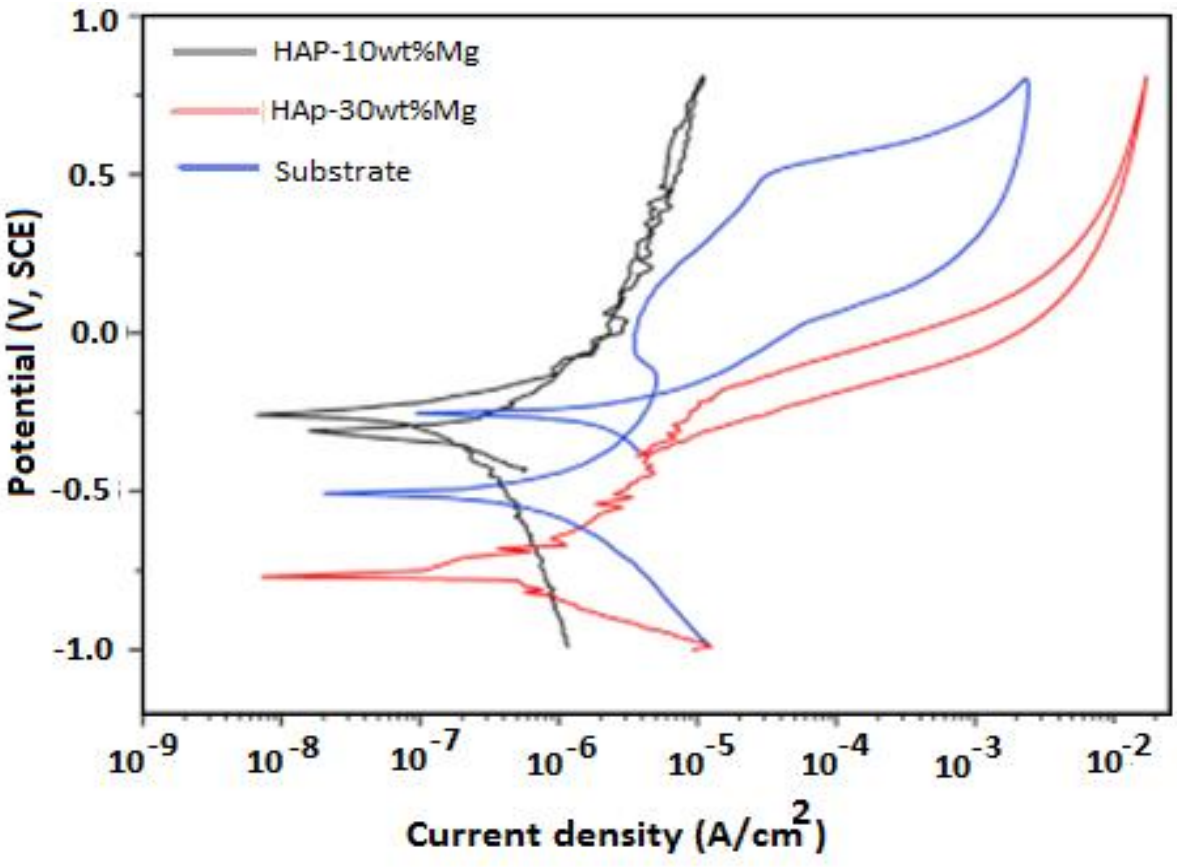


**Fig. 2.21.** Curves of potentiodynamic polarization (Rezaei et al, 2020).

It is vital to have knowledge of both the mechanical and microstructural properties of the material in order to develop Biomedical implant coatings made from hydroxyapatite. Using HT is a promising and effective for increasing material performance (Bartkowaik et al, 2020).

The microhardness of the HAp coating that is going to be placed on the host body is going to be an essential component. The ratio of calcium to phosphorus, often known as the phase ratio, is what determines hardness.

The hardness of the coatings will decrease as the percentage of amorphous phase in the layers increases. As a result of the high temperature that is required for thermal spraying, amorphous phases tend to form in as-sprayed coatings.

As a consequence of this, HT has the potential to be utilised in order to cut down on the amount of amorphous phase that is present in layers after spraying (Prashar et al, 2022). HT coating XRD patterns show that as-sprayed HAp coatings transform from amorphous to crystalline during the procedure **(Fig. 2.22).** HT involves the amorphous phase transforms into the crystalline phase, as is often believed. Based on the findings, it has been shown that the majority of the amorphous phase is composed of dehydroxylated calcium phosphate.

Crystallization of hydroxyl-rich amorphous phases is induced by HT, and this is then afterwards hydroxyl ion diffusion will occur. As a consequence of this, the coatings generated HAp, which resulted in an even greater improvement to the crystalline phase of the layers.

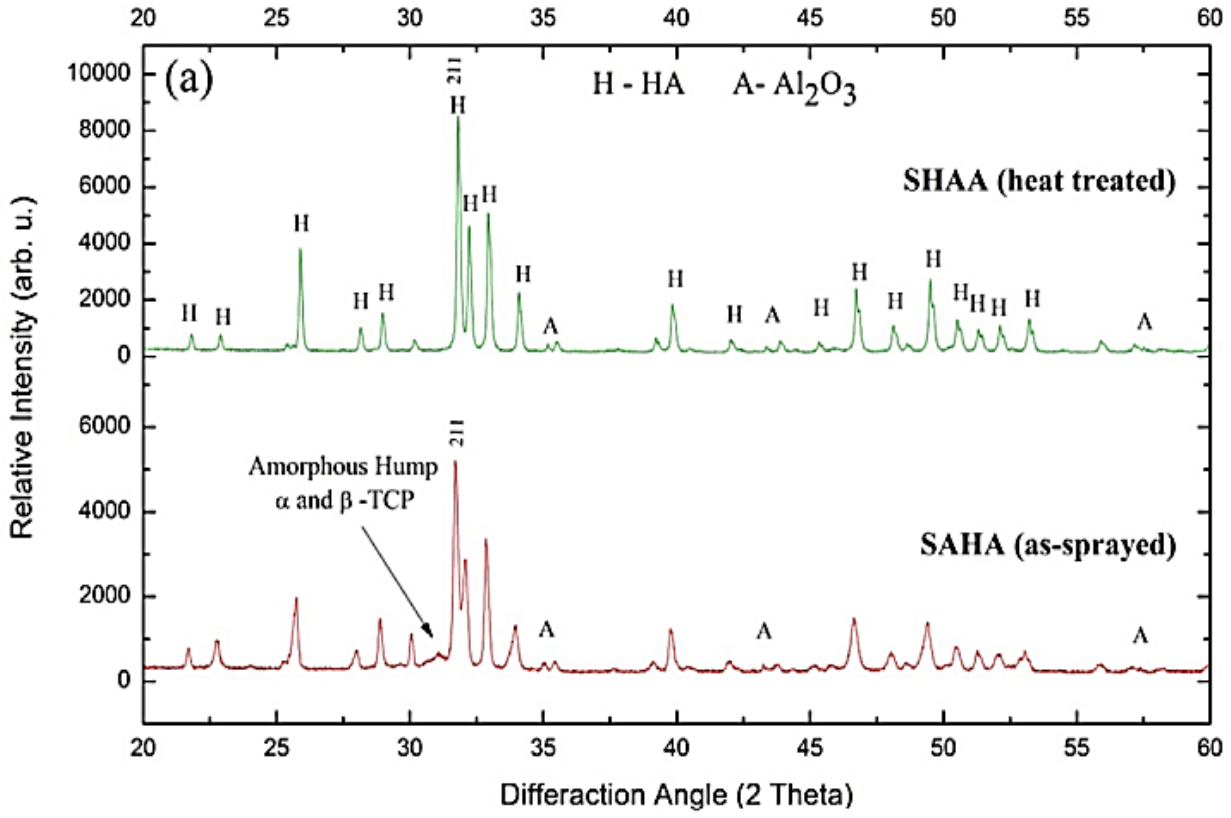


**Fig. 2.22** Coatings that are both HT and as-sprayed XRD patterns (Singh et al, 2018).

The microhardness of a selection of common pure, coatings that are reinforced, as-sprayed, or HT summarized in **Table 2.4,** which may be found here.

**Table. 2.4**

Before and after heat treatment, a comparison of the hardness levels of regularly used HAp coatings.

| Feedstock material | HT Conditions | Coating technique | Micro-hardness before HT(Hv) | Micro-hardness after HT(Hv) | Increase in crystallinity after HT (%) |
|---|---|---|---|---|---|
| • HAp<br>• HAp+10 wt% (80 $Al_2O_3$& 20 | HT Temperature-700ºC Two hours' worth of time has passed (Singh et al, 2011). | PS | • 486<br>• 598 | • 507<br>• 618 | |
| • HAp | HT Temperature-800ºC Two hours' worth of time has passed (Rocha et al, 2021) | LVOF | • 299 | • 367.2±4.8 | • 95 |
| • HAp | Maximum Operating | APS | • 276±91.2 | • 316.3±41.4 | • 93.8 |

| | | | | | |
|---|---|---|---|---|---|
| | Temperature: 700°C Timeframe of 1 hour (Singh et al, 2021) | | | | |
| • HAp+$TiO_2$ | Maximum Operating Temperature: 700°C Timeframe of 1 hour (Unune et al, 2019) | PS | • 534 | • 874±26 | • 76 |
| • HAp<br>• HAp+10 wt% (80 $Al_2O_3$& 20 | Maximum Operating Temperature: 800°C Timeframe of 2 hours (Sthish et al, 2022). | PS | • 458<br>• 496 | • 645<br>• 643 | • 82 |

**Singh et al., 2020** For orthopedic purposes, this study used the plasma spray deposition method. Researchers looked examined how adding $TiO_2$ reinforcement affected the material's microstructure, mechanical qualities, and bioactivity. The produced coatings were studied for their shape, coating thickness, elemental makeup, and phase composition. The biomimetic HA-$TiO_2$ surface, which aided apatite development and osseointegration, has holes with sizes ranging

from 200 nm to 600 nm. The β-TCP, CaO, TTCP, and TiO2 phases in the deposited layer are verified by the EDS spectra, mapping, and XRD investigation.

**Singh et al. 2023** used the hybrid microwave heating (MH) technology to change the surface layer of stainless steel (SS-316L) with the goal of increasing its bioactivity by strengthening it with hydroxyapatite (HAp) powder. Following their modification, the substrates were heated to temperatures of 400 ◦C and 700 ◦C for a duration of 1 hour. The microhardness value of the heat-treated substrates was greater than that of the as-deposited substrates because the modified layer was densified following heat-treatment. Following the application of heat, the surface's porosity, faults, and defects were reduced.

## 2.16 ADDITION OF VARIOUS ADDITIVES IN NANO FORM INTO HYDROXAPATITE

Hydroxyapatite (HAP) coatings are widely employed in biomedical implants due to their chemical similarity to bone mineral and excellent biocompatibility. However, pure HAP coatings suffer from low mechanical strength and limited corrosion resistance in physiological environments. To overcome these limitations, researchers have incorporated various nanomaterials such as nano-$Al_2O_3$, nano-$TiO_2$, and nano-Mg into HAP coatings to enhance both corrosion resistance and bioactivity. The incorporation of nano-$Al_2O_3$ into HAP has shown promising improvements in mechanical and electrochemical stability. Nano-$Al_2O_3$ particles fill microvoids and pores in the HAP matrix, thereby reducing permeability to corrosive fluids and enhancing the barrier properties of the coating. Moreover, this composite demonstrates better adhesion strength and hardness, which contribute to improved resistance against crack formation and propagation under mechanical and electrochemical stress (Gopi et al., 2015). The bioactivity of HAP+nano-$Al_2O_3$ coatings is also favorable, as the composite maintains the osteoconductive nature of HAP while improving surface roughness and wettability—key parameters for cell attachment and proliferation.

Similarly, nano-$TiO_2$-reinforced HAP coatings have been extensively investigated for their excellent corrosion resistance and enhanced cellular response. Nano-$TiO_2$ contributes to forming a compact and stable oxide film, which mitigates the diffusion of corrosive ions to the substrate. The incorporation of nano-$TiO_2$ improves not only the corrosion resistance but also the

photochemical stability and bioactivity of the coating. The anatase form of $TiO_2$ is known to support apatite nucleation in simulated body fluid (SBF), which fosters rapid osseointegration. Additionally, HAP+nano-$TiO_2$ coatings demonstrate antibacterial properties, which are crucial for preventing post-surgical infections (Feng et al., 2017). The enhanced corrosion resistance is attributed to the formation of a denser and less porous microstructure, which impedes electrolyte infiltration and delays the onset of localized corrosion.

The addition of nano-Mg into HAP coatings presents a unique combination of bioactivity enhancement and controlled biodegradability. Magnesium ions play a crucial role in bone metabolism and have been shown to promote osteoblast differentiation and angiogenesis. HAP+nano-Mg composite coatings exhibit superior bioactivity, evidenced by accelerated apatite formation in SBF, which is indicative of strong osteoinductive potential (Sun et al., 2021). From a corrosion standpoint, the presence of nano-Mg alters the electrochemical behavior of the coating by generating a more protective passive layer and buffering the acidic products resulting from corrosion. This leads to improved stability in physiological environments, although the degradation rate must be carefully optimized to avoid premature implant failure. The synergistic effect of Mg and HAP not only enhances bone bonding but also supports cell viability and proliferation due to favorable ionic interactions at the implant surface. The incorporation of nanomaterials such as $Al_2O_3$, $TiO_2$, and Mg into HAP coatings substantially improves their corrosion resistance and bioactivity. These composite coatings represent a significant advancement in surface engineering for load-bearing and long-term biomedical implants, offering a balanced combination of mechanical integrity, corrosion protection, and biological functionality.

## 2.17 RESEARCH GAP

The following conclusions have been made after doing an exhaustive review on the biomedical implants developed using different surface modification techniques:

1. The potential of LVOF sprayed coatings for the deposition of the pure HA and HA reinforced with alumina in various forms on metallic bio-implant has not been investigated till now.

2. A detailed analysis of the structure–property correlation of bio-implant coatings is needed, particularly to address challenges such as phase decomposition caused by the high temperatures involved in the coating process.
3. The effect of incorporating additives in various forms—such as micron-sized, nano-sized, and bi-modal particles—needs to be thoroughly analyzed to understand their influence on the corrosion resistance and bioactivity performance of biomedical coatings. A comparative evaluation of these additive forms can provide critical insights into optimizing coating formulations for enhanced mechanical stability, long-term durability, and improved biological responses in physiological environments.
4. On the other hand, the potential of bimodal composite coating for the deposition of the pure HA and reinforced HA (HA+10wt% micron $Al_2O_3$ and HA+10wt% nano $Al_2O_3$) coatings on metallic bio-implant has not been investigated till now using thermal spraying technology. ***[ From advanced coatings technology point of view]***

## 2.18 RESEARCH OBJECTIVES

1. To develop micrometric, nanometric and bimodal coatings such as (HA+10wt% micro-$Al_2O_3$), (HA+10wt% nano- $Al_2O_3$), (HA+5wt%micro-$Al_2O_3$+5wt% nano-$Al_2O_3$), on UNS S31254 stainless steel (254SS) using LVOF spray technique.
2. The post-treatment of developed coatings (micro, nano and bimodal) with annealing at 700°C for 2 hrs.
3. To investigate the LVOF spraying process using a detailed study of the microstructure, and mechanical properties of the developed coatings.
4. To characterize the as-deposited as well as heat-treated coatings in terms of their metallurgical and mechanical characterizations using various techniques to establish the structure property-correlation of the LVOF sprayed biomedical coatings.
5. Assessment of electrochemical corrosion behaviour of the LVOF sprayed biomedical coated specimens using a Potentiostat in Hank's balanced salt solution

## 2.19 SUMMARY

A detailed discussion on the implant corrosion has been presented. The capabilities of different existing coating techniques based on the requirements was elaborated and the limitations of such techniques have also been discussed. The use of thermal spraying has several

benefits in the field of surface engineering. An important advantage is the decreased manufacturing cost and shorter processing duration in comparison to other coating methods. Experts provide comprehensive reports on the use of thermal spraying in the treatment of metals. It has been investigated there is a lack of literature on the application of LVOF sprayed coatings in biomedical filed. It was observed that many major limitations of existing coating processes can be overcome by using LVOF sprayed coatings. The gaps observed in the literature indicate that the potential of LVOF sprayed coatings for the deposition of the pure HA and reinforced HA coatings on metallic bio-implant has not been investigated till now.

# CHAPTER 3

# EXPERIMENTAL EQUIPMENTS AND METHODOLOGY

The method of surface modifications, as well as the process parameters of the apparatus employed to modify the surface layer of SS-31254 with HA and HA+10wt%$Al_2O_3$ coatings are described in this chapter. The procedure for performing the different heat treatment of the as-deposited surface modified specimens has been discussed. The instruments/tools utilized to characterize uncoated and coated samples at different stages of the research effort have been detailed. Microstructures were characterised with scanning electron microscopy/energy dispersive X-ray spectroscopy. X-ray diffraction apparatus was used for the samples to characterize the products formed on the surface during studies. The various characterization techniques used to evaluate the performance of the coatings for the analysis of in-vitro and corrosion products formed during various tests have also been explained in this chapter. The overall process flow of this work is presented in **Fig 3.1.**

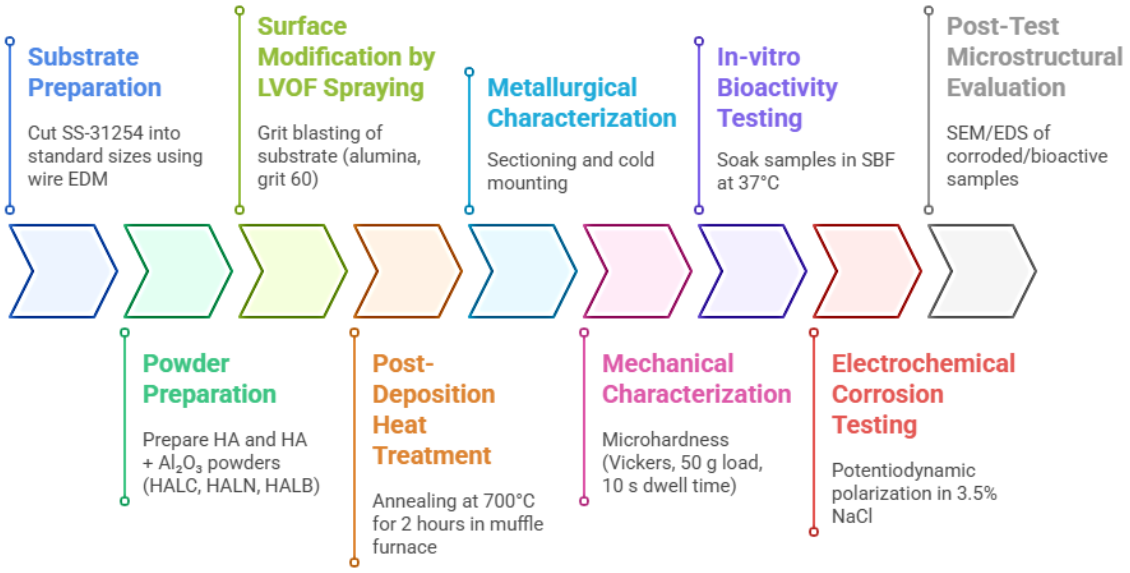


**Fig.3.1.** Process flow of the current research work.

## 3.1 SUBSTRATE PREPARATION

In this study, a substrate material was used to change the surface layer of a surgical grade stainless steel (254SS) that was purchased from Amigo Impex in Mumbai, India. Results from

the spark emission spectrometer analysis of 254SS show the following chemical compositions (wt%): 17.71Ni, 19.39Cr, 6.24Mo, 0.207N, 0.52Si, 0.018C, 0.004S, 0.017P, bal Fe.

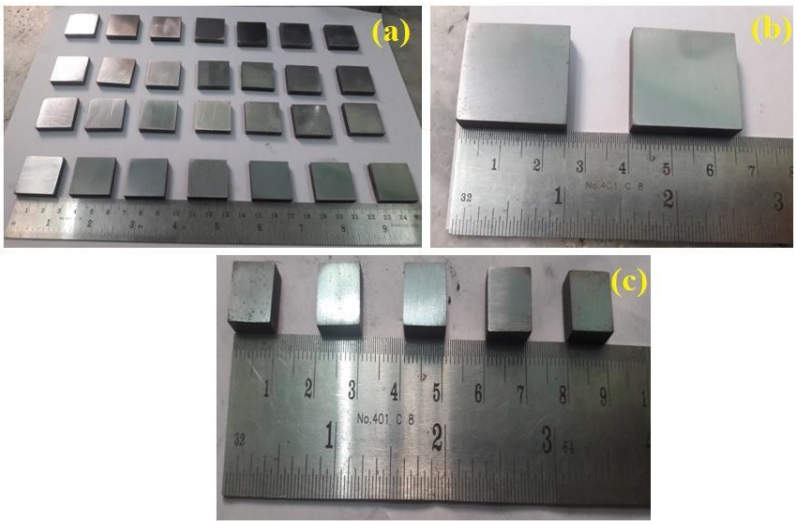


**Fig. 3.2** Specimens for various sizes for (a) XRD and SEM analysis, (b) corrosion study, and (c) invitro bioactive study.

For the surface modifications of the SS-31254, there is a requirement of specimens having various sizes like 20×20×3 $mm^3$ for XRD and SEM analysis, 25×25×3 $mm^3$ for corrosion investigations, and 10×15×3 $mm^3$ for in-vitro biocompatible study.

The specimens of required dimensions were cut through by utilizing a wire electric discharge machining apparatus as illustrated in **Fig. 3.2** from the SS-254 sheet having dimensions approximately 180 × 200 $mm^2$ with 3 mm thickness. Then the smoothing of the cut specimens was done by using an emery paper of different grades like 200, 400, 600, 800, 1000, 2000 etc.

### 3.2. POWDER DETAILS

Three distinct powder combinations containing HA and aluminium oxide ($Al_2O_3$)) were fabricated on SS-31254 substrate with LVOF thermal spraying technique. The first combination is pure HA, then 10 wt% of $Al_2O_3$ as blended with HA in the second combination, which is termed as HALC, where 10wt,% nano-$Al_2O_3$ is added is termed as HALN. The combination of 5wt.% micron-sized and T5wt.% nano-sized $Al_2O_3$ is termed as HALB. The 10% weight proportions of the hard particles are considered as optimum proportions of the reinforcement in

the HA powder. The powder was weighted initially to mix in a defined proportion and then mixed in a container for 6 hours for uniform mixing.

The selection of this 10 wt% combination is based on previous study findings by Li et al. 2002 and Morks et al. 2008, which indicate that increasing the reinforcement content in HA coatings beyond 10 wt% adversely affects certain mechanical characteristics. In addition, Chang et al. 1997, conducted a study on the impact of adding $ZrO_2$-8mol % yttria as a secondary component in plasma sprayed HA coatings with varying weight percentages. They discovered that introducing 10 wt% $ZrO_2$ in HA resulted in a substantial enhancement in bond strength.

The work was divided into three phases, where the coatings were developed in the first phase followed by post-treatment of claddings. In the second phase, the powders, coatings and post-treated coatings were characterized for micro-structural and mechanical analysis.

In the last phase of the work, the developed coatings and post-treated coatings were subjected to bio-activity and corrosion analysis followed by micro-structural characterization and phase-identification using XRD analysis.

### 3.3 SURFACE MODIFICATION THROUGH LVOF SPRAYING

The LVOF spraying was utilized in this work for surface modification of the SS-31254 through pure HA and HA10AL. The following coatings were developed in the current investigation as mentioned in **Table 3.1.**

**Table 3.1** Powders used in the current investigation

| **S.No** | **POWDERS** | **DESIGNATION SYSTEM** | **Powder (Average particle size)** |
|---|---|---|---|
| 1 | Hap | HA | 30-40 microns |
| 2 | Hap + 10% micron-sized alumina | HALC | 30-40 microns |
| 3 | Hap + 10% nano-sized alumina | HALN | 30-40 microns- Hap<br>Alumina- 200nm |
| 4 | Hap + 5% micron-sized+ alumina+5% nano-sized alumina | HALB | 30-40 microns- Hap<br>Alumina- 200nm |

Test samples were cleaned, degreased, and shot. Before LVOF Spraying, the specimens were grit blasted with alumina (Grit 60) to improve substrate-coating adherence. The coating was done by Metallizing Equipment Co. Pvt. Ltd. Jodhpur, Rajasthan 342005. Schematic representation of LVOF spray set-up is shown in **Fig.3.3.**

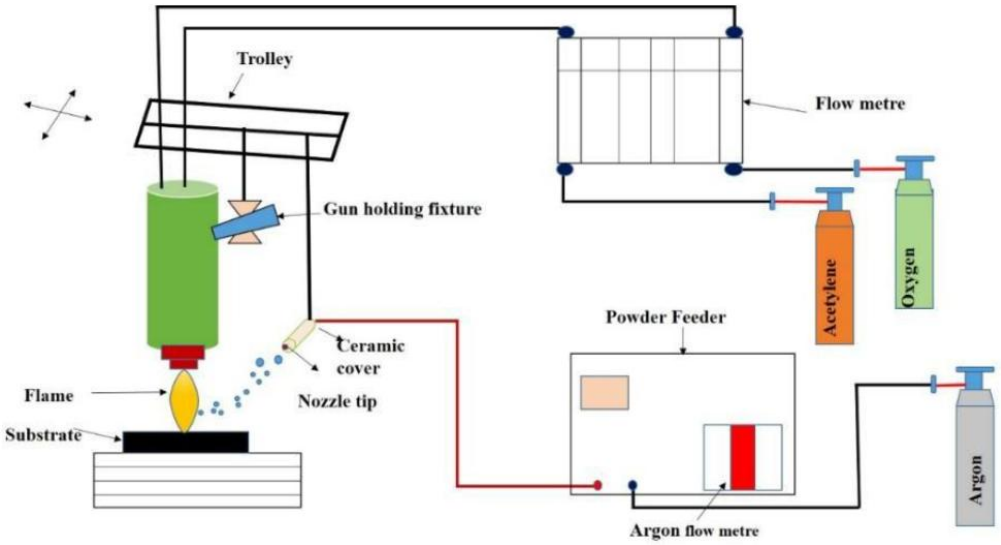


**Fig. 3.3** Schematic representation of LVOF spray set-up.

## 3.4 HEAT-TREATMENT OF COATINGS

Large-scale breakdown of the phases within the body leads to a loss of structural integrity, mechanical strength, and adhesion strength. Concrete annealing, a sort of heat treatment, has been backed as an effective way to improve coatings performance by a number of studies (He et al., 2001). Therefore, the surface modified samples at all conditions were exposed to post heat-treatment in a muffle furnace for 2 hours (heating rate 20°C/min) at 700°C to study how heat treatment affects the changed layer's microstructure, mechanical properties, and bioactivity.

## 3.5 METALLURGICAL CHARACTERIZATIONS OF THE COATINGS

Low speed diamond saw sections were used to cut through the thickness of the coatings, and the specimens were then cold mounted in epoxy to compare the differences between the as-deposited and heat-treated conditions. Cold mounting or embedding is the process of combining a resin with a hardener (or accelerator) to create the mounting compound, followed by the

polymerization process to form the block. The specimen which are sensitive to heat as well as pressure are generally prefer cold mounting. Emery sheets of varying grits were used to smooth and shine the cold-mounted specimens. **Fig. 3.4** displays optical images of the cold mounted polished samples.

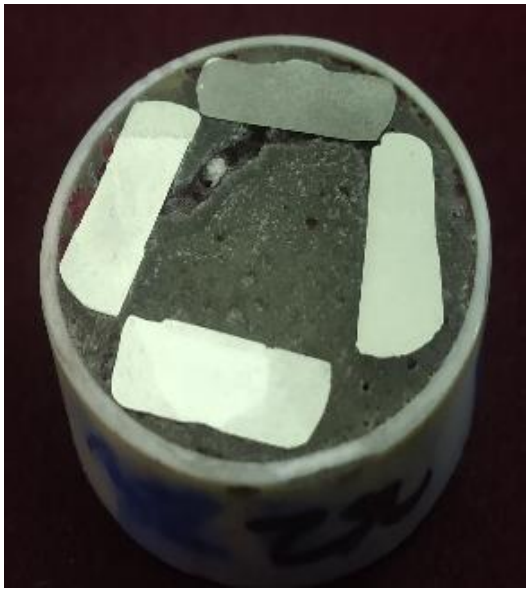

**Fig. 3.4** Sample after Cold Mounting and Polishing

The following section briefly explains the procedures and equipment used in the metallurgical characterization of coated and heat-treated specimens.

### 3.5.1 X-RAY DIFFRACTION (XRD) ANALYSIS

The XRD were used to determine the various phases present in both the coatings powder and the coatings under as-deposited and different heat treatment scenarios. Analysis of the phases generated on the surface of the coatings and heat-treated specimens, as well as the feedstock power, was performed using the XRD patterns acquired by the XRD machine. The X-ray diffraction (XRD) measurements were taken using a Bruker AXS diffractometer with 1°/min and a step range (2θ range) of 20°-80°. Cu-Kα radiation at 40 mA and 40 kV was used to perform the XRD. Appendix A provides information about the X-ray diffraction (XRD) facility that was used for the present research work (Fig. A-1).

### 3.5.2 MICROSTRUCTURAL CHARACTERIZATIONS OF COATINGS

The microstructural features in the surface modified samples such as grain boundaries, and grain size were revealed by analysing images taken on the optical microscope. The composition of the typical Kroll's reagent used in the present study is illustrated in **Table 3.2.**

**Table 3.2** Kroll's reagent etchant composition.

| Composition | In mL |
|---|---|
| Distilled water | 92 |
| $HNO_3$ | 6 |
| HF | 2 |

### 3.5.3 MICROSTRUCTURAL CHARACTERIZATIONS OF THE MICROWAVE INDUCED COATINGS SPECIMENS AT VARIOUS HEAT-TREATED CONDITIONS

Morphologies of both as-deposited and heat-treated specimens were examined with a 15kV field emission scanning electron microscopy (FE-SEM). All specimens were initially silver pasted between the samples and stub for having conductivity thereafter, gold coated for obtaining elemental-maps for the top of the surface (as-deposited and heat-treated) and across the cross-section of the coatings. The energy dispersive spectroscopy (EDS) analysis provides the elemental compositions (weight %) at the selected region. Samples were prepared as per procedure given in section 3.4 for the cross-section analysis of the samples before and after the testing. The SEM micrographs at different magnifications were taken along with the point and line scans.

### 3.5.4 MEASUREMENT OF COATINGS THICKNESS

During the deposition of coatings, the thickness was measured with a thickness gauge designed for thin films (Version: Minitest 2000; Manufacturer: Elektro-Physik Koln Company, Germany) with a precision of ±1μm. The thickness measurements were further confirmed by mounting and sectioning the deposited coatings according to the process outlined in section 3.5. The SEM/EDAX techniques was used for obtaining the cross-sectional back scattered electron (BSE) images by which the approximate thickness of the modify layer can be determined. Appendix-A contains a detailed description of the SEM apparatus (Fig. A-3). The average thickness of the deposited coating was calculated and observed using BSE images and same is presented in detailed in chapter 4 of the present research work.

### 3.5.5 POROSITY MEASUREMENT FOR THE COATINGS

The as-deposited and heat-treated surface modified samples were polished prior to the measurement of porosity. The both samples were polished down to emery papers of 1200 grit size for porosity measurement. This involved the measurement of porosity on Dewinter inverted optical microscope (Model: LT-2B, make: Chennai Metco Pvt. Ltd, Chennai, India) using STM B276 imaging software (Dewinter Material Plus, Version 4.2). The detail of the Dewinter inverted optical microscope is presented in Appendix A (Fig. A-2). Ten values of porosity were taken and their averages have been reported. The porosity values of the deposited coatings in both conditions (as-deposited and heat-treated) for all the samples are the average of the ten measurements and are given in Chapter 4 of the current research study.

## 3.6 MECHANICAL CHARACTERIZATIONS OF THE COATED SPECIMENS AT VARIOUS HEAT-TREATED CONDITIONS

The evaluation of mechanical properties was carried out in terms of microhardness. Details are explained in the following subsections.

### 3.6.1 MEASUREMENT OF MICRO-HARDNESS

The micro-hardness of the both (as-deposited and heat-treated surface modified specimens) samples were obtained by utilizing a Vickers‘s micro-hardness tester at 50 g load with load with a dwell period of 10 s. The detail of Vickers‘s micro-hardness tester used in the present investigation is presented in Appendix A (Fig. A-4). Micro-hardness was measured in layers of both as-deposited and heat-treated clad specimens. Ten indentations were made over the coating's cross-section at two separate points; five indentations were made along the layer thickness at each point (primary matrix as well as other secondary phases). Finally, their average values are reported and the distribution of micro-hardness values for clad specimens at various conditions is presented in chapter 4 of the current study.

## 3.7 FUNCTIONAL CHARACTERIZATIONS OF THE SPECIMENS

The functional evaluation is what ultimately establishes the sample's functional performance after being processed. Accordingly, aspects of specimens were evaluated using in-

vitro biocompatibility study and corrosion testing. The procedure and details of functional characterizations of the specimens are explained in the following sections.

### 3.7.1 IN-VITRO BIOCOMPATIBILITY STUDY

The as-sprayed and heat-treated surface modified samples were tested for bioactivity in vitro with a synthetic body fluid (SBF) model (Tiwari et al., 2021). The SBF had an electrical profile that was very close to that of human plasma. Used SBF had characteristics not dissimilar from human plasma. The SBF solution was prepared by dissolving the reagent grade ingredients in distilled water (700 ml) according to the following proportions: $NaHCO_3$ (0.35g), NaCl (8.03g), KCl (0.26g), $MgCl_2 \cdot 6H_2O$ (0.32 g), $K_2HPO_4 \cdot 3H_2O$ (0.23g), $CaCl_2$ (0.3 g) and $Na_2SO_4$ (0.07g). The plastic receptacles underwent a 24-hour cycle of sterilisation in an autoclave at 100 degrees Celsius and 10 atmospheres of pressure. This process helps to remove the bacteria and other living microorganisms. The experimental setup of autoclave machine established at NIT, Jalandhar as shown in **Fig. 3.5.**


**Fig. 3.5** Experimental Setup of Autoclave vertical machine

The plastic flasks were then placed in a rotating incubator set to 72 rpm, where they remained without any solution changes. The container was maintained at 37 degrees Celsius throughout

the soaking period. The experimental setup of incubator machine established at NIT, Jalandhar as shown in **Fig. 3.6.** Any weight loss or increase caused by soaking in the SBF solution was analysed by comparing the subjects' starting and ending weights.


**Fig. 3.6:** Experimental Setup of Incubator

### 3.7.2 CORROSION BEHAVIOUR THE COATED SPECIMENS AT VARIOUS HEAT TREATED CONDITIONS

Corrosion is generally initiated from the surface of material by the interaction of environment at the surface. The electrochemical reactions act as a catalyst for a corrosion to occur on the surface/ sub-surface of the material. Thus, the electrochemical testing is best for investigation of the corrosion mechanism.

For performing electrochemical study, the main requirement of the tested sample is that it must be electrical conductors and further size of the sample is small enough (few square centimeters) to be properly fitted in the Gamry instrument for the metal in a corrosive environment. There are three electrode configuration used in Gamry instrument for performing the corrosion testing. The all electrodes used for studying the corrosion behaviour are immersed

into the solution, and they are joined to an appliance called potentiostat. The electrolytic solution used in the study has closely resembles with the actual application environment of the specimen being tested. As an added bonus, a potentiostat may be used by adjusting the potential of the metal sample to the required level. The density of the corrosion current (Icorr) at the corrosion potential may be calculated using this setup (Ecorr). Electrochemistry allows for the assessment of several corrosion occurrences. Both base metal and as-deposited coated specimens and specimens treated through various heat treatment conditions were subjected to an electrochemical corrosion test in the current investigation. The corrosion behaviour of the LVOF sprayed surface-modified specimens was studied using an electrochemical test, and its schematic construction is depicted in **Fig.3.7.** The standard calomel electrode (SCE) was used as a primary reference electrode against which all other potentials were measured. A rod of pure graphite served as the counter electrode. In this investigation, a functional electrode with a corrosive area of 1.5836 $cm^2$ was constructed using surface modified specimens under both as-deposited and heat-treated circumstances. The epoxy insulation ensured that only the working portion of the coating specimen was exposed to the corrosive conditions of the electrochemical research. The coatings specimen was prepared for electrochemical testing by first being polished with emery sheets ranging in grit size from 200 to 1000, then being cleaned with an ultrasonic cleaner, and lastly being hot-dried with air. For the purpose of studying specimens under various settings, a potentiodynamic polarisation curve was drawn while the experiments were conducted in a 3.5 wt% NaCl solution at room temperature. The potentiodynamic polarisations test is conducted using a computer running the DC105 Gamry electrochemical programme and a Potentiostat/ Galvanostat (Series G-750; Gamry Instruments, War-Minster, PA). During the electrochemical tests, the potential was varied from -500 mV to 1500 mV against $E_{corr}$. Using a potentiostat with a scan rate of 1 mV/sec, the electrode potential was maintained within 1 mV of a preset value over a broad range of applied current. The experiments were performed using a fresh solution for each experiment and testing were carried out at ambient temperature. The procedure for performing experiments using Gamry Instrument is as follows:

a) Green–Blue: Working and Working Sense, connected together. A black cable was attached to the connection point, referred to from here on as Black. This is the conventional-positive electrode. The black cable was connected to the counter electrode (i.e. the anode in the electrochemical test set up).

b) Red–White: Counter and reference electrodes were also connected together. A red cable was attached to the connection point, referred to from here on as Red. This is the conventional ―counter‖ or ―negative‖ electrode.

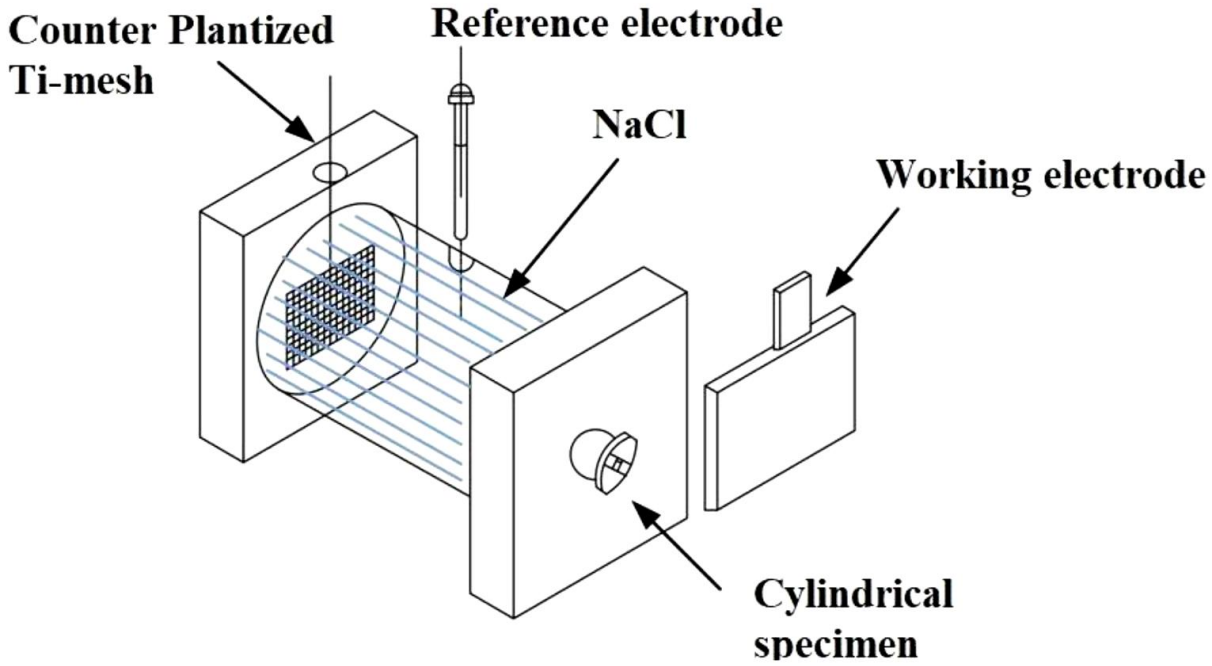


**Fig 3.7** Corrosion testing apparatus.

### 3.8 TAFEL PLOT EXPERIMENT

The electrochemical study was performed by utilizing a Tafel extrapolation method. To ensure the repeatability of the test results, the electrochemical corrosion study was done on coating samples for each condition (as-deposited and heat-treated). The Tafel extrapolation method is based on mixed-potential theory for determining the corrosion rate of samples. The data captured from anodic or cathodic polarization measurement were used in a mixed-potential theory. Further, during electrochemical study, the cathodic polarization data are generally taken because these data are easier to assess using an experimental method. A schematic construction for performing a cathodic polarization measurement is shown in **Fig. 3.8.** The sample, whose corrosion rate is to be measured served as a working electrode (W.E.), and cathodic current was provided to it by means of an auxiliary electrode which is generally made from inert material such as platinum or graphite. The current in the experimental process was measured by means of

an ammeter *A*, and the potential of the clad specimens was measured with respect to a reference electrode by a potentiometer-electrometer circuit. The results obtained during the cathodic polarization of clad specimens in an SBF solution. An indicator voltmeter shows the corrosion potential of the clad specimen being tested in relation to the reference calomel electrode before the cathodic current is applied. It is possible to plot the electrode's potential vs the logarithm of the applied current by doing the following: *E* vs *logi*. Extrapolating to the corrosion potential (Ecorr), tangents were drawn on the logi versus E graph, meeting at a single point. This X-axis value represents the current corrosion (Icorr). Log axes are used in corrosion experiments to show a wide range of current values. Passivity causes a six-fold shift in corrosion experiment current. After electrochemical analysis, the microstructure was analysed.

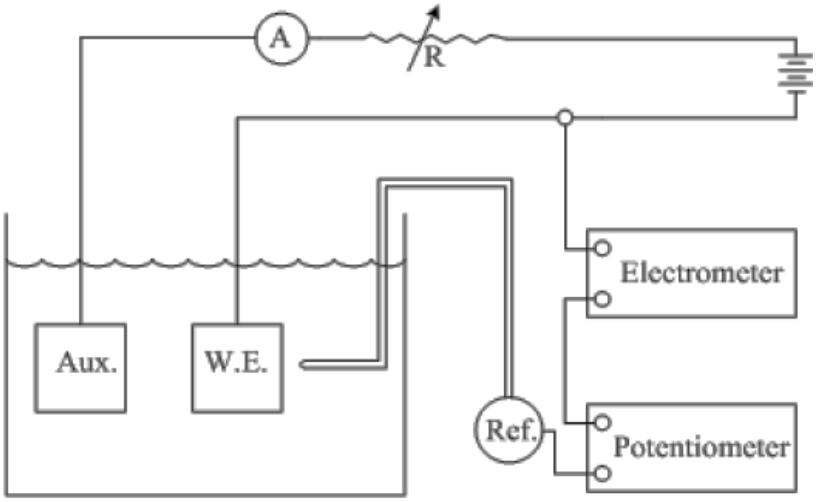


**Fig. 3.8** Schematic illustration of the electric circuit for cathodic polarization measurement.

## 3.9 SUMMARY

A detailed description of the various steps in the LVOF sprayed surface modifications were discussed. Heating the samples that have had their surfaces treated by annealing has been characterised as being crucial under all circumstances. The properties of coatings and heat-treated specimens are determined with the use of a variety of metallurgical and mechanical characterization instruments and techniques, which are discussed in detail in this chapter. Samples with their surfaces transformed by LVOF spraying technique have had their corrosion resistance and in-vitro properties reviewed at length, along with the methods and conditions used to evaluate these attributes.

# CHAPTER 4

# CHARACTERIZATION OF POWDERS AND COATINGS

## 4.1 CHARACTERIZATION OF POWDERS

Commercially available HaP and $Al_2O_3$ in the form of powder manufactured by *H.C Starck of Germany* was selected as a coating material. The powders were made available by Metallizing Equipment Co. Pvt. Ltd. Jodhpur *(India).*

Further to confirm the composition and average particle size of the coating powders; the SEM/EDAX and XRD analysis has been done. The $Al_2O_3$ powder shows an angular morphology wit 40-50µm average particle size as shown in **Fig.4.1 (a).**

The EDS corresponding to the SEM **(Fig.4.1a)** is represented in **Fig. 4.1 (b).** The XRD spectrum of aluminium oxide powder is shown in **Fig.4.2.** The peaks of alumina in this XRD correspond to the *JCPDS reference code of 00-001-1243* which corresponds to the peaks of alumina.

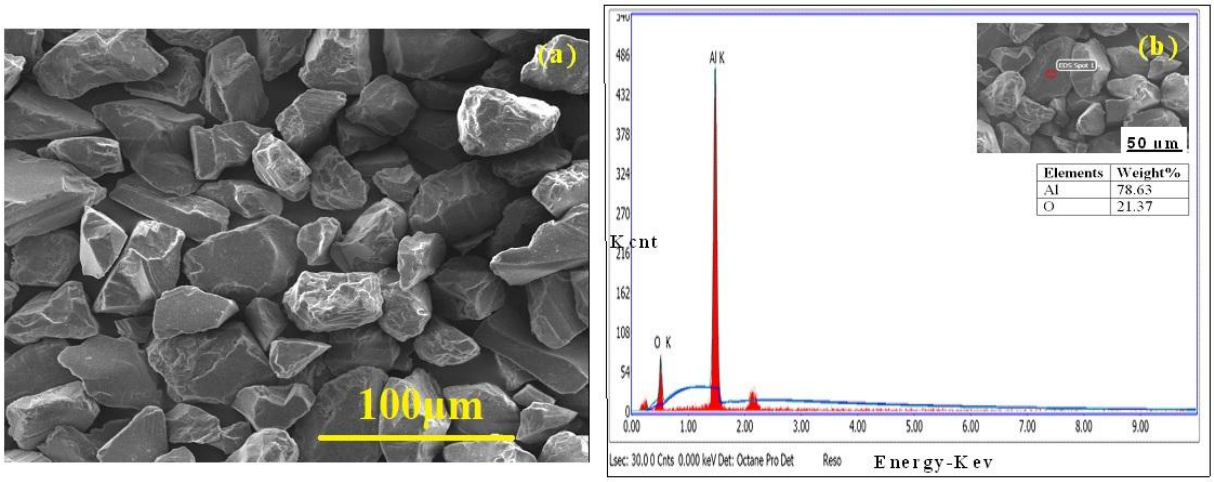


**Fig. 4.1 (a)** SEM micrograph of $Al_2O_3$ powder, and (b) EDS spectrum of $Al_2O_3$ powder.

The SEM micrograph shows particle roundness. EDS verified the existence of HAp powder's key constituents, C, P, and O. **Fig. 4.4** shows HA powder XRD. The HA powder's XRD spectrum reveals just HA peaks, indicating it is largely pure. HA powder with spherical shape was employed to deposit coatings. EDS proved the existence of HA powder's key constituents, C, P, and O.**Fig.4.3** shows HAp powder information.

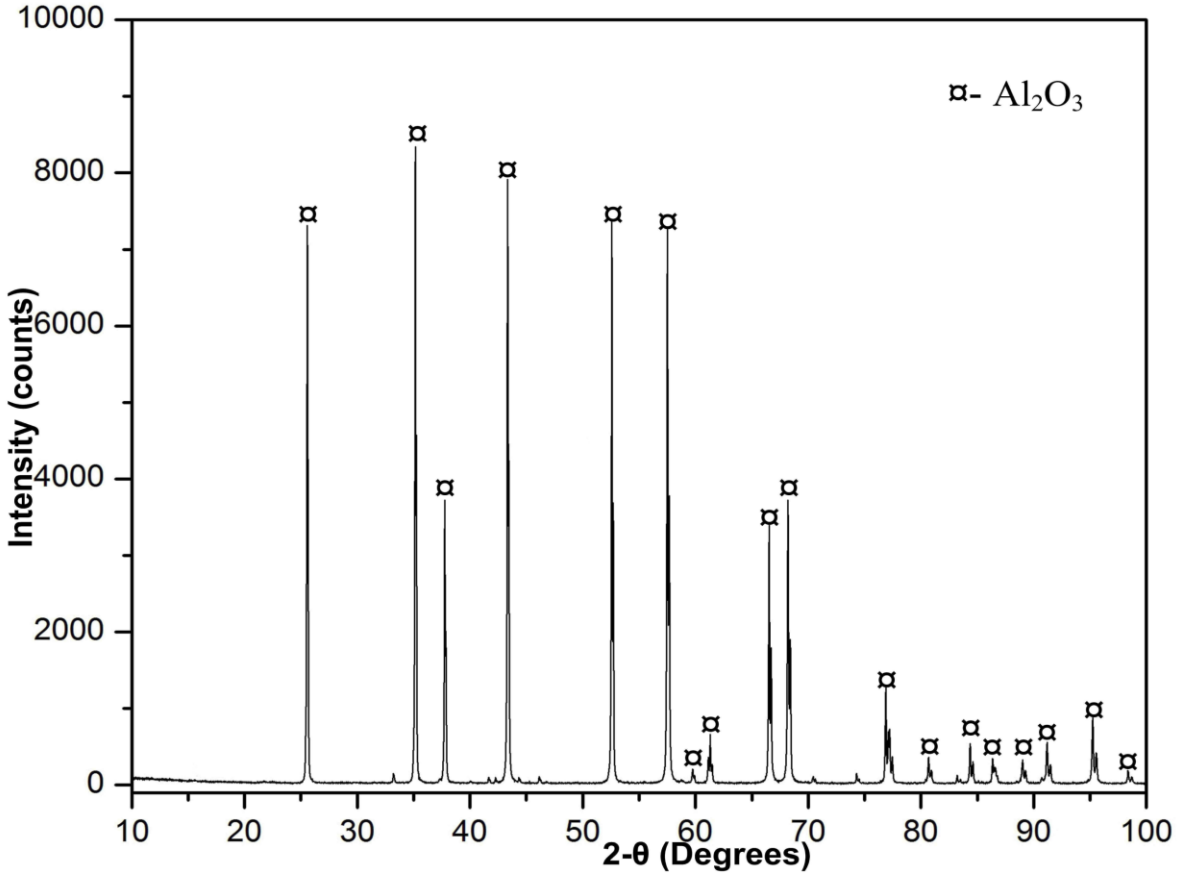


**Fig. 4.2** XRD pattern of $Al_2O_3$ powder.

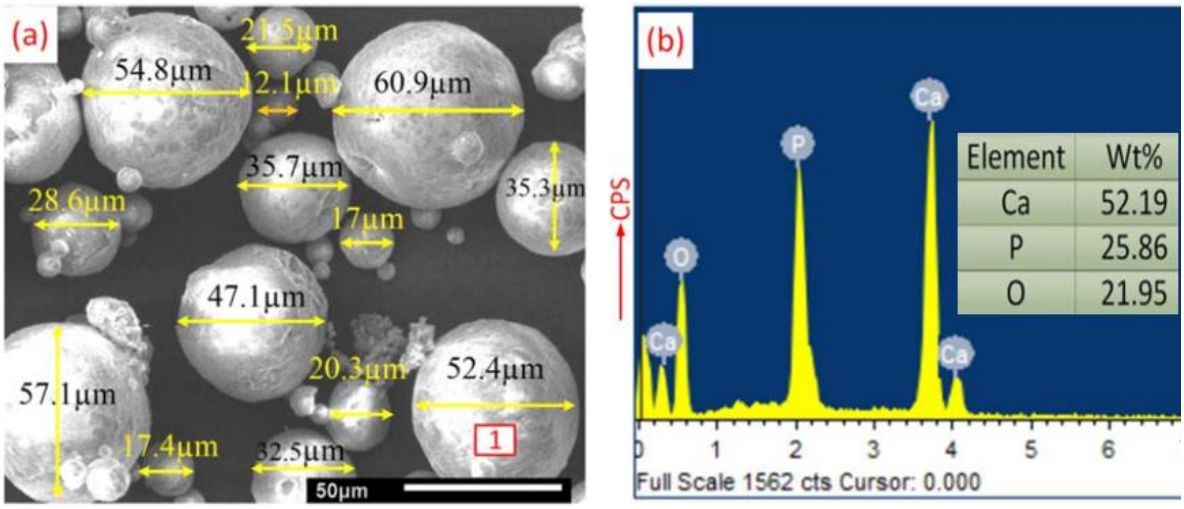


**Fig.4.3** (a) SEM and, (b) EDS of Hap powder.

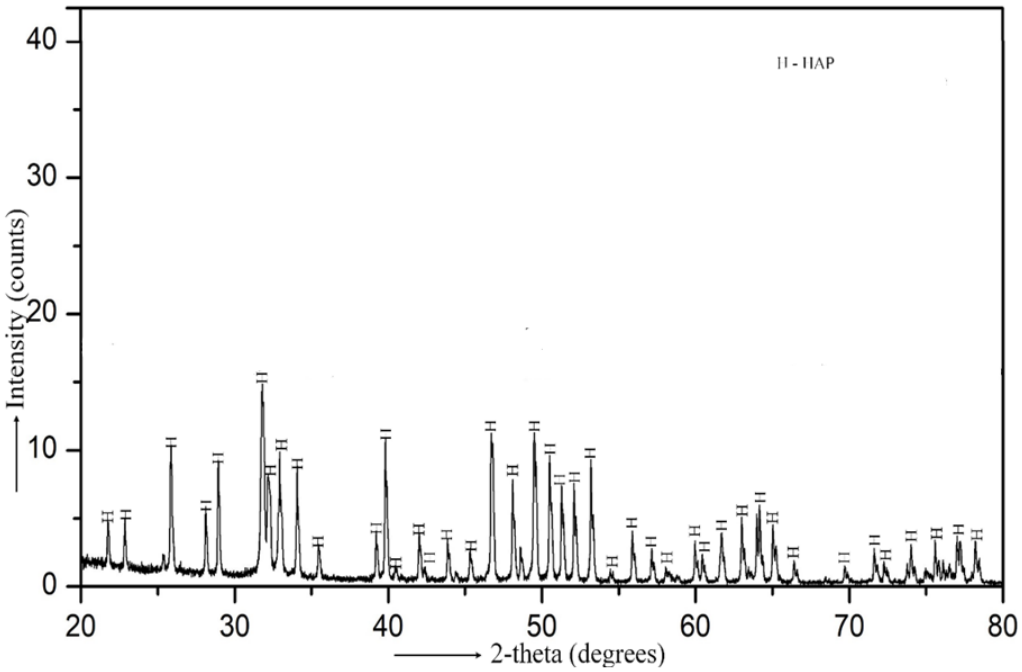


**Fig.4.4** XRD pattern of HaP powder.

The SEM micrograph and XRD of the received nano-$Al_2O_3$ powder are presented in **Fig. 4.5(a)** and (b).

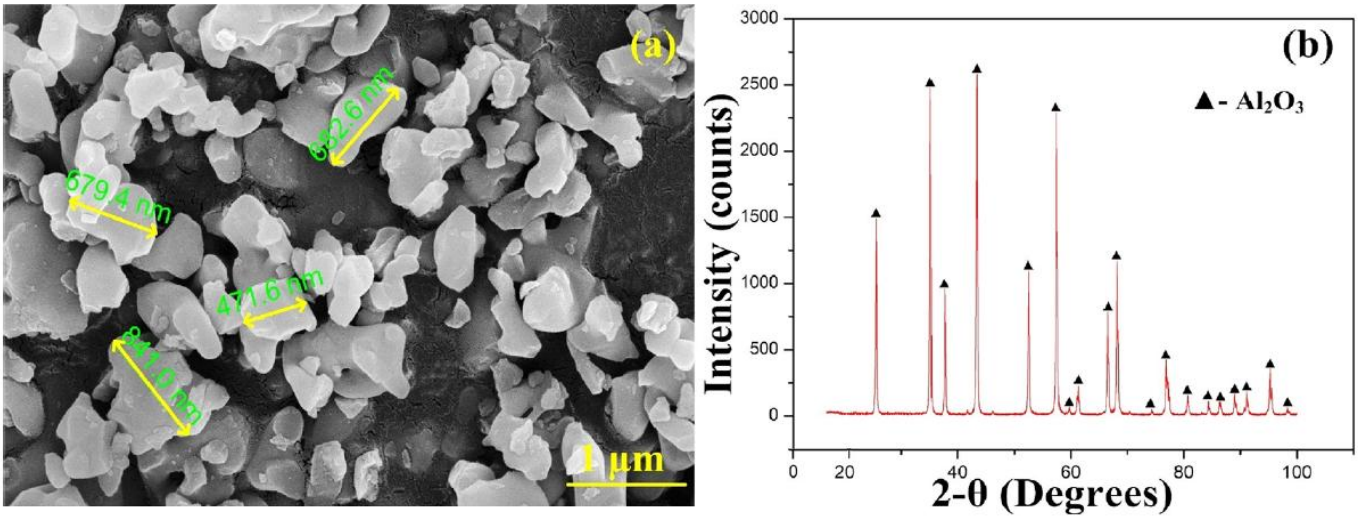


**Fig. 4.5 (a)** SEM micrograph of nano-$Al_2O_3$ powder, and (b) XRD pattern of nano-$Al_2O_3$ powder.

## 4.2 DEVELOPMENT OF COATINGS

The coatings were deposited on the substrates using LVOF Spray (a thermal spray process) apparatus **(Fig. 4.6).** The test specimens were cleaned, degreased and shot blasted. The specimens were grit blasted by alumina (Grit 60) prior to the deposition of the coatings by LVOF Spraying, for developing better adhesion between the substrates and the coatings. The LVOF coated samples are presented in **Fig. 4.7.**

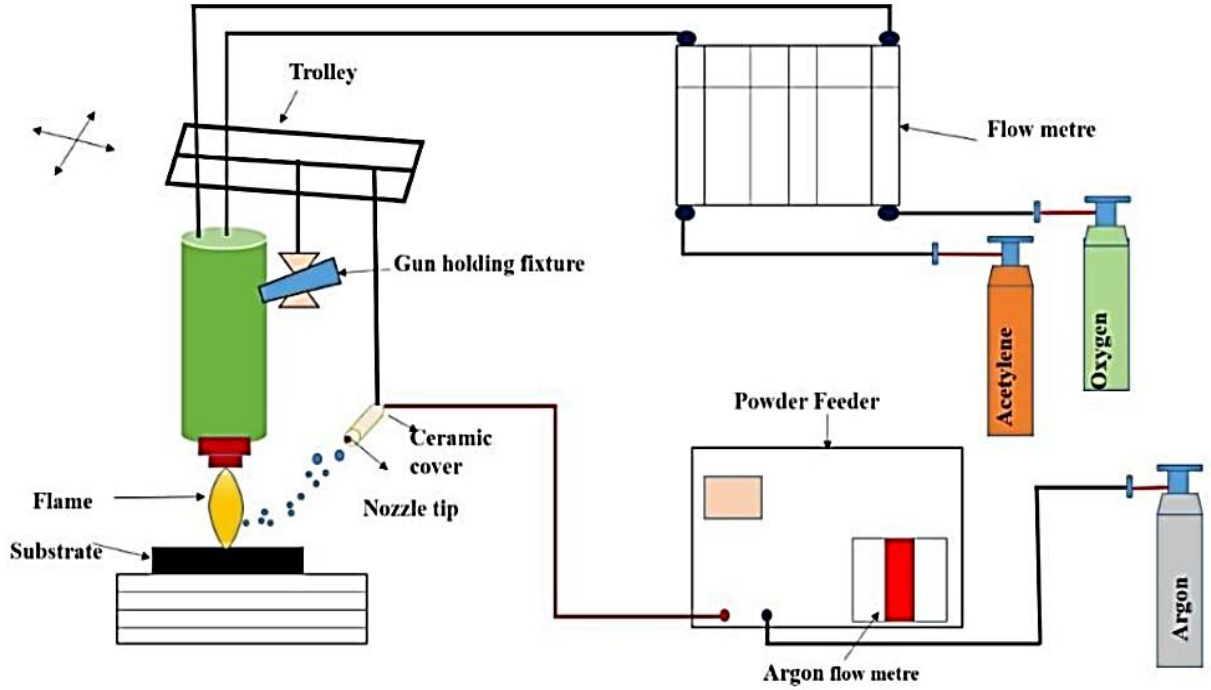


**Fig. 4.6:** Schematic representation of LVOF spray set-up (Tiwari et al, 2021).

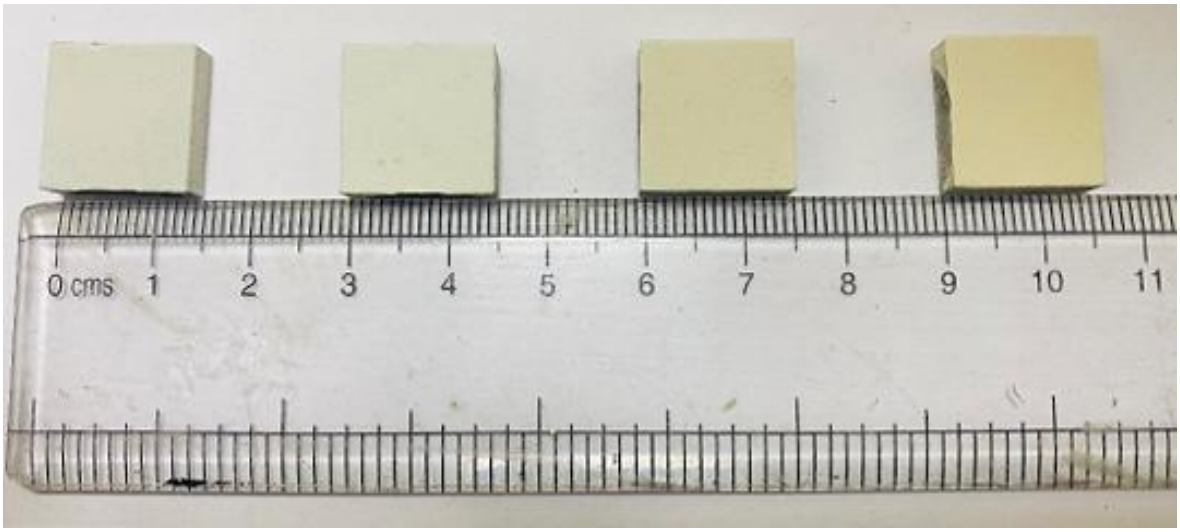


**Fig. 4.7.** Coated samples using LVOF spraying technique.

The SEM-EDS analysis of deposited coating is presented in **Fig.4.8.** The SEM surface shows the un-melted, melted and partially melted zones. This due to the temperature difference in the flame of spraying process. The EDS has confirmed the presence of Ca, P, and O present in the coating as seen in **Fig. 4.9(b).** The surface morphologies of the hydroxyapatite powder and the as-deposited HA coating were measured in the Field-Emission Scanning Electron Microscopy analysis.

The HA powder showed a spherically shaped morphology, with the same observation have been reported by Smith et al., 2023 and Johnson et al., 2024 among others. The spherically shaped HA powder indicates the manufacturing method, particularly the packing density and flow of the powder during the coating process.

According to the results of the Energy Dispersive X-ray Spectroscopy analysis, C, P, and O elements were found to be the main sources of the HA powder.

These facts describe what composition is naturally inherent to the substance of hydroxyapatite and replicate other studies regarding HA powders, among which are Lee and Kim, 2024; Wang and Chen, 2024. In this case, the role of each element is significant for creating the HA structure and its bioactivation in the physiological composition.

Henao et.al. (2024); Bioactive thermal spray coatings, manufactured via high-velocity oxygen fuel spray (HVOF), from hydroxyapatite and bioactive glasses were demonstrated by their ability to be employed on temporary implants because of both HAp and BG's potential to dissolve and promote osseointegration. It means that both phases react and dissolve at various rates under in-vitro conditions.

The 75% wt. – 25% wt. HAp-S53P4 bioactive glass powders have been HVOF-sprayed and prepared HAp/S53P4 BG composite coatings on a bioresorbable AZ31 alloy.

They investigated the HVOF parameters affected by the standoff distance and fuel/oxygen ratio variance to establish stable structural coatings and their impact on phases and microstructure formation in these coatings.

Different characterization techniques, including scanning electron microscopy, X-ray diffraction, and Fourier transform infrared spectroscopy, were utilized to investigate distinct pertinent structural microstructural aspects of the composite coatings.

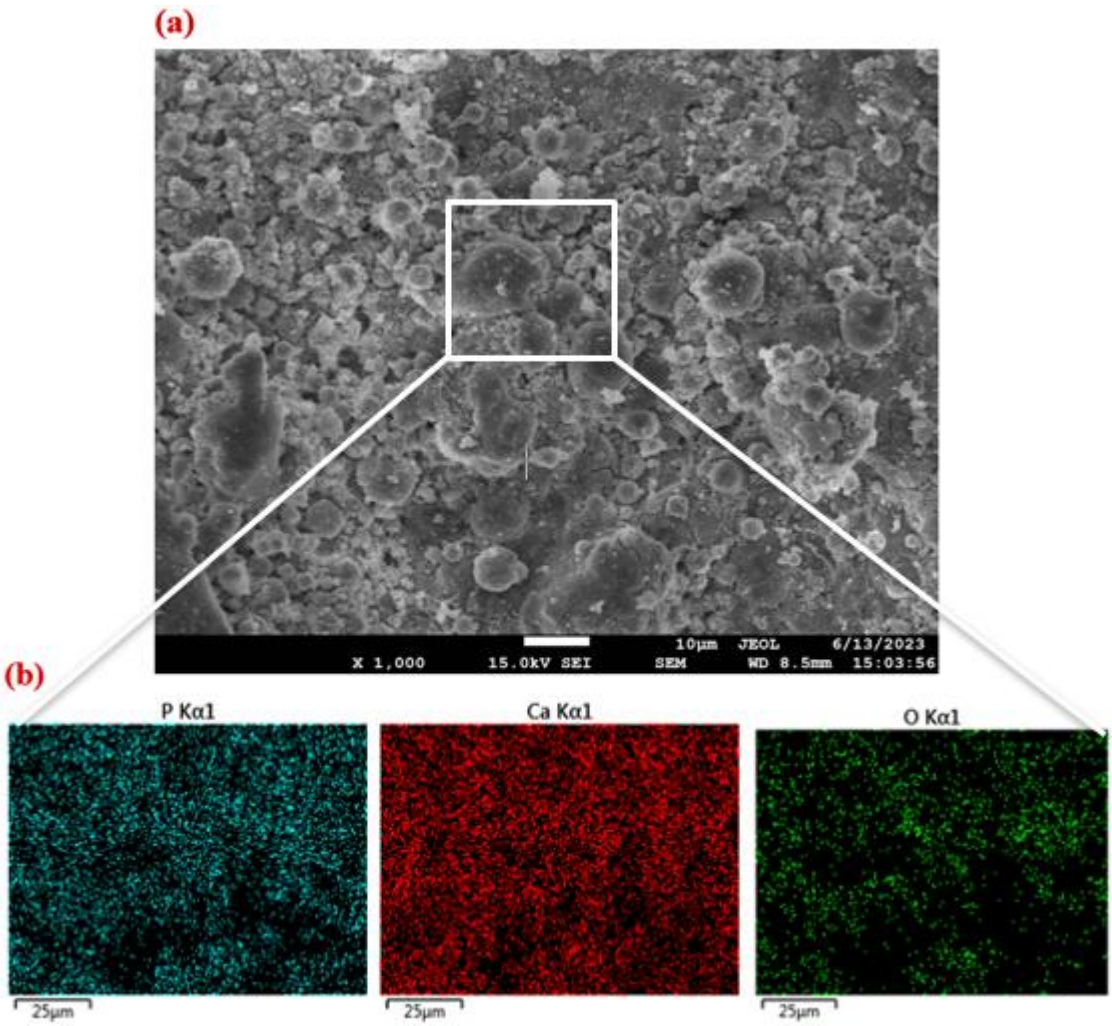


**Fig4.8. (a)** SEM micrograph of Hap coating, and (b) EDS mapping of Hap coating

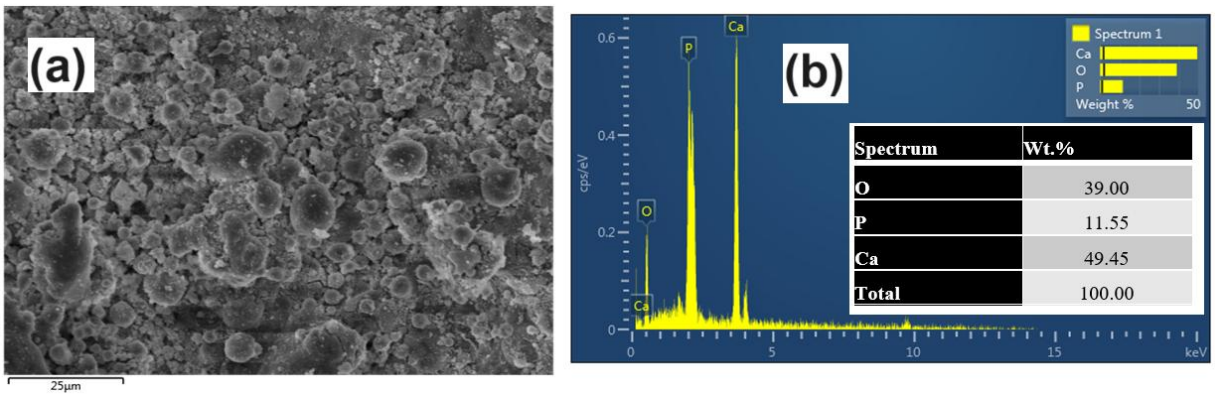


**Fig.4.9.** (a) SEM micrograph of Hap coating, and (b) EDS mapping of Hap coating

A composite coating is developed by incorporating 10% alumina into a modified hydroxyapatite coating as shown in **Fig.4.10.** The surface morphology is presented in **Fig.4.10(a)** and the EDS

mapping of Hap +10% alumina coating is shown in **Fig. 4.10(b).** This addition serves to improve the coating's mechanical qualities and resistance to wear. The composite is then applied with the Low Velocity Oxy-Fuel (LVOF) technique. The incorporation of alumina generates a secondary phase that significantly alters the microstructure and surface characteristics of the coating. The scanning electron microscopy (SEM) analysis of this composite coating reveals a complex structure, with distinctly identifiable regions with particles that are un-melted, melted, or partially melted. This morphology resembles that of pure hydroxyapatite coatings. Nonetheless, the incorporation of alumina results in an increase in the volume of partially melted areas, since alumina requires a higher temperature for full melting. The result is a surface exhibiting more diversity, with improved hardness and toughness, due to the dispersion of alumina particles inside the hydroxyapatite matrix. The temperature variations inside the LVOF spraying flame significantly influence the development of microstructural properties, especially in areas where melting is incomplete, a phenomenon that is more pronounced due to the presence of mixed materials. The EDS investigation has confirmed the presence of calcium (Ca), phosphorus (P), oxygen (O), and aluminum (Al), indicating that the alumina is well incorporated into the coating. This composite structure preserves the bioactive properties of hydroxyapatite while enhancing the mechanical strength and wear resistance of the coating. As a result, it is well-suited for biomedical applications that need both biocompatibility and durability.

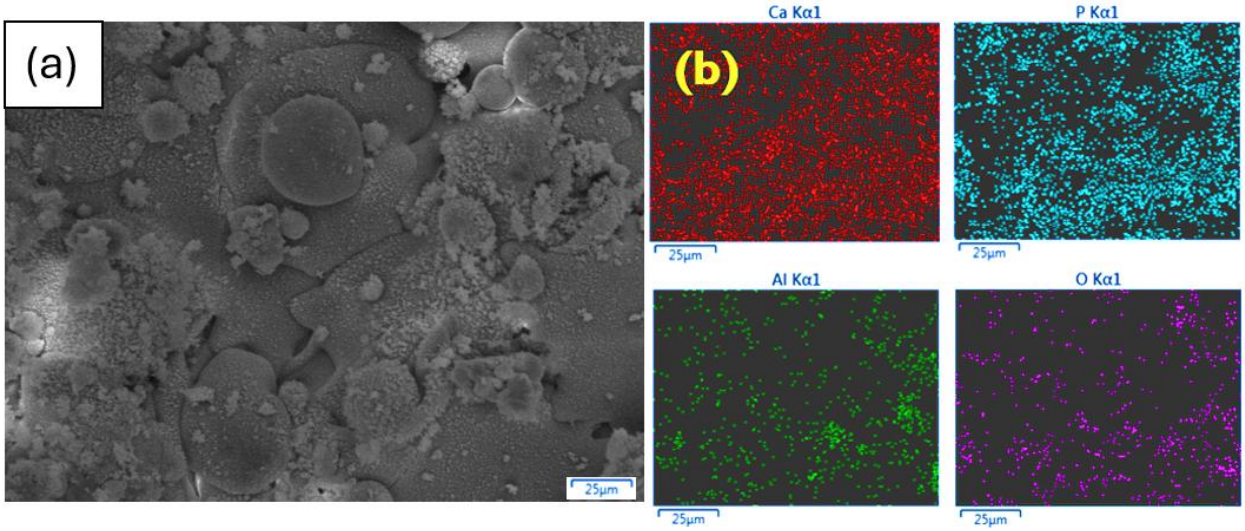


**Fig.4.10.** (a) SEM micrograph of Hap with 10% micrometric alumina coating (HALC), and (b) EDS mapping of Hap with 10% alumina coating

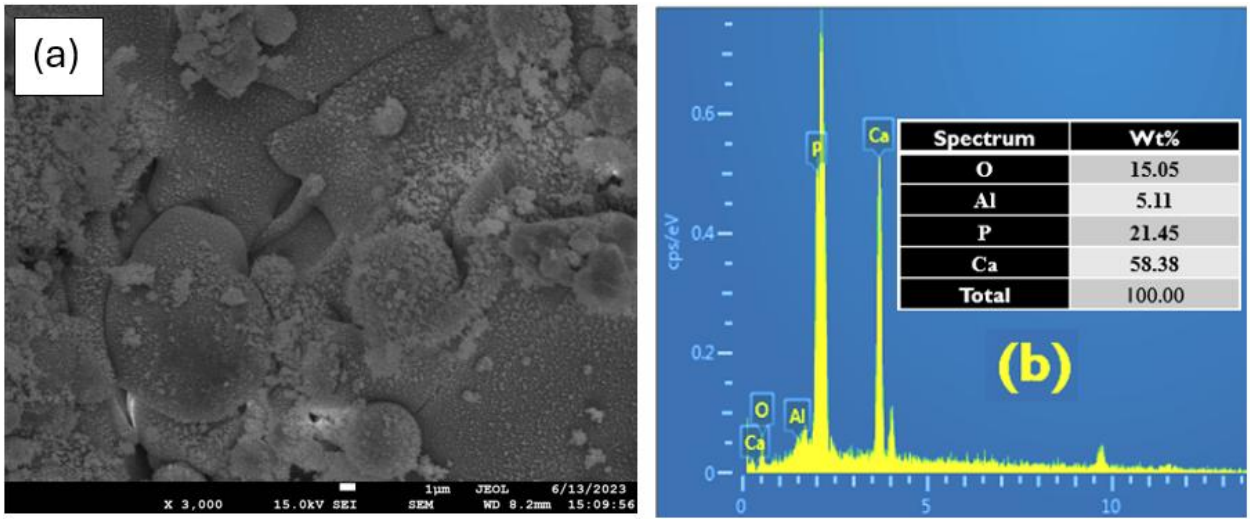


**Fig.4.11.** (a) SEM micrograph of hydroxyapatite with 10% nano alumina coating (HALN), and (b) EDS mapping of hydroxyapatite with 10% alumina coating

The SEM micrograph of hydroxyapatite with 10% nano alumina coating and EDS of this coating is presented in **Fig.4.11.** A 10% concentration of nano-alumina is incorporated into a modified hydroxyapatite coating to improve its mechanical properties, wear resistance, and surface characteristics. The coating is then applied via Low Velocity Oxy-Fuel (LVOF) technology. The incorporation of nano-alumina generates a secondary phase at the nanoscale, significantly influencing the microstructure. The scanning electron microscopy (SEM) analysis of the composite coating demonstrates a polished surface structure marked by a consistent arrangement of nanoscale features, including regions that are unmelted, fully melted, and partially melted. The use of nano-alumina enhances the formation of partially melted areas due to its high melting point and remarkable thermal stability, resulting in a denser and more compact coating structure. The nano-sized alumina particles serve as a reinforcement inside the hydroxyapatite matrix, resulting in improved hardness, toughness, and wear resistance. Furthermore, these nano-scale particles enhance the surface area and reactivity of the coating, leading to enhanced adherence to the substrate and increased biological activity. The successful incorporation of nano-alumina has been confirmed using EDS analysis, which substantiates the existence of calcium (Ca), phosphorous (P), oxygen (O), and aluminium (Al). This composite coating maintains the bioactive properties of hydroxyapatite while offering outstanding mechanical strength, making it extremely suitable for biomedical applications requiring enhanced durability and bioactivity.

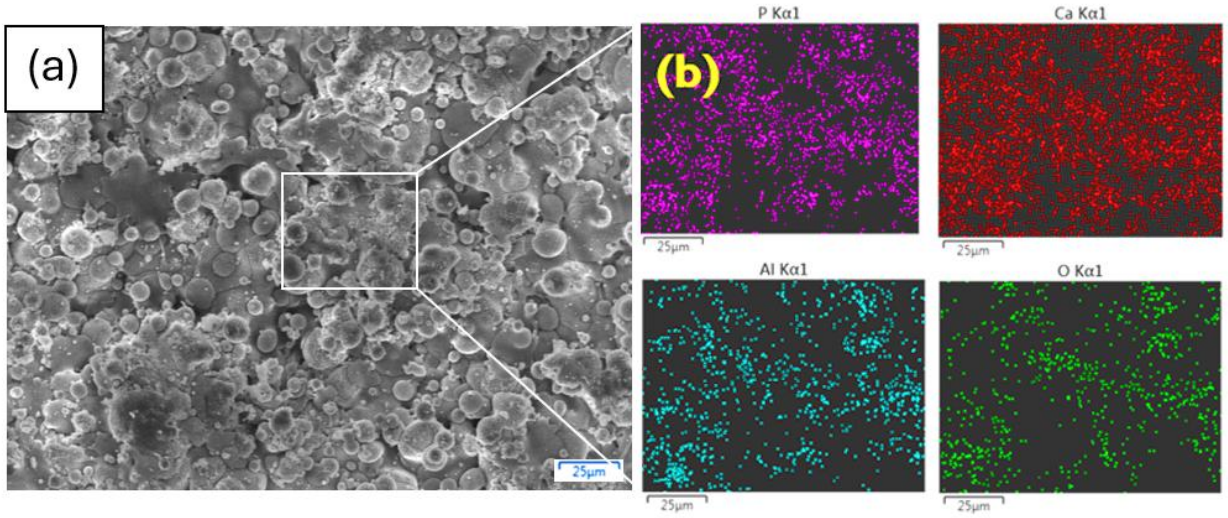


**Fig.4.12.** (a) SEM micrograph of Hap with 5% nano+ 5%micron-alumina coating (HALB), and (b) EDS mapping of coating.

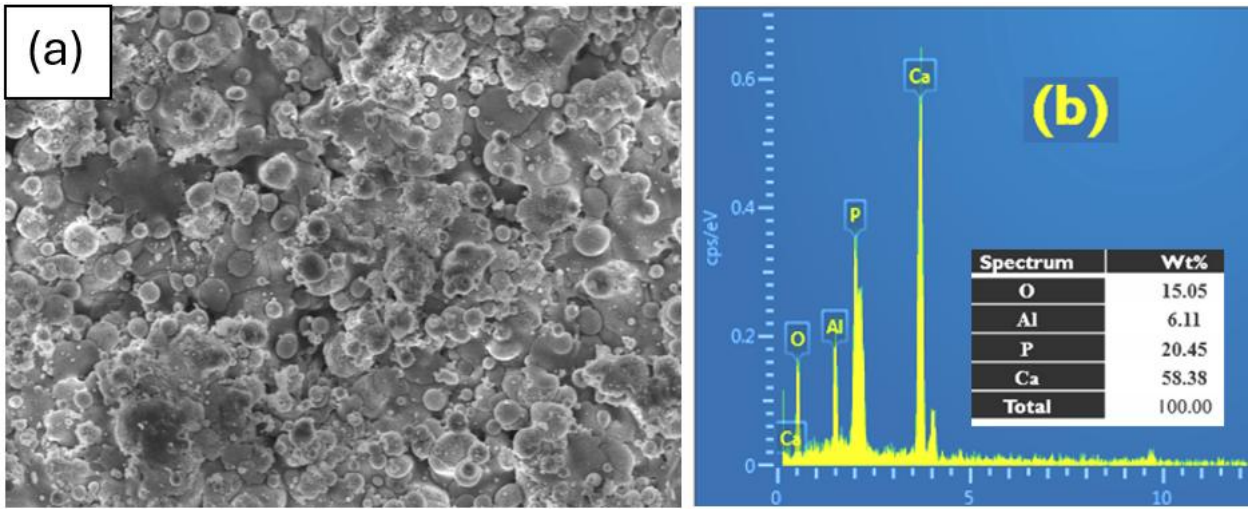


**Fig4.13.** (a) SEM micrograph of Hap + Hap with 5% nano+ 5%micron-alumina coating (HALB), and (b) EDS mapping of coating.

**Figs. 4.12 and 4.13** exhibit the facts relating to SEM and EDS, respectively. The hydroxyapatite coating is improved by including a combination of 5 wt.% micrometric alumina and 5 wt.% nano-alumina into the hydroxyapatite matrix. The mixture is then applied to the surface via the Low Velocity Oxy-Fuel (LVOF) technique. The incorporation of both micrometric and nanoscale alumina particles establishes a reinforcing mechanism at two distinct scales, leading to a significant improvement in the coating's overall properties. The micrometric alumina particles demonstrate enhanced mechanical strength and wear resistance due to their diminutive size and

ability to withstand higher impact pressures under mechanical stress **(Fig. 4.12a).** Conversely, the nano-alumina particles possess a substantial surface area, facilitating their more efficient dispersion within the hydroxyapatite matrix and minimizing the voids between micrometric particles. This results in a coating structure that is more compact and denser.

The scanning electron microscopy (SEM) analysis of this composite coating reveals a complex surface morphology, with regions with un-molten, melted, and partially melted particles **(Fig 4.13a).** This morphology resembles that seen in previous coatings. Nonetheless, the incorporation of both micrometric and nano-alumina results in a more heterogeneous surface, exhibiting improved mechanical interlocking among particles of differing dimensions. The incorporation of micrometric alumina enhances the toughness and structural integrity of the coating, whilst the inclusion of nano-alumina particles yields a smoother surface finish and increased hardness. The nano-alumina particles may occupy the interstices between other particles, so inhibiting the propagation of fractures.

The presence of both types of alumina particles ensures a more uniform distribution of mechanical stresses over the coating, hence reducing the likelihood of failure under loading circumstances. This dual reinforcement is particularly advantageous in scenarios where both durability and the facilitation of biological activity are essential. The EDS analysis confirms the presence of calcium (Ca), phosphorus (P), oxygen (O), and aluminum (Al), indicating the successful incorporation of both micrometric and nano-alumina into the hydroxyapatite matrix **(Fig 4.13b).** The resulting composite coating maintains the essential bioactive properties for biomedical applications, while providing enhanced durability and wear resistance. This makes it an exceptional option for advanced medical implants and systems requiring both mechanical integrity and biocompatibility.

The X-ray diffraction (XRD) patterns of the Low Velocity Oxy-Fuel (LVOF) sprayed coatings reveal distinct crystalline structures for each of the four coatings: pure hydroxyapatite, hydroxyapatite with 10% alumina, hydroxyapatite with 10% nano-alumina, and hydroxyapatite containing a blend of 5% micrometric alumina and 5% nano-alumina. The X-ray diffraction (XRD) pattern of the pure hydroxyapatite coating displays prominent peaks corresponding to the crystalline phases of hydroxyapatite indicating a presence of HA peaks, α-TCP, β-TCP and phases of $Al_2O_3$ (alpha &gamma) as shown in **Fig.14.4**. Supplementary peaks indicative of the

alumina phase ($Al_2O_3$) is seen in the hydroxyapatite + 10% alumina coating, hence affirming the presence of alumina inside the hydroxyapatite matrix. The XRD pattern of the hydroxyapatite with 10% nano-alumina coating displays peaks indicative of both hydroxyapatite and nano-alumina. Nonetheless, the nano-alumina peaks seem broader and less intense, signifying their reduced particle size and increased surface area. The XRD pattern of the hydroxyapatite coating, including 5% micrometric alumina and 5% nano-alumina, displays peaks indicative of both alumina phases and hydroxyapatite. The excellent incorporation of both micrometric and nano-scale alumina peaks, alongside hydroxyapatite peaks, indicates that alumina particles of both sizes have been successfully integrated into the coating matrix. The integration of micrometric and nano-alumina generates a unique diffraction pattern, signifying a more complex microstructure that may enhance mechanical properties and wear resistance while maintaining bioactivity.

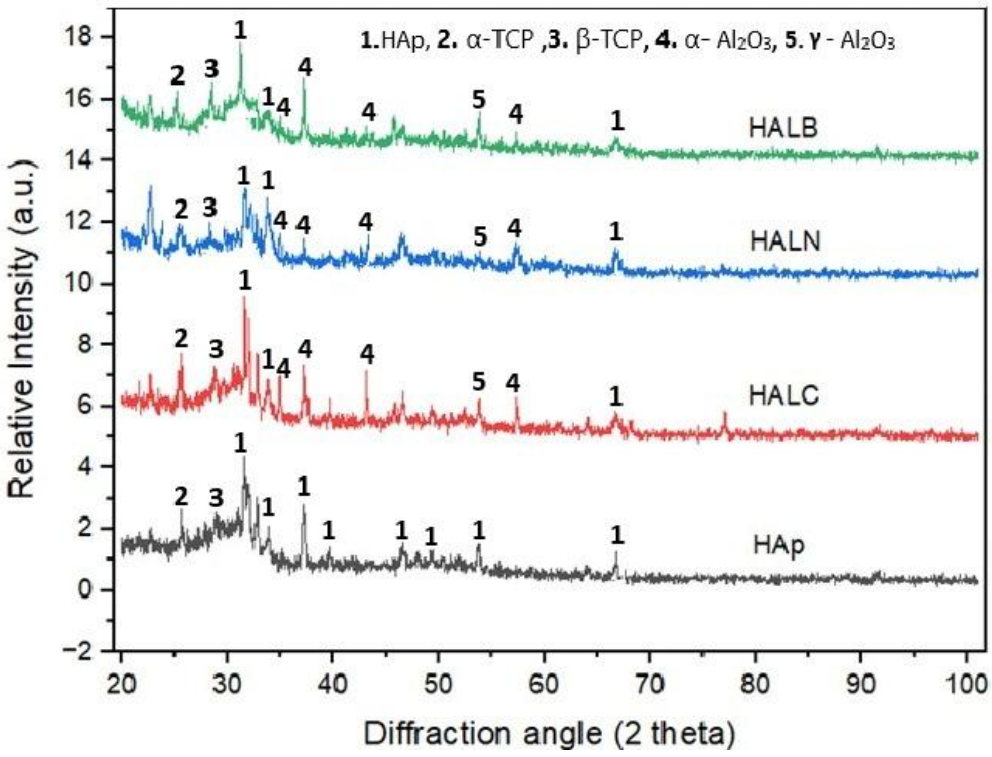


**Fig.4.14**. The XRD patterns of coatings (a) HA, (b) HALM, (c) HALN, and (d) HALB.

### 4.3 HEAT-TREATED COATINGS

Post-annealing, during which the four coatings were exposed to 700°C for 2 hours, the scanning electron microscopy (SEM) analysis reveals significant changes in the microstructure of each

coating, as seen in **Fig. 4.15.** This study effectively showcases the impact of the thermal treatment on the surface characteristics and overall shape of the coatings. The SEM pictures reveal a significant enlargement in grain size for the pure hydroxyapatite layer when compared to its as-sprayed state. The increase in grain size is caused by the introduction of thermal energy during the annealing process, which facilitates the movement of atoms and the merging of smaller grains into bigger ones. Annealing also results in a more homogeneous and sleek surface shape, accompanied by a decrease in surface porosity. The increased crystallinity of the hydroxyapatite coating upon annealing is apparent from the distinct grain boundaries and reduced surface imperfections, which may enhance the mechanical stability of the coating and decrease its dissolution rate in biological settings.

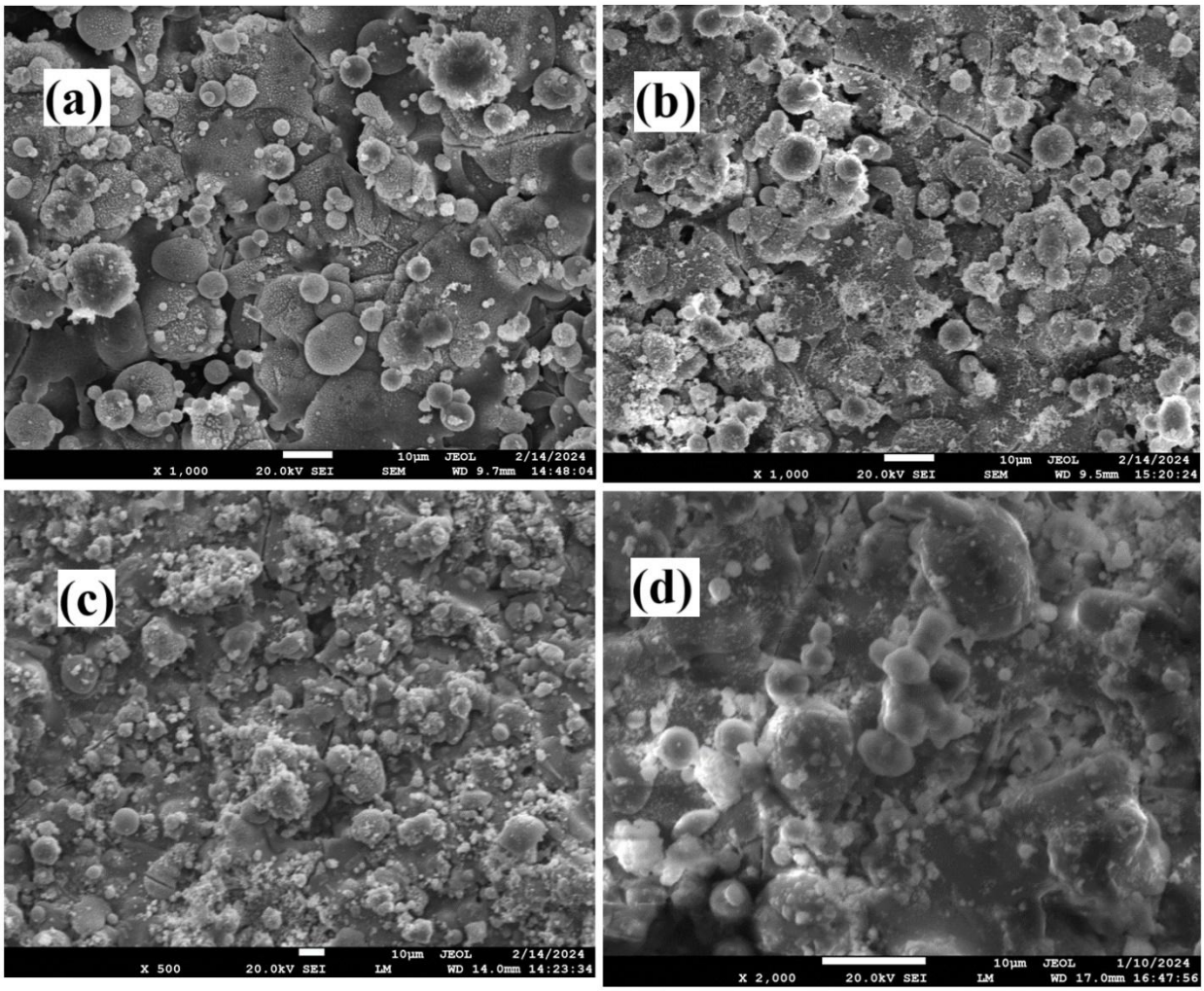


**Fig.4.15** The SEM micrographs of heat treated (a) HA, (b) HALM, (c) HALN and (d) HALB coatings.

The SEM pictures after annealing at 700°C reveal a clear change in the microstructure of the hydroxyapatite covering containing 10% alumina. Incorporating micrometric alumina particles into the hydroxyapatite matrix leads to a surface morphology that is more varied and diverse. Following the annealing process, the alumina particles, which possess a higher melting point compared to hydroxyapatite, retain their original form and size, serving as reinforcement inside the coating as shown in **Fig.4.15b.** The heat treatment boosts the mechanical characteristics of the coating by enhancing the cohesion between the hydroxyapatite matrix and the alumina particles, making the interface between them more defined and well-bonded. Nevertheless, there is evidence of localized sintering of hydroxyapatite specifically around the alumina particles, resulting in a more compact microstructure with a reduced number of empty spaces. The process of densification, which is enhanced by annealing, is advantageous for enhancing the hardness and wear resistance of the coating, so making it more suited for applications that need strong mechanical performance.

The hydroxyapatite covering containing 10% nano-alumina exhibits distinct changes in shape when annealed at 700°C, as seen by SEM analysis, in comparison to its initial as-sprayed condition as shown in **Fig.4.15c.** The nano-alumina particles exhibit a more uniform and dense distribution inside the hydroxyapatite matrix, primarily because of their short dimensions and large surface area. Annealing enhances the sintering interaction between nano-alumina and hydroxyapatite, leading to a denser structure with reduced porosity. The scanning electron microscopy (SEM) images reveal a smoother surface with fewer fractures and flaws, indicating that the incorporation of nano-alumina particles helps to prevent crack propagation during the annealing process. The annealed coating exhibits improved interfacial adhesion between hydroxyapatite and nano-alumina particles, leading to higher toughness and endurance of the coating. The improved adhesion is essential for biological applications requiring both bioactivity and mechanical strength. The incorporation of nano-alumina enhances the grain structure of hydroxyapatite, hence improving the mechanical properties of the coating.

The scanning electron microscopy (SEM) analysis of the hydroxyapatite coating, treated with a blend of 5% micrometric alumina and 5% nano-alumina and then annealed at 700°C, demonstrates a complex microstructural evolution as seen in **Fig. 4.15d.** The hydroxyapatite matrix is augmented by the integration of micrometric and nano-alumina particles, yielding a

composite structure with dual-scale reinforcement. Subsequent to the annealing procedure, the micrometric alumina particles exhibit a rather stable condition, but the nano-alumina particles experience sintering and diffusion into the adjacent hydroxyapatite matrix. The result is a hierarchical microstructure with well-defined micrometric alumina zones surrounded by a matrix rich in nano-alumina and hydroxyapatite. The scanning electron microscope (SEM) images show a coating that is highly condensed and densely packed, exhibiting little porosity. This indicates that the heat treatment has effectively facilitated sintering and grit formation. The use of micrometric and nano-alumina particles improves the mechanical interlocking in the coating, resulting in enhanced mechanical characteristics, including increased hardness. The strong interactions formed by the various particle sizes and the hydroxyapatite matrix also enhance load distribution and improve resilience to mechanical strain. The XRD pattern of the post-treated coated samples have shown in **Fig. 4.16**. The XRD pattern have shown the improved crystallinity of the coating after heat treatment, which is endorsed by the absence of amorphous phases present in the coating during the deposition.

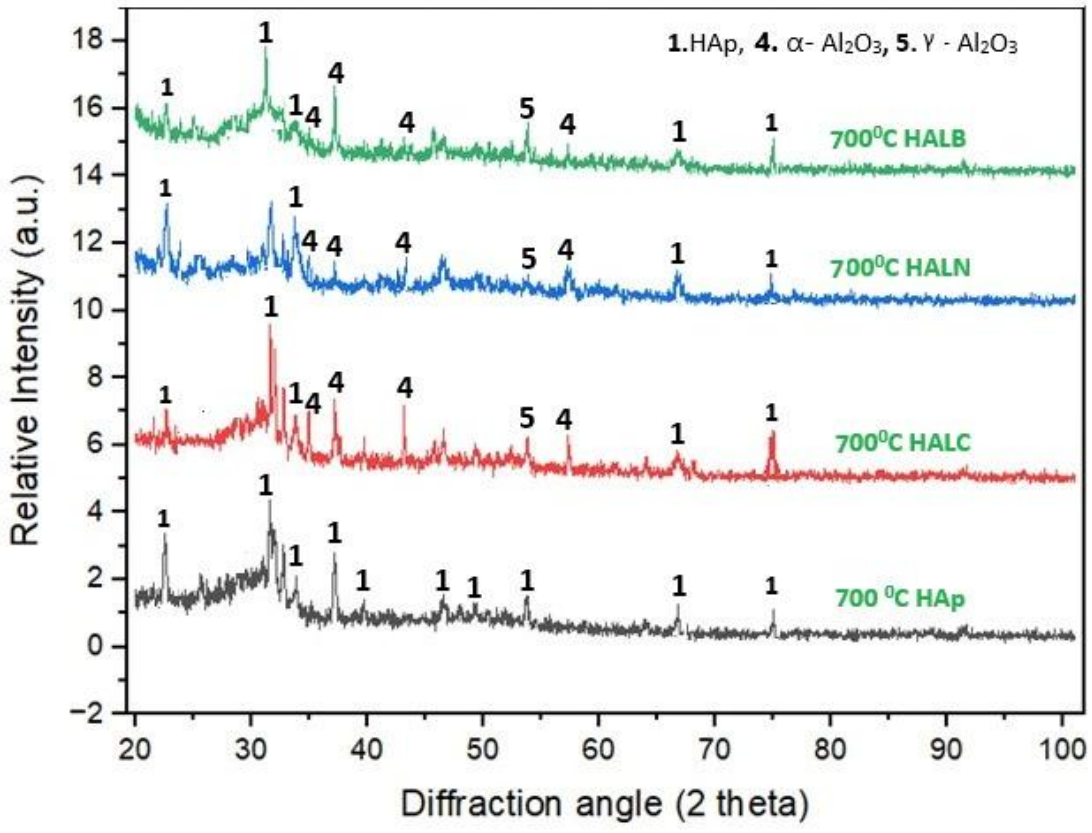


**Fig. 4.16**. The XRD pattern of the post-treated coated samples.

The crystallinity of the developed coatings and post-treated coatings calculated from the XRD patterns are presented in **Table 4.1.**

**Table 4.1** The crystallinity of the developed coatings and post-treated coatings.

| Coatings | As sprayed coating | Annealed |
|---|---|---|
| HAp | 73.4 | 79.3 |
| HALC | 76.2 | 82.5 |
| HALN | 89.7 | 90.1 |
| HALB | 90.4 | 95.5 |

The development of amorphous phases has significant impact on the performance of the biomedical implant coatings. The value of crystallinity for HA was found to be 55 % (Xue et al, 2004), when sprayed using plasma spraying technique and with addition of 10wt.% alumina into HA, the crystallinity has increased to 78.9% (Singh et al, 2018). Therefore, by adding alumina into HA, an increase of 45% crystallinity was recorded. The HA gets decomposed due to high temperature of flame and cooling rates ($10^6$-$10^8$ k/s) involved in plasma spray is responsible to the formation of α & β tri-calcium phosphate, which are non-apatite phases.

## 4.4 MICROHARDNESS OF AS-SPRAYED AND HEAT-TREATED COATINGS

The microhardness of the annealed and as-sprayed coatings was evaluated at a load of 100g load with dwell period of 10 seconds. The microhardness values are shown in **Fig.4.17.** The column graph representing the microhardness values of different coatings, both as-sprayed and annealed at 700°C, with error bars: The error bars indicate small variations or uncertainty in the microhardness measurements. The HALB coating shows the highest microhardness, especially after annealing at 700°C, indicating enhanced hardness. Annealing generally improves the hardness of all coatings, as reflected in the higher values for the heat-treated samples. The as-sprayed HA coating exhibited an average microhardness of 290.2 HV, indicating a moderate increase in surface hardness. Upon heat treatment at 700°C, the microhardness of the HA coating slightly improved to 340 HV, demonstrating the beneficial effect of annealing on particle bonding and hardness enhancement. However, the improvement is modest, suggesting that pure HA has limitations in achieving significantly higher hardness due to its brittle nature. The HALC coating (HA + 10% micron-sized $Al_2O_3$) showed an improved hardness of 335.5 HV compared to pure HA. The augmentation may be ascribed to the incorporation of micron-sized alumina,

which fortifies the HA matrix. Post-heat treatment, the microhardness of the HALC coating elevated to 415.3 HV, indicating enhanced densification and superior mechanical strength attributable to alumina's capacity to endure elevated temperatures. The HALN coating (HA + 10% nano-sized $Al_2O_3$) demonstrated superior hardness, averaging 370.1 HV. The nano-sized alumina particles enhance hardness by more efficiently filling vacancies and producing a denser covering. Post-heat treatment, the HALN coating exhibited a notable increase in microhardness to 475.1 HV, underscoring the efficacy of nano-alumina in fortifying the coating after annealing. The HALB coating (HA + 5% micron + 5% nano-sized $Al_2O_3$) exhibited the maximum hardness, with an as-sprayed microhardness of 385.2 HV.

The combination of micron- and nano-sized alumina provides optimal reinforcement, enhancing both mechanical strength and toughness. After heat treatment, the HALB coating exhibited the maximum microhardness of 493.5 HV, demonstrating the most effective improvement in hardness due to the synergistic effects of mixed particle sizes and annealing. Plasma spray thermal spray, sputtering, and techniques like sol-gel have been used for the deposition process of coatings (Singh et al, 2018). The formation of undesired phases due to high-temperature involved is enable the coatings to high dissolve rapidly in aqueous environments and are responsible for the degradation of coatings in terms of mechanical strength and biological characteristics. The role of additives has been undermined by the process parameters in these processes. The addition of various reinforcements such as $Al_2O_3$, $ZrO_2$ and $TiO_2$ into HA improves the mechanical strength in addition to the biocompatibility (Liu et al, 2025). The addition of $Al_2O_3$ up to 20% improvement the hardness and toughness of the coating. Similarly, the addition of yttria stabilized zirconia into HA improves the mechanical properties. The $ZrO_2$ addition improves the hardness and toughness of the coating (Yu et al, 2003). The microhardness of the plasma-sprayed pure HA coating has shown a 270 $HV_{0.1}$

The microhardness can be further increased up to 700 HV by blending 40wt.% $Al_2O_3$ into HA**.** In the recent studies on LVOF sprayed coatings, the hardness of the HA was observed around 290 $HV_{0.1}$. The increase is attributed in the LVOF is due to the better inter-splat bonding and melting of the powder particles even at high velocity. The particles coming out of nozzle at high velocity are impacted on the surface and gets deformed properly on the surface, whereas the powders velocity is less in case of plasma spraying. A similar study has revealed about the

LVOF sprayed 40wt% $TiO_2$-reinforced HA coating with the significant increment by 200 % hardness from 274 $HV_{0.1}$ to 820 $HV_{0.1}$. In a study on pure HA and 20 wt.% $SiO_2$-reinforced HA has shown an increase of 70 % bond strength (from 5.5 MPa to 9.4 MPa). The addition of 50 wt.% Ti-6Al-4V in pure HA has also shown an increase of 48 % bond strength (from 18 MPa to 28 MPa) (Lockwood et al, 2008). An increase of 54% in bond strength in pure HA i.e from 28 MPa to 43 MPa has been observed when 30wt.%-alumina was reinforced into HA (Singh et al, 2024).

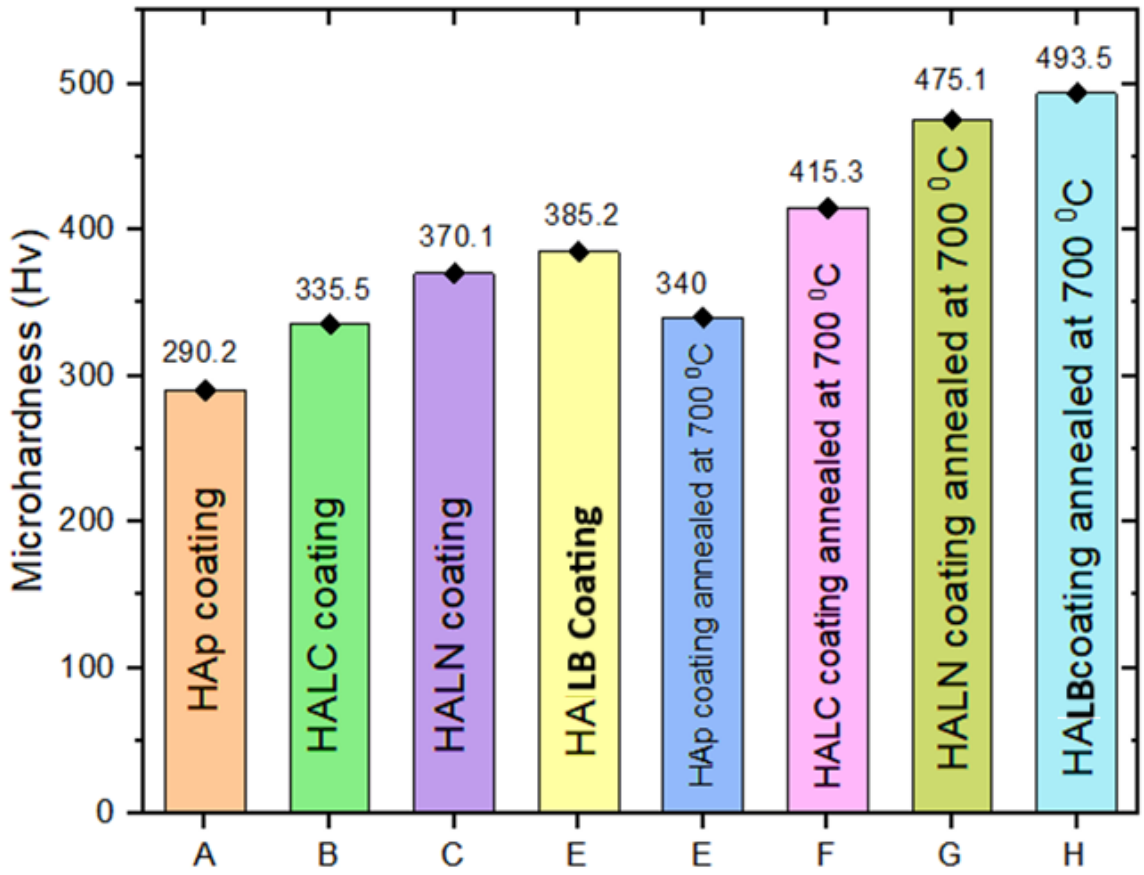


**Fig.4.17.** Microhardness of as-sprayed and heat-treated coatings.

## 4.5 POROSITY ANALYSIS OF AS-SPRAYED AND HEAT-TREATED COATINGS

The porosity values presented show the effect of coating composition and heat treatment on the porosity levels of various hydroxyapatite (HA) and alumina ($Al_2O_3$) composite coatings. Porosity is a key factor in determining the mechanical and biological performance of coatings,

particularly in applications like biomedical implants. The Porosity of as-sprayed and heat-treated coatings are shown in **Fig.4.18.**

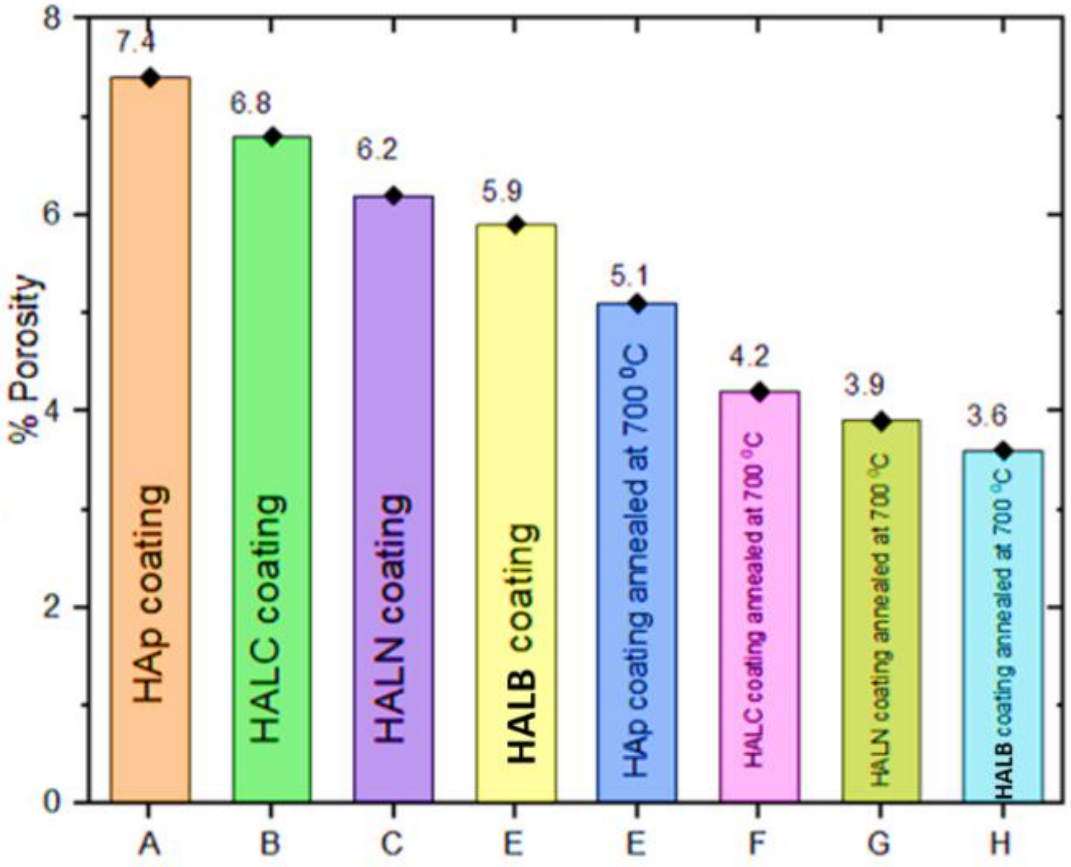


**Fig.4.18.** Porosity of as-sprayed and heat-treated coatings.

The as-sprayed HA coating shows the highest porosity (7.4%). Hydroxyapatite is a bioactive material, but it is inherently porous when sprayed. While porosity can enhance biological integration by promoting tissue in-growth, high porosity weakens mechanical strength, making it more susceptible to cracking and degradation.

The introduction of conventional alumina (HALC) reduces the porosity slightly (6.8%) compared to pure HA. Alumina improves the mechanical strength and wear resistance of the coating, which likely leads to reduced porosity by filling the gaps in the HA matrix and enhancing the coating's densification. The addition of nano-alumina (HALN) results in further porosity reduction (6.2%). Nano-sized alumina particles have a larger surface area, allowing for better packing and filling of pores within the HA matrix, leading to a denser structure. The

combination of both conventional and nano-alumina (HALB) achieves the lowest porosity among the as-sprayed coatings (5.9%). The combined effect of different particle sizes helps minimize porosity, enhancing both the mechanical properties and durability of the coating.

Heat treatment at 700°C generally reduces porosity across all coatings due to the sintering and densification effects. During annealing, particles fuse better, reducing gaps and closing pores. However, the extent of porosity reduction varies depending on the composition of the coating. After annealing, the porosity of HA drops from 7.4% to 5.1%. Heat treatment helps reduce porosity by enhancing particle bonding, but pure HA still retains significant porosity due to its inherent brittleness and less dense microstructure. The porosity in the annealed HALC coating decreases to 5.1%. Alumina, being more heat-resistant, sinters more effectively during the annealing process, further reducing porosity and increasing the coating's density and mechanical strength. The porosity of HALN drops significantly to 3.9%. Nano-alumina particles are particularly effective in reducing porosity during heat treatment due to their ability to compact more densely, allowing for a stronger, more uniform coating. The lowest porosity is observed in the HALB annealed coating, where it drops to 3.6%. This is because the combination of both conventional and nano-alumina enhances sintering during annealing, reducing porosity to the maximum extent. The presence of alumina particles of varying sizes ensures better packing and higher densification, improving mechanical integrity while maintaining good coating properties. The pure HA plasma sprayed coatings have shown a porosity of 8.6 %, whereas upon addition of 10 wt.% alumina in HA revealed a porosity of 3.86%, thereby 50% decrease in porosity level. (Tsui et al, 2015). In the initial stage of the use of LVOF spraying technique, two studies were reported for the biomedical implant coatings (Tiwari et al, 2021). The studies have shown the decrease in the porosity (from 8.6 to 6.5 %) of HA coatings by 25 % as the plasma sprayed HA coatings involves the formation of bigger splats and weak splat interfaces (Tailor et al, 202). Moreover, the high density of the reinforcements ($Al_2O_3$ and $TiO_2$) hydroxyapatite is responsible for the decrease in the porosity. In another study on LVOF sprayed coatings, the same trend of the decreased porosity (from 6.4% to 4.7%) was shown by pure HA and $TiO_2$-reinforced HA for the porosity. The addition of reinforcement and use of LVOF spraying technique has shown the decreased porosity, thereby increased coatings corrosion resistance.

## 4.6 SUMMARY

The examination of four Low Velocity Oxy-Fuel (LVOF) sprayed coatings—pure hydroxyapatite, hydroxyapatite with 10% alumina, hydroxyapatite with 10% nano-alumina, and hydroxyapatite with a blend of 5% micrometric alumina and 5% nano-alumina—demonstrates unique microstructural and compositional characteristics via SEM, EDS, and XRD methodologies. After the annealing at 700°C for 2 hours, there are considerable changes in the SEM photos of the coatings. These results support the fact that hydroxyapatite coating appears as thicker, tubular structures do not turn out to be extendable much and therefore not affect much on stacking failure of catilage cut surfaces. The hydroxyapatite with 10% alumina coated revealed the microstructure to be much heterogeneous which is due to some degree of dispersant alumina particle existing inside the matrix thereof assisting in a better covering density and tensile strength. The surface of the hydroxyapatite + 10 wt.% nano-alumina coating is flatter and more compact, showing less maintain cracking because of an increased toughness originating from the nanosized particles spread uniformly throughout it. The biocomposite coating based on unreactive laser-induced phase separation containing 5% micrometric + 5% nano-alumina has a complex, multiple-scale architecture with the mechanical reinforcing action of both micrometric and nano-alumina, resulting in the hardness and fracture toughness improvements. The XRD patterns of the coatings clearly show the crystalline phases, and each modification presents different peaks related to hydroxyapatite and alumina phases which confirms that the expected phase was reached as well as its crystallinity. The employment of different analytical techniques sheds light on the improved mechanical properties and bioactivity of the coatings, paving their way toward biomedical applications requiring strength alongside compatibility. SEM inspection of the four coatings shows that annealing 4 hours at 700°C has refined the grain, increased density and improved interfacial adhesion.

Each of these coatings has unique features on account of its material composition. The grain size of the pure hydroxyapatite coating revealed to be higher with a low porosity, in comparison. The number of vacancies is decreased as a result of mechanical reinforcement with use of 10% alumina coating and combined with hydroxyapatite. The grain size of hydroxyapatite combined with 10% nano-alumina coating is reduced, and its toughness increased. The three-dimensional dense composite structured coating is composed of hydroxyapatite developed with 5%

micrometric alumina, and up to 5% nano-alumina at the micro and nanometer scales. Annealing accelerates the results that can be obtained by these coatings, thereby improving their performance and making them ideal for biomedical applications requiring both bioactivity and mechanical strength.

The SEM micrographs of the annealed Low Velocity Oxyfuel (LVOF) sprayed coatings, on SS-254 surgical steel defined individual surface characteristics pertaining to each composition. The Hydroxyapatite (HaP) coating shows a mixed phase of molten and partially molten particles resulting in an open cell structure. In addition, the HaP + 10% $Al_2O_3$ coating with the addition of micron-sized alumina has a more uniform surface; but un-melted particles are visible in this composition, which indicates not complete melting due to lower energy input by LVOF method. The microstructure of the HaP + 10% $Al_2O_3$ (nano-sized) coating shows more homogeneously and denser morphology, due to less unmelted particles that have resulted in better melting as well as even dispersion of nano-sized alumina throughout the hydroxyapatite matrix. Apparently, this nanoscale enhancement appears to diminish porosity while augmenting the coating's smoothness. The hybrid coating of hydroxyapatite with 5% micron-sized alumina and 5% nano-sized alumina creates a synergy between the two particle scales. SEM images reveal a surface with both fully and partially melted particles, leading to a more complex surface structure. Micron-sized alumina improves mechanical stability, while nano-sized alumina enhances surface smoothness and promotes densification. The addition of alumina, particularly in the nanoscale, transitions the surface from porous in pure hydroxyapatite to a more compact and uniform structure, which significantly impacts the coating's thermal and mechanical properties. The coating with 5% micron-sized and 5% nano-sized alumina exhibits superior microstructural characteristics compared to other compositions. The combination of both particle sizes improves surface morphology, with the micron-sized particles reinforcing mechanical strength and wear resistance, while the nano-sized particles fill gaps between larger particles, resulting in a denser and smoother coating. This distribution reduces the presence of unmelted or partially melted particles, improving adhesion and surface uniformity, making it the most promising option for enhanced mechanical performance and durability.

## CHAPTER 5

# IN-VITRO BIOCOMPATIBILITY STUDY AND CORROSION BEHAVIOUR OF THE BASE METAL (SS-31254) AND SURFACE MODIFIED SPECIMENS AT ALL CONDITIONS

The experiments described in this chapter have been undertaken to investigate the various corrosion behaviour and biocompatibility of uncoated SS-31254 and coated specimens under all conditions in Ringer's solution which simulates the human body fluid. All the time the corrosion susceptibility of uncoated SS-31254 and microwave-assisted surface modified specimens was assessed by using the Polarization approach. The final results of the FE-SEM/EDS examination of the test materials are summarized

## 5.1 IN-VITRO STUDY FOR HA SURFACE MODIFIED SPECIMENS FOR AS-DEPOSITED CONDITIONS

Fig. 5.1 represents the surface morphology and elemental composition of specific hydroxyapatite (HA) coatings and their alumina ($Al_2O_3$) composites, captured using scanning electron microscopy (SEM) coupled with energy-dispersive X-ray spectroscopy (EDS). Fig. 5.1(a) shows the SEM image of the HA coating, revealing a porous structure characterized by surface cavities.

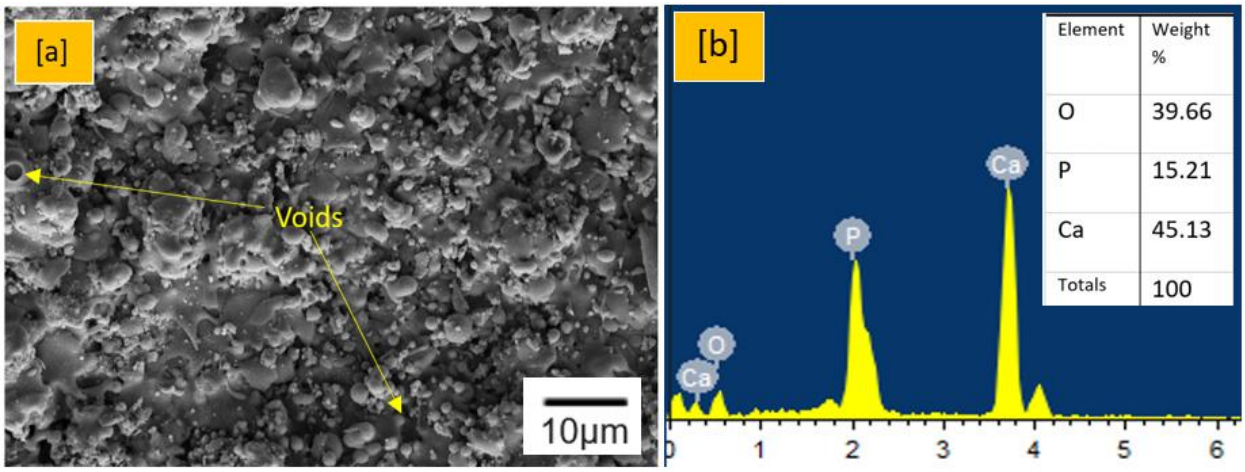


**Fig. 5.1.** (a)Corrosion analysis of surface as-sprayed **HA** coating and, (b) corresponding EDS.

These pores are inherent to HA and play a fundamental role in biomedical applications by facilitating cell adhesion and proliferation within the matrix, which is essential for effective osseointegration in implant devices (Zhang et al., 2020; Kumar et al., 2019).

While porosity enhances biological integration, it can compromise the mechanical integrity of the coating. Fig. 5.1(b) displays the EDS spectrum of the HA coating, indicating a high concentration of oxygen (O), phosphorus (P), and calcium (Ca)—the principal constituents of

hydroxyapatite ($Ca_{10}(PO_4)_6(OH)_2$). The observed Ca/P atomic ratio is critical, as it directly influences the coating's bioactivity and resorption behavior (Lee et al., 2018; Singh et al., 2021). The surface morphology reveals the presence of larger, denser particles embedded within the HA matrix, along with distinct whisker-like structures. These whisker-like features are likely alumina ($Al_2O_3$) particles integrated into the hydroxyapatite matrix, which contribute to enhanced wear resistance and increased hardness of the coating (Chen et al., 2020; Patel et al., 2019). This hybrid structure improves the mechanical strength of the coating while maintaining the inherent bioactivity of hydroxyapatite, a key requirement for load-bearing biomedical applications. **Fig. 5.2(b)** displays the EDS spectrum, which shows an additional peak corresponding to aluminum (Al), confirming the successful incorporation of alumina. The measured weight percentages of oxygen (O), phosphorus (P), calcium (Ca), and aluminum (Al) further support the effective integration of alumina into the HA matrix (Liu et al., 2021). The HA–alumina composite thus offers a balanced enhancement of both mechanical properties and biological performance, making it suitable for orthopedic and dental implants (Wang et al., 2018).

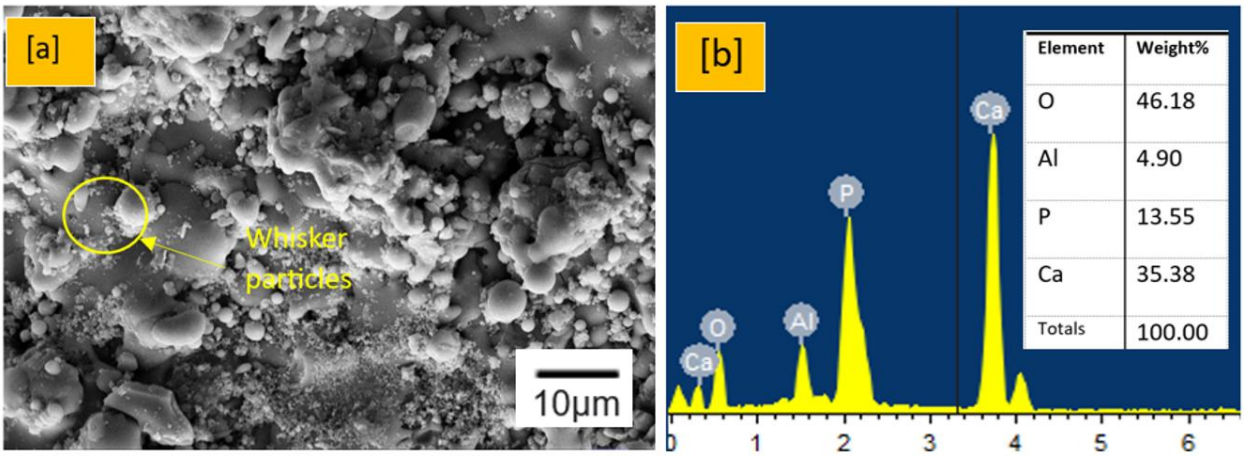


**Fig. 5.2.** (a)Corrosion analysis of surface as-sprayed **HALC** coating and, (b) corresponding EDS.

**Fig. 5.3(a)** shows the SEM image of the HA combined with nano-alumina particles (HALN). This coating exhibits a smoother surface morphology compared to the conventional alumina, likely due to the finer nano-sized alumina particles.

The nano-sized particles increase surface area, which could improve the coating's mechanical properties, such as toughness and wear resistance. **Fig. 5.3(b)** displays the EDS spectrum for

HALN, again showing the presence of O, P, Ca, and Al. The inclusion of nano-alumina leads to a more uniform dispersion of particles, which is beneficial for mechanical strength and may also reduce the brittleness typically associated with HA coatings.

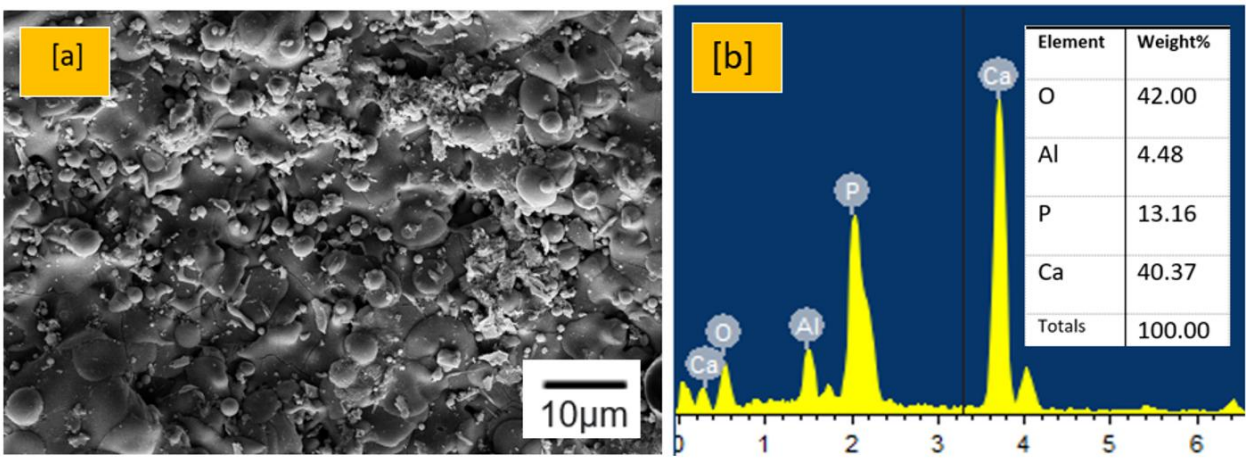


**Fig. 5.3.** (a)Corrosion analysis of surface as-sprayed HALN coating and, (b) corresponding EDS.

**Fig. 5.4(a)** presents the SEM image of the HALB coating, which combines HA with both 5% conventional alumina and 5% nano alumina. This coating appears to have a more granular and uniform surface, benefiting from the combined properties of both conventional and nano-alumina. The granular morphology might indicate a balance between increased mechanical strength and the maintenance of porosity for biological applications. **Fig. 5.4(b)** shows the EDS spectrum for the HALB coating, which reflects a similar elemental composition as the previous coatings with O, P, Ca, and Al.

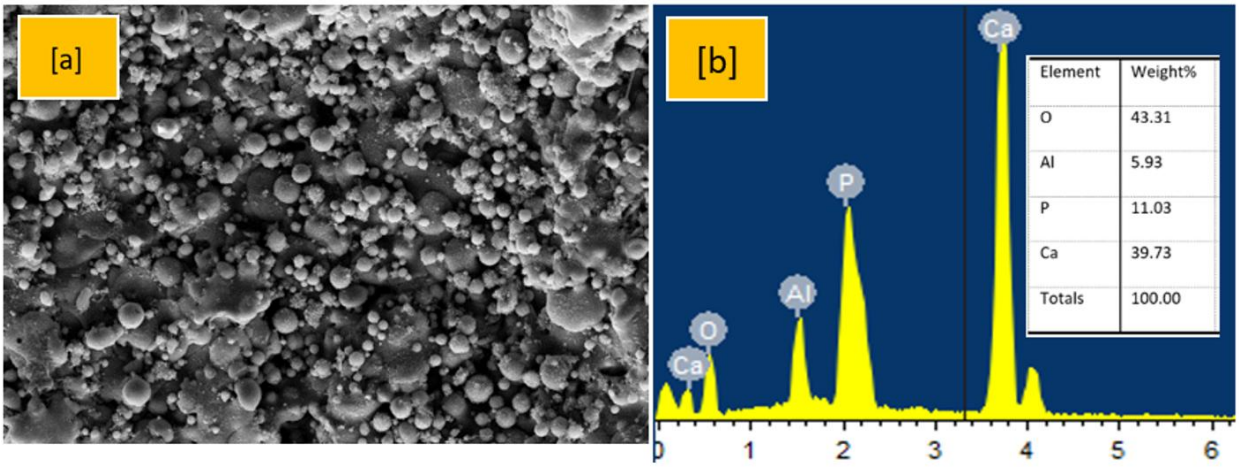


**Fig. 5.4.** (a)Corrosion analysis of surface as-sprayed HALB coating and, (b) corresponding EDS.

The combination of conventional and nano alumina provides a dual advantage: conventional alumina contributes to hardness, while nano-alumina ensures a finer surface finish and enhanced toughness. The dual-phase system is designed to optimize both the mechanical and biological performance of the coating.

The SEM and EDS analyses collectively show how the inclusion of alumina, in both conventional and nano forms, affects the surface morphology and elemental composition of hydroxyapatite-based coatings. These coatings are typically developed for biomedical implants where the bioactivity of HA is combined with the mechanical robustness of alumina to provide improved corrosion resistance, hardness, and overall durability without compromising biocompatibility.

## 5.2 IN-VITRO STUDY FOR HA SURFACE MODIFIED SPECIMENS FOR HEAT-TREATED CONDITIONS

The heat treatment at 700°C likely influenced the coating's grain structure, causing changes in porosity, crack formation, and voids that predispose the coating to corrosion as shown in **Fig. 5.5.**

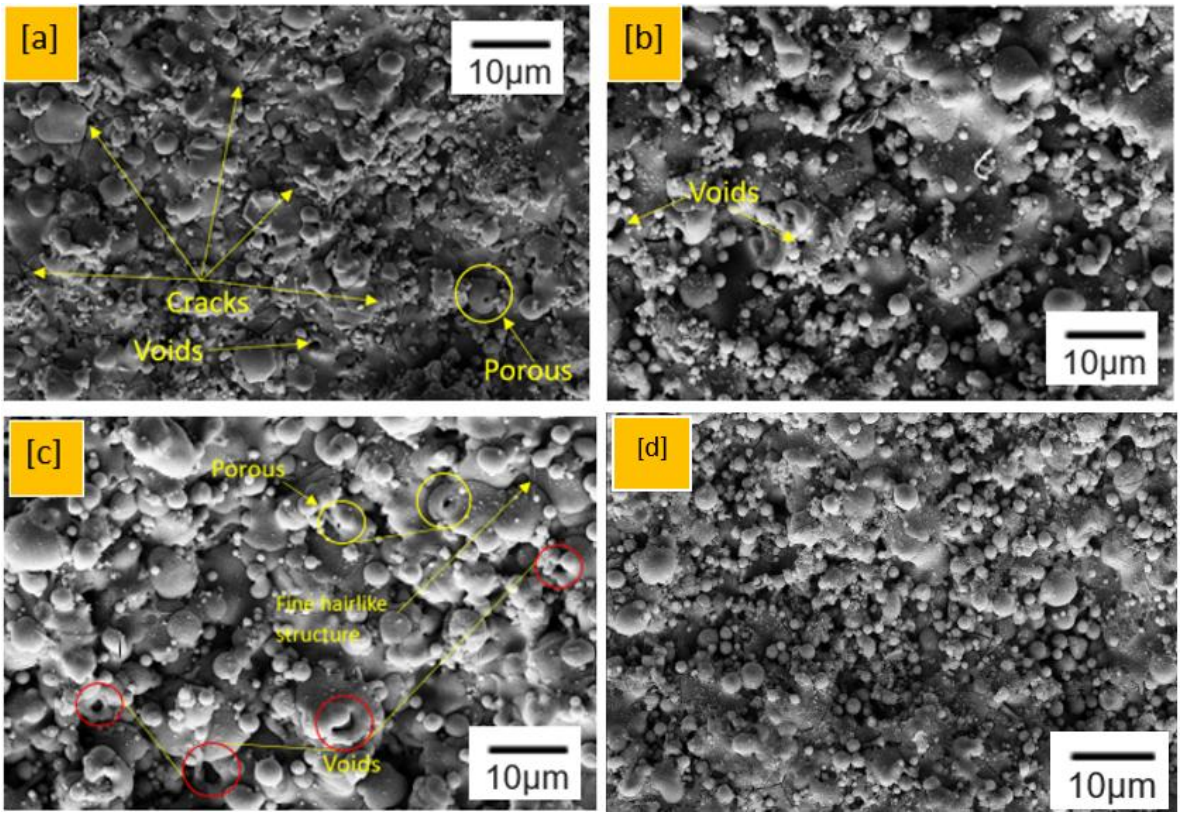


**Fig. 5.5.** Corrosion analysis of heat-treated coating at 700º C.

While the heat treatment can improve the mechanical properties of certain materials, it may also cause microstructural changes, such as grain growth, that negatively impact corrosion resistance. The observed cracks could have originated from thermal stresses, while the voids and porous regions may facilitate corrosion by allowing corrosive agents to penetrate into the coating.

In practical applications, optimizing the balance between mechanical strength and corrosion resistance is crucial. The heat-treated coatings need to maintain enough integrity to resist cracking and corrosion, especially in environments where they will be exposed to both high temperatures and corrosive substances. This study suggests that while heat treatment can improve some properties, it might compromise the coating's resistance to corrosion, depending on the material's microstructure and the conditions it faces. The values of corrosion resistance have been presented in **Table 5.1.**

The corrosion performance of SS-254 surgical steel and various Hydroxyapatite (HaP) coatings, with and without heat treatment, was evaluated using parameters like anodic (ba) and cathodic (bc) Tafel slopes, corrosion potential (Ecorr), corrosion current density (Icorr), and corrosion rate in a simulated body fluid environment. Uncoated 254 SS showed the poorest corrosion resistance, with the most negative corrosion potential (-0.537 V), highest Icorr (1.02 µA/cm²), and a corrosion rate of 0.328 mm/year. These values indicate a high susceptibility to corrosion in the given environment. As-sprayed HA coating provided moderate protection compared to the uncoated steel, reducing the corrosion rate to 0.075 mm/year and lowering Icorr to 0.987 µA/cm². However, the anodic slope (ba = 0.512 V/dec) remained relatively high, indicating ongoing corrosion activity, albeit reduced. HA coating at 700°C 700°C improved the coating's performance. The Ecorr shifted positively to -0.340 V, and both Icorr (0.864 µA/cm²) and the corrosion rate (0.063 mm/year) decreased, indicating enhanced corrosion protection. HALC composite coating provided better corrosion protection than pure HA. It exhibited a more positive Ecorr (-0.293 V), significantly lower Icorr (0.668 µA/cm²), and a reduced corrosion rate of 0.031 mm/year. The heat-treated version (700°C) showed further improvement with the lowest ba (0.128 V/dec), and a corrosion rate of 0.034 mm/year, demonstrating that both $Al_2O_3$ addition and heat treatment effectively enhanced corrosion resistance. HALN showed impressive corrosion resistance with Ecorr of -0.195 V and Icorr of just 0.070 µA/cm², reducing the corrosion rate to 0.032 mm/year. After heat treatment at 700°C, these parameters improved even

further, with Icorr reduced to 0.104 µA/cm² and a corrosion rate of 0.021 mm/year, making it one of the best-performing coatings.

1. Annealed HA coating showed moderate performance, with Ecorr (-0.263 V) and Icorr (0.079 µA/cm²) values comparable to the HALN coating. The corrosion rate (0.029 mm/year) was slightly lower than the as-sprayed HA but higher than the composite coatings.

2. HALB, the combination of micro and nano $Al_2O_3$ particles in HaP offered excellent corrosion resistance, with Ecorr of -0.318 V, Icorr of 0.081 µA/cm², and a corrosion rate of 0.022 mm/year. The heat-treated version further reduced these values, with an Icorr of 0.067 µA/cm² and a remarkably low corrosion rate of just 0.005 mm/year, showing superior corrosion protection.

All coatings improved corrosion resistance compared to uncoated SS-254, the best results were achieved with heat-treated HALN and HALB coatings, indicating that the incorporation of nano-sized alumina particles, particularly after annealing, significantly enhances corrosion performance.

**Table. 5.1.** Corrosion results for SS 254, as-sprayed and heat-treated coatings.

| **Specimen** | **ba(V/dec)** | **bc(V/dec)** | **$E_{corr}$ (bolt)** | **$I_{corr}$(µA/cm²)** | **Corrosion rate(mm/year)** |
|---|---|---|---|---|---|
| **254 SS** | 0.550 | 0.814 | -0.537 | 1.02 | 0.328 |
| **As sprayed HA coating** | 0.512 | 0.941 | -0.436 | 0.987 | 0.075 |
| **HA coating at 700 $^0$C** | 0.446 | 0.785 | -0.340 | 0.864 | 0.063 |
| **HALC coating** | 0.317 | 0.124 | -0.293 | 0.668 | 0.031 |
| **HALC coating at 700 $^0$C** | 0.128 | 0.131 | -0.268 | 0.318 | 0.034 |

| | | | | | |
|---|---|---|---|---|---|
| **HALN coating** | 0.971 | 0.112 | -0.195 | 0.070 | 0.032 |
| **Annealed at 700 $^0$C HALN coating** | 0.599 | 0.130 | -0.222 | 0.104 | 0.021 |
| **Annealed HA coating at 800 $^0$C** | 0.408 | 0.136 | -0.263 | 0.079 | 0.029 |
| **HALB coating** | 0.453 | 0.130 | -0.318 | 0.081 | 0.022 |
| **Annealed at 700 $^0$C HALB coating** | 0.731 | 0.154 | -0.260 | 0.067 | 0.005 |

## 5.3 BIOACTIVITY ANALYSIS

The bioactivity test involved immersing the uncoated, coated (HA, HALC, HALN and HALB), and annealed (700 $^0$C) samples in simulated body fluid (SBF) for 14 days without changing the solution. The FE-SEM images reveal the formation of a bone-like apatite layer **(refer to Figs. 5.6 and 5.7).** Uncoated SS-254 steel showed no weight change and no apatite layer formation, indicating its lack of bioactivity. **Table 5.2** presents the weight change data for the samples. Coatings annealed at 400 °C exhibited the initial formation of calcium phosphate phases and enhanced surface mineralization activity, indicative of an early bioactive response essential for osseointegration. This is consistent with studies showing that moderate annealing improves crystallinity and surface wettability, thereby promoting apatite nucleation (Zhao et al., 2019; Kumar et al., 2020). However, prolonged annealing at 800 °C can lead to phase separation and grain growth, which reduces bioactivity due to the diminished ion exchange capacity (Lee et al., 2018). The incorporation of $Al_2O_3$ nanoparticles modifies the nucleation and ion release kinetics, positively influencing the surface reactivity and bioactive behavior of the coating (Singh et al., 2021). Ion exchange with SBF induces apatite layer formation, which is crucial for successful biomaterial–tissue integration (Wang et al., 2017).

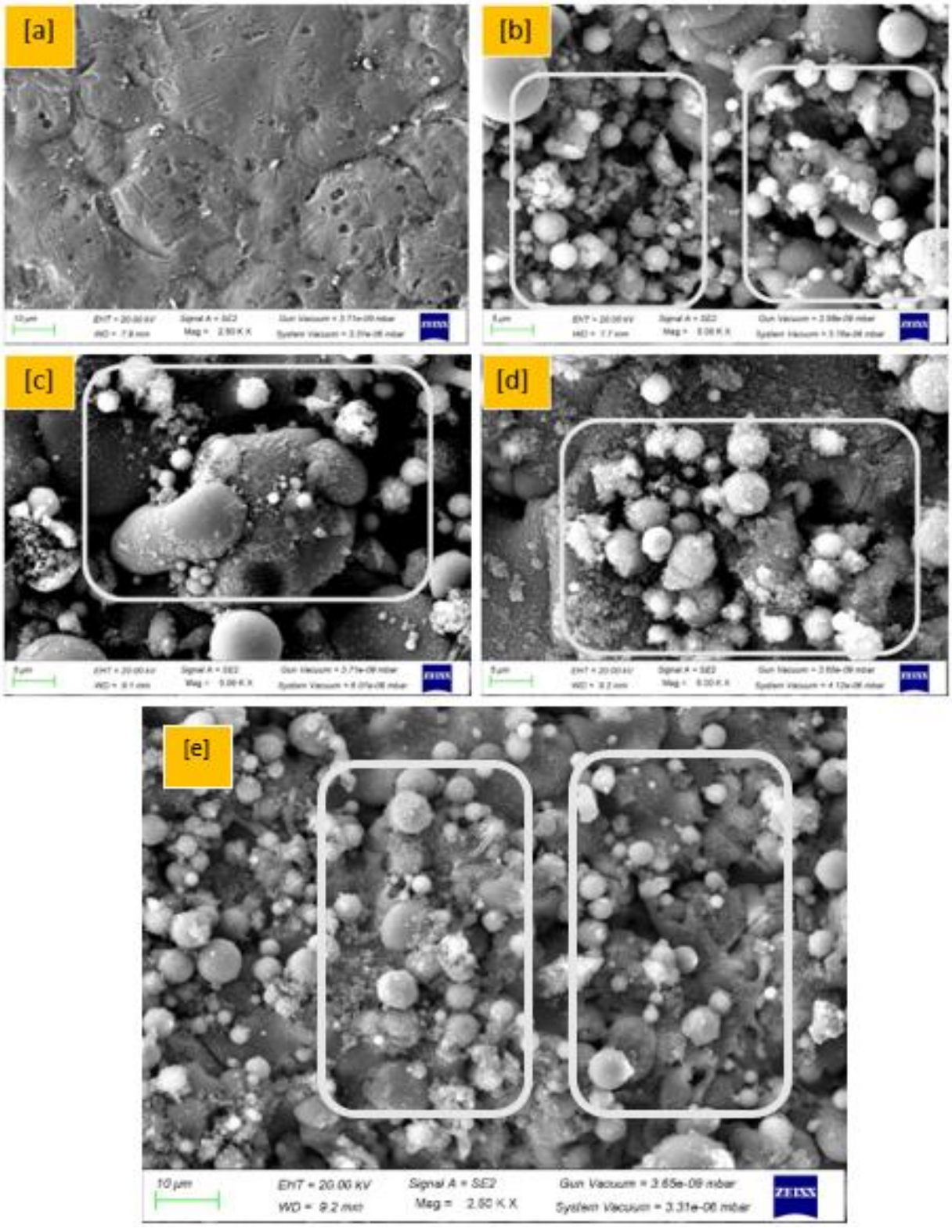


**Fig 5.6**. Apatite layer formation on (a) uncoated substrate (b) coated HA (c) Coated HALM (d) coated HALN and (e) HALB coating

In the case of the HA coating, the formation of α-tricalcium phosphate (α-TCP) and β-tricalcium phosphate (β-TCP) phases may occur concurrently with the development of the apatite layer, which is crucial for enhancing osteoconductivity (Zhao et al., 2019; Kim et al., 2020). **Fig. 5.6** presents the FESEM images showing surface morphologies that confirm the formation of the apatite layer on the coatings and the SEM micrographs of post-treated samples are shown in **Fig. 5.7**.

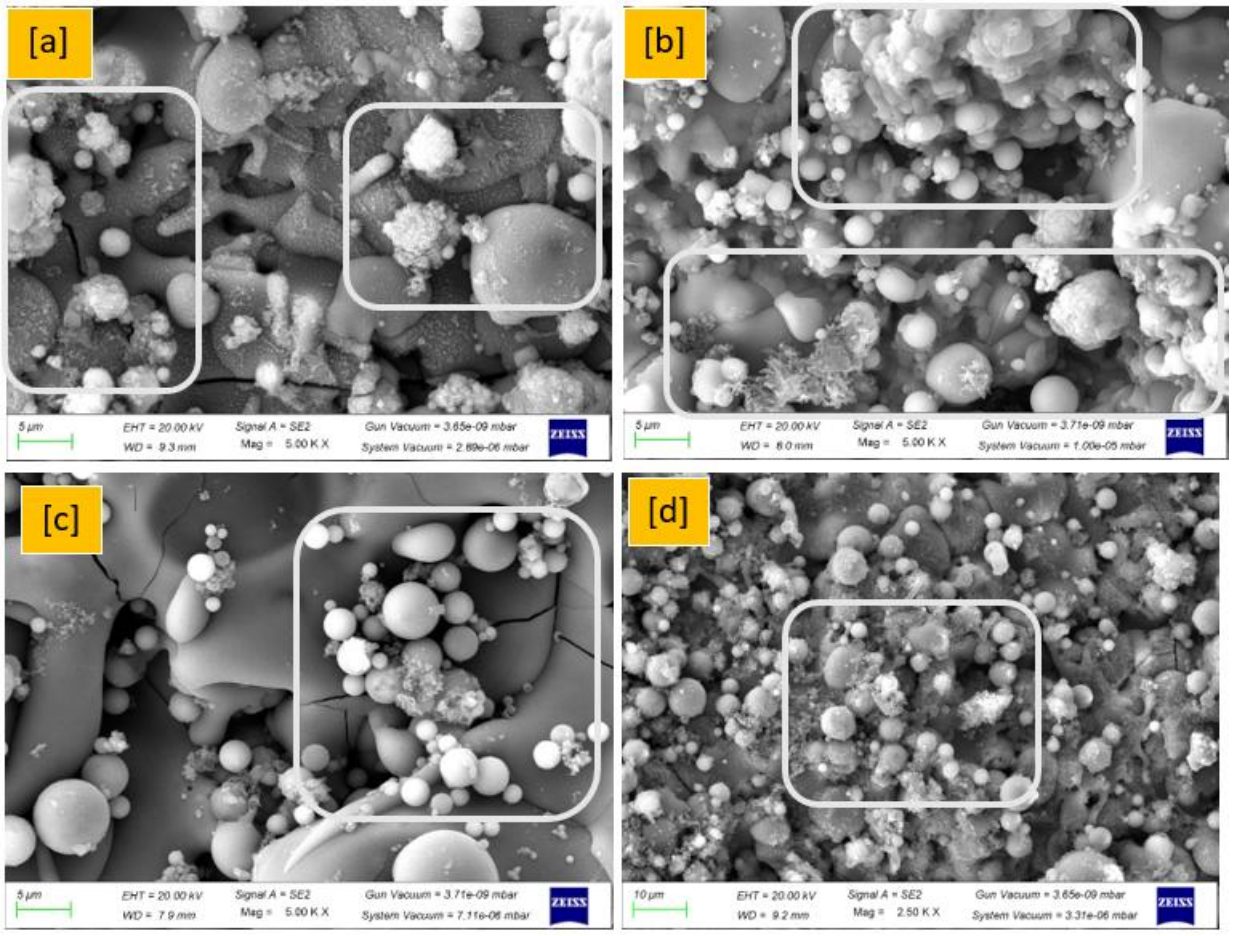


**Fig 5.7**. Apatite layer formation on (a) coated HA (b) Coated HALM (c) coated HALN and (d) HALB coating annealed at 700º C

The micrographs indicate that the capacity for apatite formation increases with higher annealing temperatures, supporting prior findings that thermal treatment improves crystallinity and bioactivity (Liu et al., 2020). As demonstrated by the weight changes in **Table 5**, HALM coatings exhibited reduced bioactivity, likely due to their larger particle size and structural

discontinuities that impede ion exchange and cell adhesion (Patel et al., 2021). In contrast, HALN coatings slightly enhanced bioactivity by promoting greater cell interaction and bone tissue integration. Notably, HALN coatings (**Fig. 5.7**) annealed at 700 °C showed improved bioactivity, attributed to the synergistic effect of nanometric alumina, which increases surface area and enhances cellular response (Wang et al., 2018; Singh et al., 2022).

A bioactivity test was conducted on SS-254 surgical steel and various hydroxyapatite (HaP) coatings to evaluate the formation of a bone-like apatite layer after immersion in simulated body fluid (SBF). The initial and final weights of the samples were measured to assess apatite formation, with weight gain indicating bioactivity. The uncoated SS-254 showed a negligible weight change of only 0.0006 g, signifying no apatite layer formation and confirming its lack of bioactivity (Singh et al., 2019). In contrast, all coated samples exhibited measurable weight gain, indicating their bioactivity and ability to support apatite nucleation and growth (Zhou et al., 2020; Patel et al., 2021). These findings are consistent with prior research demonstrating that hydroxyapatite coatings enhance surface reactivity and promote mineralization in physiological conditions (Li et al., 2018).

Table 5.2 illustrates the weight change for LVOF sprayed and annealed HA, HALM, HALN, and HALB coatings. As-sprayed HaP coating gained 0.20 g weight, which exhibited mild bioactivity. The bioactivity slightly improved after being annealed at 700°C, with a weight gain of 0.24 g (Table 1), indicating the treatment either produced an appetite layer or accelerated its formation on the surface coating surface under SBF action. The annealed and unannealed HALC (HaP + 10% micron-sized $Al_2O_3$) coating had less weight gain, 0.09 vs. 0.13 g however the annealed form showed a higher growth suggesting that the bioactivity may be improved post-heat treatment of this complex plasma sprayed microplasma layered coating against Ca/P rich solutions.Both the HALN (HaP + 10% nano $Al_2O_3$) coating and its heat-treated counterpart showed significant bioactivity with a weight gain of ~0.22 g for the former and 0.26 g for the latter, indicating their ability to produce more apatite compared to micron sized $Al_2O_3$ at the same time intervals. The highest bioactivity was found in the HALB (HaP + 5% micron + 5% nano-sized $Al_2O_3$) coating with weight increases of 0.26 g and after heat treatment at 700°C, displayed the greatest gain of mass equal to 0.28 g. All this confirms that, blending of both

types of alumina, in conjunction with annealing considerably enhances HaP coating's bioactivity.

**Table 5.2** Weight difference of LVOF-sprayed and annealed coatings of HA, HALM, HALN, and HALB.

| **Coated Specimens** | **Initial weight ($W_i$) in g** | **Final weight ($W_f$) in g** | **Weight change ($W_f - W_i$) in g** |
|---|---|---|---|
| SS 254 | 7.7418 | 7.7424 | 0.0006 |
| As sprayed HA | 7.6315 | 7.8314 | 0.20 |
| HA annealed at 700 $^0$C | 7.6681 | 7.90481 | 0.24 |
| HALC | 7.6132 | 7.7026 | 0.09 |
| HALC annealed at 700 $^0$C | 7.7141 | 7.8447 | 0.13 |
| HALN | 7.5624 | 7.7855 | 0.22 |
| HALN annealed at 700 $^0$C | 7.5193 | 7.7806 | 0.26 |
| HALB | 7.6407 | 7.8997 | 0.26 |
| HALB annealed at 700 $^0$C | 7.5121 | 7.7965 | 0.28 |

## 5.4 SUMMARY

This chapter focuses on the corrosion behaviour of uncoated SS-31254 stainless steel and various surface-modified specimens coated with hydroxyapatite (HA) and HA-alumina ($Al_2O_3$) composites under simulated physiological conditions using Ringer's solution. Corrosion analysis was performed through electrochemical polarization testing, and microstructural observations were made using FE-SEM and EDS.

**Figures 5.1 to 5.4** display the SEM and EDS images of as-sprayed coatings: pure HA (**Fig. 5.1**), HA + conventional alumina (HALC, **Fig. 5.2**), HA + nano-alumina (HALN, **Fig. 5.3**), and HA +

hybrid alumina (HALB, **Fig. 5.4**). The coatings exhibited varying porosities, grain distributions, and elemental compositions. The HA coating was porous and bioactive, while alumina-reinforced variants displayed denser, more structured morphologies. Heat-treated coatings at 700 °C (**Fig. 5.5**) showed crack formation and microstructural changes, which influenced corrosion behaviour. **Table 5.1** outlines electrochemical data for all specimens. Uncoated SS-254 exhibited the poorest corrosion resistance (Ecorr = –0.537 V, Icorr = 1.02 µA/cm², corrosion rate = 0.328 mm/year). As-sprayed HA showed improved performance, with a corrosion rate of 0.075 mm/year.

HALC coatings (with 10% micron-sized $Al_2O_3$) further improved resistance (corrosion rate = 0.031 mm/year), and post-annealing at 700 °C slightly enhanced the results (0.034 mm/year). HALN coatings (with 10% nano-$Al_2O_3$) demonstrated excellent corrosion resistance (0.032 mm/year as-sprayed, 0.021 mm/year after annealing). HALB coatings, combining 5% micron + 5% nano-$Al_2O_3$, showed the best performance, with an as-sprayed corrosion rate of 0.022 mm/year and just 0.005 mm/year after heat treatment.

The bioactivity of all specimens was evaluated by immersing them in simulated body fluid (SBF) for 14 days and observing the formation of bone-like apatite layers through SEM imaging (**Figs. 5.6 and 5.7**) and weight gain measurements (**Table 5.2**). The uncoated SS-254 showed negligible weight gain (0.0006 g), confirming its non-bioactive nature. In contrast, the HA-coated samples exhibited notable apatite formation. The as-sprayed HA coating gained 0.20 g, and after annealing at 700 °C, the weight increased to 0.24 g, indicating enhanced bioactivity due to improved microstructural densification.

HALC coatings showed moderate bioactivity with weight gains of 0.09 g (as-sprayed) and 0.13 g (annealed). HALN coatings were more effective, with 0.22 g and 0.26 g for as-sprayed and annealed conditions, respectively. The HALB coatings exhibited the highest bioactivity: 0.26 g (as-sprayed) and 0.28 g after 700 °C heat treatment. This improvement is attributed to the synergistic effect of both micro and nano-sized alumina particles enhancing surface reactivity and apatite nucleation. SEM images (**Figs. 5.6 and 5.7**) supported these findings, showing dense, nodular apatite structures on the HALB surface post-treatment, affirming the coating's superior biological integration potential.

# CHAPTER 6

# CONCLUSIONS AND FUTURE SCOPE

The metallic materials in a pure or alloy form are widely applied as bio-implants in human body for several clinical applications due to their excellent mechanical properties and reasonable biocompatibility. Research and development on metallic biomaterials has shown that surface coating/ modifications of metallic implants by using a suitable bioactive material is a widely accepted alternative to minimize the harmful effects of corrosion.

In the present research work, a microwave assisted surface modifications has been used in metallic implants (SS-31254) by using hydroxyapatite (HA) coatings. SS-31254 is a widely used material in clinical applications. However, it has poor biocompatibility when these materials are actually used in the human body system. Therefore, the surface layer of SS-31254 was modified with bioactive HA powder by using LVOF technique. Because the HA coatings is very brittle in nature. Therefore, the effect of additions of reinforcement ($Al_2O_3$ by weight in 10%) in HA in suitable amount has also been discussed. The effect of heat-treatment on the microwave surface modified samples at all conditions at 700$^o$ C has also been described.

## 6.1 CONCLUSIONS

Based upon experimental results obtained and its analysis in the present work, the following conclusions have been drawn:

1. It is feasible to modify the surface properties of SS-31254 using bioactive powders such as HA and HA reinforced with 10 wt% $Al_2O_3$ (micron and nano-sized) through the Low-Velocity Oxy-Fuel (LVOF) technique. The LVOF process provides high particle velocities at relatively low flame temperatures, which minimizes thermal decomposition of hydroxyapatite and allows better retention of bioactive phases during deposition.

2. Surface modification using HA, HALC (HA + 10 wt% micron-sized $Al_2O_3$), HALN (HA + 10 wt% nano-sized $Al_2O_3$), and HALB (HA + 5 wt% micron + 5 wt% nano $Al_2O_3$) was effectively carried out using LVOF. The use of both micro- and nano-scaled reinforcements enables control over coating density, thermal conductivity, and mechanical properties due to differential particle behavior during spraying.

3. The coating-substrate system exhibited a strong mechanical bond without significant interfacial cracking or delamination, as confirmed by cross-sectional SEM. This is attributed to the high kinetic energy of particles in LVOF, which facilitates good inter-particle cohesion and mechanical interlocking with the substrate surface, enhancing adhesion strength.

4. All coatings, both as-sprayed and post-treated at 700 °C for 2 hours, showed improved mechanical properties due to the transformation of the amorphous matrix into a more crystalline phase. Direct aging promotes nucleation and growth of stable crystalline phases, improving hardness, residual stress relaxation, and crack resistance.

5. XRD analysis revealed the presence of α- and β-tricalcium phosphates (TCP) and octacalcium phosphate (OCP) in the coatings. The reduction of amorphous content and peak sharpening after heat treatment indicates stress relief and enhanced crystallinity, contributing to phase stability and improved corrosion resistance.

6. Porosity measurements demonstrated that the as-sprayed HA coating had the highest porosity (7.4%), which was significantly reduced by alumina addition in HALC (6.8%), HALN (6.2%), and HALB (5.9%). This is due to better particle packing and densification facilitated by the incorporation of $Al_2O_3$. Post-deposition annealing further decreased porosity (down to 3.6% in HALB) by sintering necks and sealing open pores, which enhances corrosion resistance and mechanical strength.

7. Microhardness results confirmed that the reinforcement with $Al_2O_3$ improves the hardness of the coatings, with HALC (335.5 HV), HALN (370.1 HV), and HALB (493.5 HV) outperforming the pure HA coating (290.2 HV). The highest hardness in annealed HALB coatings (493.5 HV) is attributed to solid particle strengthening, grain refinement, and reduced porosity, which collectively increase resistance to plastic deformation.

8. Electrochemical corrosion testing showed a significant improvement in corrosion resistance for all coatings. Uncoated SS-254 exhibited a high corrosion rate (0.328 mm/year), while coatings like HALC (0.031 mm/year), HALN (0.032 mm/year), and HALB (0.022 mm/year) demonstrated lower corrosion rates due to enhanced barrier properties. Post-heat treatment, HALN (0.021 mm/year) and HALB (0.005 mm/year)

showed further improvement, attributed to reduced porosity, better phase stability, and refined microstructure.

9. Bioactivity tests in simulated body fluid (SBF) revealed apatite layer formation on all coated samples. The weight gain observed-0.20 g (HA), 0.22 g (HALN), and 0.26 g (HALB), with annealed HALB showing the highest (0.28 g)-confirms superior bioactivity. The enhanced ion-exchange kinetics and high surface area of nano-alumina in HALN and HALB promote nucleation of calcium phosphate, accelerating osseointegration potential.

## 6.2 SCOPE FOR FUTURE WORK

The present investigation opens up several opportunities for future work. Some of scopes can be summarised as follows:

1. Nano HA powder could be used instead of micron sized HA based powder and results can be compared.

2. The other techniques such as laser cladding can be used for the fabrication of coatings.

3. The in-vivo test of the surface modified SS-31254 may also performed for used in actual applications.

4. A unique novel futuristic method of surface modification via electrical discharge machining (EDM) can be used for the processing of biomaterials.

## BIBLIOGRAPHY


1. Awasthi, S., Pandey, S.K., Arunan, E. and Srivastava, C., 2021. A review on hydroxyapatite coatings for the biomedical applications: Experimental and theoretical perspectives. *Journal of Materials Chemistry B*, *9*(2), pp.228-249.
2. Balamurugan, A., Kannan, S. and Rajeswari, S., 2002. Bioactive sol-gel hydroxyapatite surface for biomedical applications--in vitro study. *Trends in Biomaterials and Artificial Organs*, *16*(1), p.18-21.
3. Balani, K., Anderson, R., Laha, T., Andara, M., Tercero, J., Crumpler, E. and Agarwal, A., 2007. Plasma-sprayed carbon nanotube reinforced hydroxyapatite coatings and their interaction with human osteoblasts in vitro. *Biomaterials*, *28*(4), pp.618-624.
4. Balla, V.K., Das, M., Bose, S., Ram, G.J. and Manna, I., 2013. Laser surface modification of 316 L stainless steel with bioactive hydroxyapatite. *Materials Science and Engineering: C*, *33*(8), pp.4594-4598.
5. Bansal, A. and Zafar, S., 2017. Influence of heat treatment on microstructure and mechanical properties of Inconel-625 clad deposited on mild steel.
6. Bauer, S., Schmuki, P., Von Der Mark, K. and Park, J., 2013. Engineering biocompatible implant surfaces: Part I: Materials and surfaces. *Progress in Materials Science*, *58*(3), pp.261-326.
7. Beheri, H.H., Mohamed, K.R. and El-Bassyouni, G.T., 2013. Mechanical and microstructure of reinforced hydroxyapatite/calcium silicate nano-composites materials. *Materials and Design*, *44*, pp.461-468.
8. Bellucci, D., Veronesi, E., Strusi, V., Petrachi, T., Murgia, A., Mastrolia, I., Dominici, M. and Cannillo, V., 2019. Human mesenchymal stem cell combined with a new strontium-enriched bioactive glass: An ex-vivo model for bone regeneration. *Materials*, *12*(21), p.3633.
9. Bergant, Z. and Grum, J., 2009. Quality improvement of flame sprayed, heat treated, and remelted NiCrBSi coatings. *Journal of thermal spray technology*, *18*(3), pp.380-391.
10. Bergant, Z., Trdan, U. and Grum, J., 2014. Effect of high-temperature furnace treatment on the microstructure and corrosion behavior of NiCrBSi flame-sprayed coatings. *Corrosion Science*, *88*, pp.372-386.

11. Bergmann, C.P. and Vicenzi, J., 2011. Protection against erosive wear using thermal sprayed cermet: a review. *Protection against Erosive Wear Using Thermal Sprayed Cermet*, pp.1-77.
12. Birks, N., Meier, G.H. and Pettit, F.S., 2006. *Introduction to the high temperature oxidation of metals*. Cambridge university press.
13. Bolelli, G., Lusvarghi, L. and Barletta, M., 2008a. Heat treatment effects on the corrosion resistance of some HVOF-sprayed metal alloy coatings. *Surface and Coatings Technology*, *202*(19), pp.4839-4847.
14. Bolelli, G., Lusvarghi, L. and Giovanardi, R., 2008b. A comparison between the corrosion resistances of some HVOF-sprayed metal alloy coatings. *Surface and Coatings Technology*, *202*(19), pp.4793-4809.
15. Boulos, M.I., Fauchais, P.L. and Heberlein, J.V., 2021. *Thermal spray fundamentals: from powder to part*. Springer International Publishing.
16. Calvarin, G., Molins, R. and Huntz, A.M., 2000. Oxidation mechanism of Ni—20Cr foils and its relation to the oxide-scale microstructure. *Oxidation of Metals*, *53*(1), pp.25-48.
17. Campo, M., Carboneras, M., López, M.D., Torres, B., Rodrigo, P., Otero, E. and Rams, J., 2009. Corrosion resistance of thermally sprayed Al and Al/SiC coatings on Mg. *Surface and Coatings Technology*, *203*(20-21), pp.3224-3230.
18. Carlisle, E.M., 1970. Silicon: a possible factor in bone calcification. *Science*, *167*(3916), pp.279-280.
19. Chatha, S.S., Sidhu, H.S. and Sidhu, B.S., 2013. High-temperature behavior of a NiCr-coated T91 boiler steel in the platen superheater of coal-fired boiler. *Journal of thermal spray technology*, *22*(5), pp.838-847.
20. Chatha, S.S., Sidhu, H.S. and Sidhu, B.S., 2016. Performance of 75Cr3C2-25NiCr coating produced by HVOF process in a coal-fired thermal power plant. In *Advanced Materials Research* (Vol. 1137, pp. 88-100). Trans Tech Publications Ltd.
21. Chatterjee, U.K., Bose, S.K. and Roy, S.K., 2001. *Environmental degradation of metals: corrosion technology series/14*. CRC Press.
22. Chen, H., Zhang, E. and Yang, K., 2014. Microstructure, corrosion properties and bio-compatibility of calcium zinc phosphate coating on pure iron for biomedical application. *Materials Science and Engineering: C*, *34*, pp.201-206.

23. Chen, Y., Xu, Z., Smith, C. and Sankar, J., 2014. Recent advances on the development of magnesium alloys for biodegradable implants. *Acta biomaterialia*, *10*(11), pp.4561-4573.
24. Chen, Y., Zhang, T.H., Gan, C.H. and Yu, G., 2007. Wear studies of hydroxyapatite composite coating reinforced by carbon nanotubes. *Carbon*, *45*(5), pp.998-1004.
25. Chou, B.Y. and Chang, E., 2002. Plasma-sprayed hydroxyapatite coating on titanium alloy with ZrO2 second phase and ZrO2 intermediate layer. *Surface and Coatings Technology*, *153*(1), pp.84-92.
26. Ctibor, P., Lechnerová, R. and Beneš, V., 2006. Quantitative analysis of pores of two types in a plasma-sprayed coating. *Materials Characterization*, *56*(4-5), pp.297-304.
27. Daram, P. and Banjongprasert, C., 2020. The influence of post treatments on the microstructure and corrosion behavior of thermally sprayed NiCrMoAl alloy coating. *Surface and Coatings Technology*, *384*, p.125166.
28. Das, A. and Shukla, M., 2019. Surface morphology, bioactivity, and antibacterial studies of pulsed laser deposited hydroxyapatite coatings on stainless steel 254 for orthopedic implant applications. *Proceedings of the Institution of Mechanical Engineers, Part L: Journal of Materials: Design and Applications*, *233*(2), p.120-127.
29. Davis, J.R. ed., 2004. *Handbook of thermal spray technology*. ASM international.
30. Deb, D., Iyer, S.R. and Radhakrishnan, V.M., 1996. A comparative study of oxidation and hot corrosion of a cast nickel base superalloy in different corrosive environments. *Materials Letters*, *29*(1-3), pp.19-23.
31. Dehnavi, F., Eslami, A. and Ashrafizadeh, F., 2017. A case study on failure of superheater tubes in an industrial power plant. *Engineering Failure Analysis*, *80*, pp.368-377.
32. Delaunay, F., Berthier, C., Lenglet, M. and Lameille, J.M., 2000. SEM-EDS and XPS studies of the high temperature oxidation behaviour of Inconel 718. *Microchimica Acta*, *132*(2), pp.337-343.
33. Deng, K., Shi, J., Wang, C., Wang, X., Wu, Y., Nie, K. and Wu, K., 2012a. Microstructure and strengthening mechanism of bimodal size particle reinforced magnesium matrix composite. *Composites Part A: Applied Science and Manufacturing*, *43*(8), pp.1280-1284.
34. Deng, K.K., Wang, X.J., Wang, C.J., Shi, J.Y., Hu, X.S. and Wu, K., 2012b. Effects of bimodal size SiC particles on the microstructure evolution and fracture mechanism of AZ91 matrix at room temperature. *Materials Science and Engineering: A*, *553*, pp.74-79.

35. Deuerling, C., Maguhn, J., Nordsieck, H., Benker, B., Zimmermann, R. and Warnecke, R., 2009. Investigation of the mechanisms of heat exchanger corrosion in a municipal waste incineration plant by analysis of the raw gas and variation of operating parameters. *Heat transfer engineering*, *30*(10-11), pp.822-831.
36. Doleker, K.M., Odabas, O., Ozgurluk, Y., Askerov, H. and Karaoglanli, A.C., 2019. Effect of high temperature oxidation on Inconel 718 and Inconel 718/YSZ/Gd2Zr2O7. *Materials Research Express*, *6*(8), p.086456.
37. Dooley, R. and Wiertel, E., 2009, January. A survey of erosion and corrosion resistant materials being used on boiler tubes in waste to energy boilers. In *North American Waste-to-Energy Conference* (Vol. 48807, pp. 37-41).
38. Eliaz, N., Shemesh, G. and Latanision, R.M., 2002. Hot corrosion in gas turbine components. *Engineering failure analysis*, *9*(1), pp.31-43.
39. Fathi, M.H., Salehi, M.A.H.D.I., Saatchi, A., Mortazavi, V. and Moosavi, S.B., 2003. In vitro corrosion behavior of bioceramic, metallic, and bioceramic–metallic coated stainless steel dental implants. *Dental materials*, *19*(3), p.188-198.
40. Fontana, M.G., Corrosion Engineering, 3rd ed., McGraw-Hill Book Company, New York, (1987).
41. Frazier, W.E., 2014. Metal additive manufacturing: a review. *Journal of Materials Engineering and performance*, *23*(6), pp.1917-1928.
42. Fu, L., Khor, K.A. and Lim, J.P., 2000. Yttria stabilized zirconia reinforced hydroxyapatite coatings. *Surface and Coatings Technology*, *127*(1), pp.66-75.
43. Gao, T., Aro, H.T., Ylänen, H. and Vuorio, E., 2001. Silica-based bioactive glasses modulate expression of bone morphogenetic protein-2 mRNA in Saos-2 osteoblasts in vitro. *Biomaterials*, *22*(12), pp.1475-1483.
44. Geetha, M., Singh, A.K., Asokamani, R. and Gogia, A.K., 2009. Ti based biomaterials, the ultimate choice for orthopaedic implants–a review. *Progress in materials science*, *54*(3), p. 397-425.
45. Gross, K.A., Gross, V. and Berndt, C.C., 1998. Thermal analysis of amorphous phases in hydroxyapatite coatings. *Journal of the American Ceramic Society*, *81*(1), pp.106-112.

46. Gu, Y.W., Khor, K.A., Pan, D. and Cheang, P., 2004. Activity of plasma sprayed yttria stabilized zirconia reinforced hydroxyapatite/Ti–6Al–4V composite coatings in simulated body fluid. *Biomaterials*, *25*(16), pp.3177-3185.
47. Hannink, G. and Arts, J.C., 2011. Bioresorbability, porosity and mechanical strength of bone substitutes: what is optimal for bone regeneration?. *Injury*, *42*, pp.S22-S25.
48. He, J.L., Chen, K.C., Chen, C.C., Leyland, A. and Matthews, A., 2001. Cyclic oxidation resistance of Ni–Al alloy coatings deposited on steel by a cathodic arc plasma process. *Surface and Coatings Technology*, *135*(2-3), pp.158-165.
49. Hench, L.L. and Polak, J.M., 2002. Third-generation biomedical materials. *Science*, *295*(5557), pp.1014-1017.
50. Hijón, N., Cabanas, M.V., Pena, J. and Vallet-Regí, M., 2006. Dip coated silicon-substituted hydroxyapatite films. *Acta Biomaterialia*, *2*(5), pp.567-574.
51. Hofmann, D.C., Roberts, S., Otis, R., Kolodziejska, J., Dillon, R.P., Suh, J.O., Shapiro, A.A., Liu, Z.K. and Borgonia, J.P., 2014. Developing gradient metal alloys through radial deposition additive manufacturing. *Scientific reports*, *4*(1), pp.1-8.
52. https://nrc.canada.ca/en/research-development/research-collaboration/industrial-rd groups/cold-spray-additive-manufacturing-csam-industrial-rd-group.
53. https://www.impact-innovations.com/en/coldgas/cg_index_en.html.
54. https://www.spee3d.com/.
55. Huang, Y., Hao, M., Nian, X., Qiao, H., Zhang, X., Zhang, X., Song, G., Guo, J., Pang, X. and Zhang, H., 2016. Strontium and copper co-substituted hydroxyapatite-based coatings with improved antibacterial activity and cytocompatibility fabricated by electrodeposition. *Ceramics International*, *42*(10), pp.11876-11888.
56. ITIRAVIVONG, P., 2001. Biomaterials: an Overview. *Journal of Metals, Materials and Minerals*, *11*(1), pp. 15-21.
57. Kamachimudali, U., Sridhar, T.M. and Raj, B., 2003. Corrosion of bio implants. *Sadhana*, *28*, p. 601-637.
58. Kannan, S., Balamurugan, A. and Rajeswari, S., 2003. Hydroxyapatite coatings on sulfuric acid treated type 316L SS and its electrochemical behaviour in Ringer's solution. *Materials letters*, *57*(16-17), p. 2382-2389.

59. Kaushal, S., Gupta, D. and Bhowmick, H., 2018. On processing of Ni-Cr3C2 based functionally graded clads through microwave heating. *Materials Research Express*, *5*(6), p.066405.
60. Kaya, C., 2008. Electrophoretic deposition of carbon nanotube-reinforced hydroxyapatite bioactive layers on Ti–6Al–4V alloys for biomedical applications. *Ceramics International*, *34*(8), pp.1843-1847.
61. Li, H., Khor, K.A. and Cheang, P., 2002. Properties of heat-treated calcium phosphate coatings deposited by high-velocity oxy-fuel (HVOF) spray. *Biomaterials*, *23*(10), pp.2105-2112.
62. Li, H., Khor, K.A. and Cheang, P., 2002. Titanium dioxide reinforced hydroxyapatite coatings deposited by high velocity oxy-fuel (HVOF) spray. *Biomaterials*, *23*(1), pp.85-91.
63. Li, H., Khor, K.A., Kumar, R. and Cheang, P., 2004. Characterization of hydroxyapatite/nano-zirconia composite coatings deposited by high velocity oxy-fuel (HVOF) spray process. *Surface and Coatings Technology*, *182*(2-3), pp.227-236.
64. Lin, K., Zhang, M., Zhai, W., Qu, H. and Chang, J., 2011. Fabrication and characterization of hydroxyapatite/wollastonite composite bioceramics with controllable properties for hard tissue repair. *Journal of the American Ceramic Society*, *94*(1), pp.99-105.
65. Lysaght, M.J. and O'Loughlin, J.A., 2000. Demographic scope and economic magnitude of contemporary organ replacement therapies. *ASAIO journal*, *46*(5), pp.515-521.
66. Mancini, C.E., Berndt, C.C., Sun, L. and Kucuk, A., 2001. Porosity determinations in thermally sprayed hydroxyapatite coatings. *Journal of materials science*, *36*(16), pp.3891-3896.
67. Manivasagam, G., Dhinasekaran, D. and Rajamanickam, A., 2010. Biomedical implants: corrosion and its prevention-a review. *Recent patents on corrosion science*, *2*(1). p. 40-54.
68. Marcelo, T., Mascarenhas, J.M. and Oliveira, F.A.C., 2010. Microwave sintering–a novel approach to powder technology. In *Materials Science Forum* (Vol. 636, pp. 946-951). Trans Tech Publications Ltd.
69. Martin, J.H., Yahata, B.D., Hundley, J.M., Mayer, J.A., Schaedler, T.A. and Pollock, T.M., 2017. 3D printing of high-strength aluminium alloys. *Nature*, *549*(7672), pp.365-369.

70. Meng, Y.H., Tang, C.Y. and Tsui, C.P., 2008. Fabrication and characterization of needle-like nano-HA and HA/MWNT composites. *Journal of Materials Science: Materials in Medicine*, *19*(1), pp.75-81.
71. Mohajernia, S., Pour-Ali, S., Hejazi, S., Saremi, M. and Kiani-Rashid, A.R., 2018. Hydroxyapatite coating containing multi-walled carbon nanotubes on AZ31 magnesium: Mechanical-electrochemical degradation in a physiological environment. *Ceramics International*, *44*(7), pp.8297-8305.
72. Moridi, A., 2016. *Powder Consolidation Using Cold Spray: Process Modeling and Emerging Applications*. Springer.
73. Moridi, A., Hassani-Gangaraj, S.M., Guagliano, M. and Dao, M., 2014. Cold spray coating: review of material systems and future perspectives. *Surface Engineering*, *30*(6), pp.369-395.
74. Moridi, A., Stewart, E.J., Wakai, A., Assadi, H., Gartner, F., Guagliano, M., Klassen, T. and Dao, M., 2020. Solid-state additive manufacturing of porous Ti-6Al-4V by supersonic impact. *Applied Materials Today*, *21*, p.100865.
75. Nasab, M.B., Hassan, M.R. and Sahari, B.B., 2010. Metallic biomaterials of knee and hip-a review. *Trends Biomater. Artif. Organs*, *24*(1), p. 69-82.
76. Ni, J., Ling, H., Zhang, S., Wang, Z., Peng, Z., Benyshek, C., Zan, R., Miri, A.K., Li, Z., Zhang, X. and Lee, J., 2019. Three-dimensional printing of metals for biomedical applications. *Materials Today Bio*, *3*, p.100024.
77. Niinomi, M., 2008. Metallic biomaterials. *Journal of Artificial Organs*, *11*, p.105-110.
78. Oshkour, A.A., Pramanik, S., Mehrali, M., Yau, Y.H., Tarlochan, F. and Osman, N.A.A., 2015. Mechanical and physical behavior of newly developed functionally graded materials and composites of stainless steel 316L with calcium silicate and hydroxyapatite. *Journal of the mechanical behavior of biomedical materials*, *49*, p. 321-331.
79. Patterson, S.P., Daffner, R.H. and Gallo, R.A., 2005. Electrochemical corrosion of metal implants. *American Journal of Roentgenology*, *184*(4), p. 1219-1222.
80. Rath, P.C., Besra, L., Singh, B.P. and Bhattacharjee, S., 2012. Titania/hydroxyapatite bi-layer coating on Ti metal by electrophoretic deposition: Characterization and corrosion studies. *Ceramics International*, *38*(4), pp.3209-3216.

81. Rezaei, A., Golenji, R.B., Alipour, F., Hadavi, M.M. and Mobasherpour, I., 2020. Hydroxyapatite/hydroxyapatite-magnesium double-layer coatings as potential candidates for surface modification of 316 LVM stainless steel implants. *Ceramics International*, *46*(16), pp.25374-25381.
82. Rocha, R.C., Galdino, A.G.D.S., Silva, S.N.D. and Machado, M.L.P., 2018. Surface, microstructural, and adhesion strength investigations of a bioactive hydroxyapatite-titanium oxide ceramic coating applied to Ti-6Al-4V alloys by plasma thermal spraying. *Materials Research*, *21*(4).
83. Roohani-Esfahani, S.I., Newman, P. and Zreiqat, H., 2016. Design and fabrication of 3D printed scaffolds with a mechanical strength comparable to cortical bone to repair large bone defects. *Scientific reports*, *6*(1), pp.1-8.
84. Roychowdhury, A., Gupta, S., Vidyasagara, P.E.C. and Pal, S., 2004. Wear studies of frequently used implant materials. *Trends in Biomaterials and Artificial Organs*, *17*(2), pp.135-141.
85. Sames, W.J., List, F.A., Pannala, S., Dehoff, R.R. and Babu, S.S., 2016. The metallurgy and processing science of metal additive manufacturing. *International materials reviews*, *61*(5), pp.315-360.
86. Singh, A., Singh, G. and Chawla, V., 2018. Influence of post coating heat treatment on microstructural, mechanical and electrochemical corrosion behaviour of vacuum plasma sprayed reinforced hydroxyapatite coatings. *Journal of the mechanical behavior of biomedical materials*, *85*, pp.20-36.
87. Singh, B., Singh, G. and Sidhu, B.S., 2018. Analysis of corrosion behavior and surface properties of plasma-sprayed HA/Ta coating on CoCr alloy. *Journal of Thermal Spray Technology*, *27*(8), pp.1401-1413.
88. Singh, B., Singh, G. and Sidhu, B.S., 2019. Investigation of the in vitro corrosion behavior and biocompatibility of niobium (Nb)-reinforced hydroxyapatite (HA) coating on CoCr alloy for medical implants. *Journal of Materials Research*, *34*(10), pp.1678-1691.
89. Singh, G., Singh, S. and Prakash, S., 2011. Post Heat Treatment of Plasma Sprayed Pure and Alumina-Titania Reinforced Hydroxyapatite Coating on SS 304 Steel. *Journal of Minerals and Materials Characterization and Engineering*, *10*(2), pp.173-184.

90. Singh, G., Singh, S. and Prakash, S., 2011. Surface characterization of plasma sprayed pure and reinforced hydroxyapatite coating on Ti6Al4V alloy. *Surface and Coatings Technology*, *205*(20), pp.4814-4820.
91. Singh, J., Chatha, S.S. and Singh, H., 2021. Characterization and corrosion behavior of plasma sprayed calcium silicate reinforced hydroxyapatite composite coatings for medical implant applications. *Ceramics International*, *47*(1), pp.782-792.
92. Singh, R. and Dahotre, N.B., 2007. Corrosion degradation and prevention by surface modification of biometallic materials. *Journal of Materials Science: Materials in Medicine*, *18*(5), p. 725-751.
93. Singh, S., Pandey, K.K., Rahman, O.A., Haldar, S., Lahiri, D. and Keshri, A.K., 2020. Investigation of crystallinity, mechanical properties, fracture toughness and cell proliferation in plasma sprayed graphene nano platelets reinforced hydroxyapatite coating. *Materials Research Express*, *7*(1), p.015415.
94. Sridhar, T.M., Mudali, U.K. and Subbaiyan, M., 2003. Preparation and characterisation of electrophoretically deposited hydroxyapatite coatings on type 316L stainless steel. *Corrosion Science*, *45*(2), p. 237-252.
95. Tao, Y., Ke, G., Xie, Y., Chen, Y., Shi, S. and Guo, H., 2015. Adhesion strength and nucleation thermodynamics of four metals (Al, Cu, Ti, Zr) on AlN substrates. *Applied Surface Science*, *357*, pp.8-13.
96. Tian, P., Hu, H., Wang, H., Liu, X. and Ding, C., 2014. TiO2/CaF2 composite coating on titanium for biomedical application. *Materials Letters*, *117*, pp.98-100.
97. Tiwari, S. and Mishra, S.B., 2021. Post annealing effect on corrosion behavior, bacterial adhesion, and bioactivity of LVOF sprayed hydroxyapatite coating. *Surface and Coatings Technology*, *405*, p.126500.
98. Tsui, Y.C., Doyle, C. and Clyne, T.W., 1998. Plasma sprayed hydroxyapatite coatings on titanium substrates Part 1: Mechanical properties and residual stress levels. *Biomaterials*, *19*(22), pp.2015-2029.
99. Vasudev, H., Singh, G., Bansal, A., Vardhan, S. and Thakur, L., 2019. Microwave heating and its applications in surface engineering: a review. *Materials Research Express*, *6*(10), p.102001.

100. Vayre, B., Vignat, F. and Villeneuve, F., 2012. Metallic additive manufacturing: state-of-the-art review and prospects. *Mechanics and Industry*, *13*(2), pp.89-96.

101. Wang, G. and Zreiqat, H., 2010. Functional coatings or films for hard-tissue applications. *Materials*, *3*(7), p. 3994-4050.

102. Wang, M., 2003. Developing novel biomaterials for new challenges. In *Materials Science and Technology in Engineering Conference Now, New and Next*, The Hong Kong Institution of Engineers, Hong Kong.

103. Wang, Y.M., Voisin, T., McKeown, J.T., Ye, J., Calta, N.P., Li, Z., Zeng, Z., Zhang, Y., Chen, W., Roehling, T.T. and Ott, R.T., 2018. Additively manufactured hierarchical stainless steels with high strength and ductility. *Nature materials*, *17*(1), pp.63-71.

104. Williams, C.B., Cochran, J.K. and Rosen, D.W., 2011. Additive manufacturing of metallic cellular materials via three-dimensional printing. *The International Journal of Advanced Manufacturing Technology*, *53*(1), pp.231-239.

105. Williams, D.F., 2003. Biomaterials and tissue engineering in reconstructive surgery. *Sadhana*, *28*, p. 563-574.

106. Yang, C.W. and Lui, T.S., 2007. Effect of crystallization on the bonding strength and failures of plasma-sprayed hydroxyapatite. *Materials transactions*, *48*(2), pp.211-218.

107. Yang, Y.C., Chen, C.C., Wang, J.B., Wang, Y.C. and Lin, F.H., 2017. Flame sprayed zinc doped hydroxyapatite coating with antibacterial and biocompatible properties. *Ceramics International*, *43*, pp.S829-S835.

108. Yao, H.L., Wang, H.T., Bai, X.B., Ji, G.C. and Chen, Q.Y., 2018. Improvement in mechanical properties of nano-structured HA/TiO2 multilayer coatings deposited by high velocity suspension flame spraying (HVSFS). *Surface and Coatings Technology*, *342*, pp.94-104.

109. Yugeswaran, S., Yoganand, C.P., Kobayashi, A., Paraskevopoulos, K.M. and Subramanian, B., 2012. Mechanical properties, electrochemical corrosion and in-vitro bioactivity of yttria stabilized zirconia reinforced hydroxyapatite coatings prepared by gas tunnel type plasma spraying. *Journal of the mechanical behavior of biomedical materials*, *9*, pp.22-33.

110. Zakaria, M.Y., Sulong, A.B., Muhamad, N., Raza, M.R. and Ramli, M.I., 2019. Incorporation of wollastonite bioactive ceramic with titanium for medical applications: An overview. *Materials Science and Engineering: C*, *97*, pp.884-895.

111. Zhao, G.L., Wen, G.W. and Kun, W., 2009. Influence of processing parameters and heat treatment on phase composition and microstructure of plasma sprayed hydroxyapatite coatings. *Transactions of Nonferrous Metals Society of China*, *19*, pp.s463-s469.

112. Zhao, Z., Du, L., Tao, Y., Li, Q. and Luo, L., 2016. Enhancing the adhesion strength of micro electroforming layer by ultrasonic agitation method and the application. *Ultrasonicssonochemistry*, *33*, pp.10-17.

113. B. Beig, U. Liaqat, M. F. K. Niazi, I. Douna, M. Zahoor and M. B. K. Niazi, Coatings 10 (2020) 1249.

114. S. Bodhak, S. Bose and A. Bandyopadhyay, Mater. Sci. Eng. C 31 (2011) 755

115. Y. Chai et al., Bioactive Mater. 6 (2021) 4772.

116. A. Bartkowiak, A. Zarzycki, S. Kac, M. Perzanowski and M. Marszalek, Materials 13 (2020) 5290.

117. W. J. Basirun, B. Nasiri-Tabrizi and S. Baradaran, Crit. Rev. Solid State Mater. Sci. 43 (2018) 177.

118. F. E. Baştan et al., Coll. Surf. B: Biointerf. 169 (2018) 176.

119. J.A. Disegi, L. Eschbach, Stainless steel in bone surgery, Injury 31 (2001) 2–6.

120. M.L.C.A. Afonso, R.V. Jaimes, E.P.G. Arêas, M.R. Capri, E. Oliveira, S.M.L. Agostinho, The influence of albumin on the anodic dissolution of chromium present in UNS S31254 stainless steel in chloride environment, Colloids Surf. 317 (2008) 760–763.

121. Q. Chen, G.A. Thouas, Metallic implant biomaterials, Mater. Sci. Eng. R. Rep. 87 (2015) 1–57.

122. M.L.D.A. Afonso, R.F. Jaimes, P.A. Nascente, S.O. Rogero, S.M. Agostinho, Surface characterization, electrochemical behavior and cytotoxicity of UNS S31254 stainless steel for orthopedic applications, Mater. Lett. 148 (2015) 71–75.

123. A. Dziubińska, K. Majerski, E. Siemionek, Effect of forging temperature on the microstructure and properties of REX 734 implantable stainless steel, Procedia Manuf 15 (2018) 411–418.

124. E. Salahinejad, M.J. Hadianfard, D.D. Macdonald, S. Sharifi-Asl, M. Mozafari, K.J. Walker, A.T. Rad, S.V. Madihally, L. Tayebi, In vitro electrochemical corrosion and cell viability studies on nickel-free stainless steel orthopedic implants, PLoS One 8 (4) (2013) 61633.

125. R.F.V.V. Jaimes, M.L.C. de Andrade Afonso, S.O. Rogero, S.M.L. Agostinho, C.A. Barbosa, New material for orthopedic implants: electrochemical study of nickel free P558 stainless steel in minimum essential medium, Mater. Lett. 64 (13) (2010) 1476–1479.

126. L. De Micheli, A.H.P. Andrade, C.A. Barbosa, S.M.L. Agostinho, Electrochemical studies of 254SMO stainless steel in comparison with 316L stainless steel and Hastelloy C276 in phosphoric acid media in absence and presence of chloride ions, Br. Corros. J. 34 (1) (1999) 67–70.

127. E.A. El Meguid, A.A. El Latif, Critical pitting temperature for type 254 SMO stainless steel in chloride solutions, Corros. Sci. 49 (2) (2007) 263–275.

128. A. Das, M. Shukla, Hydroxyapatite coatings on high nitrogen stainless steel by laser rapid manufacturing, JOM 69 (11) (2017) 2292–2296.

129. A. Subash, A. Basanth and B. Kandasubramanian, Int. J. Polym. Mater. Polym. Biomater. (2022) 1.

130. L. Sun, C. C. Berndt and K. A. Gross, J. Biomater. Sci. Polym. Ed. 13 (2002) 977.

131. R. B. Thompson et al., Proc. Natl. Acad. Sci. 112 (2015) 1565.

132. A. Vladescu et al., Biomed. Mater. 13 (2018) 025011.

133. N. Vladislavić, I. Š. Rončević, M. Buzuk, M. Buljac and I. Drventić, J. Solid State Electrochem. 25 (2021) 841.

134. Tiwari, S. and Mishra, S.B., 2021. Post annealing effect on corrosion behavior, bacterial adhesion, and bioactivity of LVOF sprayed hydroxyapatite coating. Surface and Coatings Technology, 405, p.126500.

135. Vladescu A, Cotrut CM, Azem FA, Bramowicz M, Pana I, Braic V, et al. Sputtered Si and Mg doped hydroxyapatite for biomedical applications. 2018;13:025011.

136. Chen Q, Thouas GAJMS, Reports ER. Metallic implant biomaterials. 2015;87:1-57.

137. Ahmed W, Zhai Z, Gao CJMTB. Adaptive antibacterial biomaterial surfaces and their applications. 2019;2:100017.

138. Priyadarshini B, Rama M, Chetan, Vijayalakshmi UJJoACS. Bioactive coating as a surface modification technique for biocompatible metallic implants: a review. 2019;7:397-406.
139. Alijani S, Anvari AJJoCE, Science M. Cycle numbers to failure for magnesium and its alloys in human body fluid. 2018;9:1-8.
140. Degaard KS, Torgersen J, Elverum CWJM. Structural and biomedical properties of common additively manufactured biomaterials: A concise review. 2020;10:1677.
141. Velu R, Calais T, Jayakumar A, Raspall FJM. A comprehensive review on bio-nanomaterials for medical implants and feasibility studies on fabrication of such implants by additive manufacturing technique. 2019;13:92.
142. Dehghanghadikolaei A, Fotovvati BJM. Coating techniques for functional enhancement of metal implants for bone replacement: a review. 2019;12:1795.
143. Kamrani S, Fleck CJB. Biodegradable magnesium alloys as temporary orthopaedic implants: a review. 2019;32:185-93.
144. Resnik M, Benčina M, Levičnik E, Rawat N, Iglič A, Junkar IJM. Strategies for improving antimicrobial properties of stainless steel. 2020;13:2944.
145. Ur Rehman MA, Bastan FE, Nawaz A, Nawaz Q, Wadood AJTIJoAMT. Electrophoretic deposition of PEEK/bioactive glass composite coatings on stainless steel for orthopedic applications: an optimization for in vitro bioactivity and adhesion strength. 2020;108:1849-62.
146. Morsiya CJAJoME. A review on parameters affecting properties of biomaterial SS 316L. 2022;20:803-13.
147. Vignesh RV, Padmanaban R, Govindaraju MJSTM, Properties. Investigations on the surface topography, corrosion behavior, and biocompatibility of friction stir processed magnesium alloy AZ91D. 2019;7:025020.
148. Nguyen N, Ha-Van N, Seo CJIA, Letters WP. Midfield wireless power transfer for deep-tissue biomedical implants. 2020;19:2270-4.
149. Munir K, Lin J, Wen C, Wright PF, Li YJAb. Mechanical, corrosion, and biocompatibility properties of Mg-Zr-Sr-Sc alloys for biodegradable implant applications. 2020;102:493-507.

150. Shittu J, Pole M, Cockerill I, Sadeghilaridjani M, Reddy LVK, Manivasagam G, et al. Biocompatible high entropy alloys with excellent degradation resistance in a simulated physiological environment. 2020;3:8890-900.
151. Hufenbach J, Sander J, Kochta F, Pilz S, Voss A, Kühn U, et al. Effect of selective laser melting on microstructure, mechanical, and corrosion properties of biodegradable FeMnCS for implant applications. 2020;22:2000182.
152. Ali S, Rani AMA, Baig Z, Ahmed SW, Hussain G, Subramaniam K, et al. Biocompatibility and corrosion resistance of metallic biomaterials. 2020;38:381-402.
153. Jia Y, Ba Z, Chen X, Zhou B, Zhou W, Liu H, et al. Controlled surface mechanical property and corrosion resistance of ZK60 magnesium alloy treated by zirconium ion implantation. 2020;8:025015.
154. Manivasagam G, Dhinasekaran D, Rajamanickam AJRpocs. Biomedical implants: corrosion and its prevention-a review. 2010;2.
155. Kopova I, Kronek J, Bacakova L, Fencl JJD, Materials R. A cytotoxicity and wear analysis of trapeziometacarpal total joint replacement implant consisting of DLC-coated Co-Cr-Mo alloy with the use of titanium gradient interlayer. 2019;97:107456.
156. Hintermann B, Susdorf R, Krähenbühl N, Ruiz RJF, International A. Axial rotational alignment in mobile-bearing total ankle arthroplasty. 2020;41:521-8.
157. Mondal S, Ghosh RJJoo. Experimental and finite element investigation of total ankle replacement: A review of literature and recommendations. 2020;18:41-9.
158. Barg A, Elsner A, Anderson AE, Hintermann BJJ. The effect of three-component total ankle replacement malalignment on clinical outcome: pain relief and functional outcome in 317 consecutive patients. 2011;93:1969-78.
159. Kumar P, Rajnish RK, Sharma S, Dhillon MSJIo. Proximal femoral nailing is superior to hemiarthroplasty in AO/OTA A2 and A3 intertrochanteric femur fractures in the elderly: a systematic literature review and meta-analysis. 2020;44:623-33.
160. Ståhl A, Westerdahl EJCIiA. Postoperative physical therapy to prevent hospital-acquired pneumonia in patients over 80 years undergoing hip fracture surgery—a quasi-experimental study. 2020;15:1821.

161. Gibbs VN, McCulloch RA, Dhiman P, McGill A, Taylor AH, Palmer AJ, et al. Modifiable risk factors for mortality in revision total hip arthroplasty for periprosthetic fracture. 2020;102:580-5.
162. Quinn J, McFadden R, Chan C-W, Carson LJI. Titanium for orthopedic applications: an overview of surface modification to improve biocompatibility and prevent bacterial biofilm formation. 2020;23:101745.
163. Zafar M. Fabrication, Characterization and In Vitro Biological Evaluation of Periosteum Bilayered Composite Scaffolds for Bone Repair and Regeneration 2021.
164. Rivera-Muñoz EMJBE-F, Challenges. Hydroxyapatite-based materials: synthesis and characterization. 2011:75-98.
165. Arcos D, Vallet-Regí MJJoMCB. Substituted hydroxyapatite coatings of bone implants. 2020;8:1781-800.
166. Beig B, Liaqat U, Niazi MFK, Douna I, Zahoor M, Niazi MBKJC. Current challenges and innovative developments in hydroxyapatite-based coatings on metallic materials for bone implantation: A review. 2020;10:1249.
167. Cheng GJ, Pirzada D, Cai M, Mohanty P, Bandyopadhyay AJMS, C E. Bioceramic coating of hydroxyapatite on titanium substrate with Nd-YAG laser. 2005;25:541-7.
168. Awasthi S, Pandey SK, Arunan E, Srivastava CJJoMCB. A review on hydroxyapatite coatings for the biomedical applications: Experimental and theoretical perspectives. 2021;9:228-49.
169. Liu Y-C, Lin G-S, Lee Y-T, Huang T-C, Chang T-W, Chen Y-W, et al. Microstructures and cell reaction of porous hydroxyapatite coatings on titanium discs using a novel vapour-induced pore-forming atmospheric plasma spraying. 2020;393:125837.
170. Maximov M, Maximov O-C, Craciun L, Ficai D, Ficai A, Andronescu EJC. Bioactive Glass—An Extensive Study of the Preparation and Coating Methods. 2021;11:1386.
171. Vuornos K. In vitro studies of composite biomaterials and human adipose stem cells in bone and tendon tissue engineering applications. 2020.
172. Rainer G, Christian F, Andreas K, Miriam FJJoWR, Protection. Development of atmospheric plasma sprayed dielectric ceramic coatings for high efficiency tubular ozone generators. 2010;2010.

173. Singh H, Prakash C, Singh SJJoBE. Plasma spray deposition of HA-TiO2 on β-phase Ti-35Nb-7Ta-5Zr alloy for hip stem: characterization of bio-mechanical properties, wettability, and wear resistance. 2020;17:1029-44.
174. Heimann RBJJoVS, Technology A: Vacuum S, Films. Functional plasma-sprayed hydroxylapatite coatings for medical application: Clinical performance requirements and key property enhancement. 2021;39:050801.
175. Kravanja KA, Finšgar MJM, Design. A review of techniques for the application of bioactive coatings on metal-based implants to achieve controlled release of active ingredients. 2022:110653.
176. Yadav V, Sankar M, Pandey LJJoM, Alloys. Coating of bioactive glass on magnesium alloys to improve its degradation behavior: Interfacial aspects. 2020;8:999-1015.
177. Salhi Z, Klein D, Gougeon P, Coddet CJV. Development of coating by thermal plasma spraying under very low-pressure condition< 1 mbar. 2005;77:145-50.
178. Ratha I, Datta P, Balla VK, Nandi SK, Kundu BJCI. Effect of doping in hydroxyapatite as coating material on biomedical implants by plasma spraying method: A review. 2021;47:4426-45.
179. Grafts IB, Substitutes BJBiO, Marcel Dekker INY, NY, USA. Three-dimensionally engineered hydroxyapatite ceramics with interconnected pores as a bone substitute and tissue engineering scaffold. 2004.
180. Hameed P, Gopal V, Bjorklund S, Ganvir A, Sen D, Markocsan N, et al. Axial suspension plasma spraying: An ultimate technique to tailor Ti6Al4V surface with HAp for orthopaedic applications. 2019;173:806-15.
181. Rauch J, Bolelli G, Killinger A, Gadow R, Cannillo V, Lusvarghi LJS, et al. Advances in high velocity suspension flame spraying (HVSFS). 2009;203:2131-8.
182. Thompson RB, Reffatto V, Bundy JG, Kortvely E, Flinn JM, Lanzirotti A, et al. Identification of hydroxyapatite spherules provides new insight into subretinal pigment epithelial deposit formation in the aging eye. 2015;112:1565-70.
183. Gupta VJIJfAR, Development. Smart materials in dentistry: A review. 2018;3:89-96.
184. Baranwal A, Kumar A, Priyadharshini A, Oggu GS, Bhatnagar I, Srivastava A, et al. Chitosan: an undisputed bio-fabrication material for tissue engineering and bio-sensing applications. 2018;110:110-23.

185. Basirun WJ, Nasiri-Tabrizi B, Baradaran SJCriss, sciences m. Overview of hydroxyapatite–graphene nanoplatelets composite as bone graft substitute: mechanical behavior and in-vitro biofunctionality. 2018;43:177-212.
186. Sun L, Berndt CC, Gross KAJJoBS, Polymer Edition. Hydroxyapatite/polymer composite flame-sprayed coatings for orthopedic applications. 2002;13:977-90.
187. Balani K, Chen Y, Harimkar SP, Dahotre NB, Agarwal AJAB. Tribological behavior of plasma-sprayed carbon nanotube-reinforced hydroxyapatite coating in physiological solution. 2007;3:944-51.
188. Morks MJJotmbobm. Fabrication and characterization of plasma-sprayed HA/SiO2 coatings for biomedical application. 2008;1:105-11.
189. Singh G, Singh S, Prakash SJS, Technology C. Surface characterization of plasma sprayed pure and reinforced hydroxyapatite coating on Ti6Al4V alloy. 2011;205:4814-20.
190. Yugeswaran S, Yoganand C, Kobayashi A, Paraskevopoulos K, Subramanian BJJotmbobm. Mechanical properties, electrochemical corrosion and in-vitro bioactivity of yttria stabilized zirconia reinforced hydroxyapatite coatings prepared by gas tunnel type plasma spraying. 2012;9:22-33.
191. Rath PC, Besra L, Singh BP, Bhattacharjee SJCI. Titania/hydroxyapatite bi-layer coating on Ti metal by electrophoretic deposition: Characterization and corrosion studies. 2012;38:3209-16.
192. Yang Y-C, Chen C-C, Wang J-B, Wang Y-C, Lin F-HJCI. Flame sprayed zinc doped hydroxyapatite coating with antibacterial and biocompatible properties. 2017;43:S829-S35.
193. Yao H-L, Wang H-T, Bai X-B, Ji G-C, Chen Q-YJS, Technology C. Improvement in mechanical properties of nano-structured HA/TiO2 multilayer coatings deposited by high velocity suspension flame spraying (HVSFS). 2018;342:94-104.
194. Singh A, Singh G, Chawla VJJotmbobm. Influence of post coating heat treatment on microstructural, mechanical and electrochemical corrosion behaviour of vacuum plasma sprayed reinforced hydroxyapatite coatings. 2018;85:20-36.
195. Safavi MS, Surmeneva MA, Surmenev RA, Khalil-Allafi JJCI. RF-magnetron sputter deposited hydroxyapatite-based composite & multilayer coatings: A systematic review from mechanical, corrosion, and biological points of view. 2021;47:3031-53.

196. Fathyunes L, Khalil-Allafi J, Moosavifar MJJotmbobm. Development of graphene oxide/calcium phosphate coating by pulse electrodeposition on anodized titanium: Biocorrosion and mechanical behavior. 2019;90:575-86.
197. Safavi MS, Walsh FC, Surmeneva MA, Surmenev RA, Khalil-Allafi JJC. Electrodeposited hydroxyapatite-based biocoatings: Recent progress and future challenges. 2021;11:110.
198. Sharifianjazi F, Pakseresht AH, Asl MS, Esmaeilkhanian A, Jang HW, Shokouhimehr MJJoC, et al. Hydroxyapatite consolidated by zirconia: applications for dental implant. 2020;2:26-34.
199. Farhadian M, Raeissi K, Golozar M, Labbaf S, Hajilou T, Barnoush AJASS. 3D-Focused ion beam tomography and quantitative porosity evaluation of ZrO2-SiO2 composite coating; amorphous SiO2 as a porosity tailoring agent. 2020;511:145567.
200. Stevanović M, Djošić M, Janković A, Kojić V, Stojanović J, Grujić S, et al. The chitosan-based bioactive composite coating on titanium. 2021;15:4461-74.
201. Thanigachalam M, Muthusamy Subramanian AVJJoBS, Polymer Edition. Evaluation of PEEK-TiO2-SiO2 nanocomposite as biomedical implants with regard to in-vitro biocompatibility and material characterization. 2022;33:727-46.
202. Dulski M, Balcerzak J, Simka W, Dudek KJM. Innovative Bioactive Ag-SiO2/TiO2 Coating on a NiTi Shape Memory Alloy: Structure and Mechanism of Its Formation. 2020;14:99.
203. Dulski M, Gawecki R, Sułowicz S, Cichomski M, Kazek-Kęsik A, Wala M, et al. Key properties of a bioactive Ag-SiO2/TiO2 coating on NiTi shape memory alloy as necessary at the development of a new class of biomedical materials. 2021;22:507.
204. Singh J, Chatha SS, Singh HJCI. Characterization and corrosion behavior of plasma sprayed calcium silicate reinforced hydroxyapatite composite coatings for medical implant applications. 2021;47:782-92.
205. Chai Y, Liu Z, Du Y, Wang L, Lu J, Zhang Q, et al. Hydroxyapatite reinforced inorganic-organic hybrid nanocomposite as high-performance adsorbents for bilirubin removal in vitro and in pig models. 2021;6:4772-85.

206. Daroonparvar M, Bakhsheshi-Rad HR, Saberi A, Razzaghi M, Kasar AK, Ramakrishna S, et al. Surface modification of magnesium alloys using thermal and solid-state cold spray processes: Challenges and latest progresses. 2022.
207. Zakhireh S, Barar J, Adibkia K, Beygi-Khosrowshahi Y, Fathi M, Omidain H, et al. Bioactive Chitosan-Based Organometallic Scaffolds for Tissue Engineering and Regeneration. 2022;380:1-47.
208. Rezaei A, Golenji RB, Alipour F, Hadavi MM, Mobasherpour IJCI. Hydroxyapatite/hydroxyapatite-magnesium double-layer coatings as potential candidates for surface modification of 316 LVM stainless steel implants. 2020;46:25374-81.
209. Bartkowiak A, Zarzycki A, Kac S, Perzanowski M, Marszalek MJM. Mechanical properties of different nanopatterned TiO2 substrates and their effect on hydrothermally synthesized bioactive hydroxyapatite coatings. 2020;13:5290.
210. Prashar G, Vasudev H, Thakur L, Bansal AJSR, Letters. Performance of thermally sprayed Hydroxyapatite coatings for biomedical implants: A comprehensive review. 2022.
211. Rocha RC, Galdino AGdS, Silva SNd, Machado MLPJMR. Surface, microstructural, and adhesion strength investigations of a bioactive hydroxyapatite-titanium oxide ceramic coating applied to Ti-6Al-4V alloys by plasma thermal spraying. 2018;21.
212. Unune DR, Brown GR, Reilly GCJV. Thermal based surface modification techniques for enhancing the corrosion and wear resistance of metallic implants: A review. 2022:111298.
213. Sathish M, Radhika N, Saleh BJM, International M. Duplex and Composite Coatings: A Thematic Review on Thermal Spray Techniques and Applications. 2022:1-69.
214. Geetha, M., Singh, A. K., Asokamani, R., & Gogia, A. K. (2009). Ti based biomaterials, the ultimate choice for orthopaedic implants – A review. *Progress in Materials Science*,
215.
216. 54(3), 397–425. https://doi.org/10.1016/j.pmatsci.2008.06.004
217. Wang L, Shaw LL. Characterization of plasma-sprayed hydroxyapatite coatings. *Acta Biomaterialia*. 2009;5(8): 3067–3074.
218. Ramesh S, Tan CY, Bhaduri SB, Teng WD, Cheang P. Processing and characterization of plasma-sprayed nano HA coatings. *Materials & Design*. 2007;28(7):2088–2093.

219. Han Z, Zhang E, Yang K. In vitro degradation and cytotoxicity of composite coatings of hydroxyapatite and alumina on biodegradable magnesium alloys. *Surface and Coatings Technology*. 2012;206(24):4893–4901.

220. Heimann RB. Plasma-sprayed hydroxyapatite-based coatings: Chemical, mechanical, and biomedical properties. *Journal of Thermal Spray Technology*. 2016;25(5):827–850.

221. Gothaman NSK, Sundararajan G, Sampathkumaran P. Influence of alumina reinforcement on corrosion behavior of hydroxyapatite coatings. *Journal of Materials Science: Materials in Medicine*. 2014;25(4):1095–1105.

222. Jastrzębska A, Sitarz M, Gubernator J. Effect of alumina addition on the structure and properties of hydroxyapatite coatings obtained by plasma spraying. *Journal of Thermal Spray Technology*. 2018;27(6):1008–1017.

223. Parcharoen, Y., Poologasundarampillai, G., & Reaney, I. M. (2022). Wear mechanisms in orthopedic implants: A review. *Materials Science and Engineering: C*, *132*, 112527.

224. Revathi, A., Borrás, A. D., Muñoz, A. I., Richard, C., & Manivasagam, G. (2017). Degradation mechanisms and future challenges of titanium and its alloys for dental implant applications in oral environment. *Materials Science and Engineering: C*, *76*, 1354–1368.

225. Gopi, D., Shinyjoy, E., & Kavitha, L. (2015). Development of electrochemically assisted hydroxyapatite–alumina composite coatings on surgical grade stainless steel for biomedical applications. *Journal of Alloys and Compounds*, *640*, 408–415.

226. Feng, B., Wang, W., Xu, J., et al. (2017). Improved bioactivity and antibacterial properties of $TiO_2$/HAP composite coatings on titanium implants. *Surface and Coatings Technology*, *324*, 204–210.

227. Sun, M., Ma, K., Wang, H., & Wang, J. (2021). Enhanced corrosion resistance and biocompatibility of Mg-doped hydroxyapatite coatings for orthopedic implants. *Journal of Materials Science: Materials in Medicine*, *32*(3), 30.

228. Liu X, Huang J, Liu Y, Yan Q, Wu S, Zhou P, Li H. Microstructure control of c-axis preferentially oriented hydroxyapatite coating by plasma spraying and its biological impacts. Ceramics International. 2025 Jan 25.

229. Yu LG, Khor KA, Li H, Cheang P. Effect of spark plasma sintering on the microstructure and in vitro behavior of plasma sprayed HA coatings. Biomaterials. 2003 Jul 1;24(16):2695-705.

230. Xue, W., Tao, S., Liu, X., Zheng, X. and Ding, C., 2004. In vivo evaluation of plasma sprayed hydroxyapatite coatings having different crystallinity. *Biomaterials*, *25*(3), pp.415-421.

231. A. Singh, G. Singh, V. Chawla, Influence of post coating heat treatment on microstructural, mechanical and electrochemical corrosion behaviour of vacuum plasma sprayed reinforced hydroxyapatite coatings. *Journal of the mechanical behavior of biomedical materials*, ***85*** (2018) 20-36.

232. Tsui YC, Doyle C, Clyne TW. Plasma sprayed hydroxyapatite coatings on titanium substrates Part 1: Mechanical properties and residual stress levels. Biomaterials. 1998 Nov 1;19(22):2015-29.

233. Tiwari S, Mishra SB. Post annealing effect on corrosion behavior, bacterial adhesion, and bioactivity of LVOF sprayed hydroxyapatite coating. Surface and Coatings Technology. 2021 Jan 15;405:126500.

234. Tiwari S, Mishra SB. Low velocity oxy fuel spraying of hydroxyapatite coating on a multifunctional UNS S31254 austenitic stainless steel. Proceedings of the Institution of Mechanical Engineers, Part H: Journal of Engineering in Medicine. 2021 Aug;235(8):958-72.

235. Tailor S, Vashishtha N, Modi A, Modi SC. High-performance $Al_2O_3$ coating by hybrid-Lvof (low-velocity oxyfuel) process. Journal of Thermal Spray Technology. 2020 Jun;29(5):1134-43.

236. Shankar D, Jayaganesh K, Gowda N, Lakshmi KS, Jayanthi KJ, Jambagi SC. Thermal spray processes influencing surface chemistry and in-vitro hemocompatibility of hydroxyapatite-based orthopedic implants. Biomaterials Advances. 2024 Apr 1;158:213791.

237. Gu, Y.W., Khor, K.A. and Cheang, P., 2003. In vitro studies of plasma-sprayed hydroxyapatite/Ti-6Al-4V composite coatings in simulated body fluid (SBF). *Biomaterials*, *24*(9), pp.1603-1611.

238. Morks, M.F., 2008. Fabrication and characterization of plasma-sprayed HA/$SiO_2$ coatings for biomedical application. *Journal of the mechanical behavior of biomedical materials*, *1*(1), pp.105-111.

239. Aruna ST, Balaji N, Shedthi J, Grips VW. Effect of critical plasma spray parameters on the microstructure, microhardness and wear and corrosion resistance of plasma sprayed alumina coatings. Surface and Coatings Technology. 2012 Sep 15;208:92-100.
240. Lockwood GK, Zhang S, Garofalini SH. Anisotropic Dissolution of α-Alumina (0001) and (11 2 0) Surfaces into Adjoining Silicates. Journal of the American Ceramic Society. 2008 Nov;91(11):3536-41.
241. Singh G, Mittal M, Singh J, Gill AS, Pal D, Bhavya K. Enhancing the performance of reinforced hydroxyapatite coatings through post coating treatment. Results in Surfaces and Interfaces. 2024 Feb 1;14:100207.

## LIST OF PUBLICATIONS

1. Bafila, G., Mehta, A., & Vasudev, H. (2024). A review on the mechanical and tribological properties of thermally sprayed hydroxyapatite coatings for biomedical implant materials. *Surface Review and Letters*. https://doi.org/10.1142/S0218625X25300047 **(Q3; SC1; I.F-1.1).**
2. Bafila, G., & Vasudev, H. (2024). Electrochemical corrosion analysis of HA-based coating deposited using LVOF technique on austenitic stainless steel surgical grade. *Journal of The Institution of Engineers (India): Series D*, 1-10. https://doi.org/10.1007/s40033-024-00310-0
   **(Q2; Scopus Indexed)**